UNIVERSITÀ
DEGLI STUDI
DI PADOVA

Sede Amministrativa: Università degli Studi di Padova

Dipartimento di Ingegneria Industriale

SCUOLA DI DOTTORATO DI RICERCA IN INGEGNERIA INDUSTRIALE
INDIRIZZO: INGEGNERIA CHIMICA, DEI MATERIALI E MECCANICA
CICLO XXX

Computed tomography based quality optimization of micro injection molding

Direttore della Scuola: Ch.mo Prof. Paolo Colombo
Coordinatore d'indirizzo: Ch.mo Prof. Giovanni Meneghetti
Supervisore: Ch.mo Prof. Simone Carmignato
Correlatore: Ch.mo Prof. Giovanni Lucchetta

Dottorando: Jitendra Singh Rathore

Preface

This thesis has been prepared as one of the requirements for the doctoral (Ph.D.) degree at the University of Padova (Padova, Italy). The work has been carried out from September 2014 to August 2017 at Department of Industrial Engineering (University of Padova) under the supervision of Prof. Simone Carmignato and Prof. Giovanni Lucchetta. Four weeks were spent at Volume Graphics GmbH (Heidelberg, Germany) from mid-November 2016 to mid-December 2016 as a part of secondment.

First of all, I would like to thank both my supervisors, Prof. Simone Carmignato and Prof. Giovanni Lucchetta for their valuable contributions and guidance throughout the work. I would also like to express my gratitude to Davide Masato and Dr. Marco Sorgato for their collaborations on the micro injection molding. Furthermore, I am extremely thankful to Tomasz Konopczyński from Volume Graphics for hosting me and for the great collaboration on the fiber work. Finally, I would thank all my PhD colleagues especially Dr. Filippo Zanini for providing initial training on the CT system and the procedures. Moreover, the technical support provided by the various industrial partners is also very much appreciated.

The financial support was provided by the European Union's Seventh Framework Programme under grant agreement No. 607817; which is gratefully acknowledged.

Padova, October 2017

Jitendra Singh Rathore

Abstract

Micro injection molding is a well-established manufacturing techniques for mass replication of micro parts. However, a new product development requires a process optimization with respect to the desired quality criteria. From the quality aspect, there has been demands for new technologies for quality assessment of the micro products. X-ray computed tomography (CT) is an emerging technology for industrial quality control. The current project focuses on application based quality optimization of micro injection molded parts utilizing X-ray CT. Processing parameters play a significant role in the final part quality; the most crucial parameters are: melt temperature, mold temperature, cooling time, packing pressure etc. The influence of the process parameters on the part quality is investigated by means of design of experiment approach.

X-ray CT is an extremely powerful tool which can used for different evaluations and analyses e.g. dimensional metrology, internal porosity, fiber orientation etc. Within the framework of this project, three different studies have been performed based on their critical quality aspects.

First study was focused on microfluidics where holistic dimensional quality control is desired. X-ray CT was used for the overall part measurement related to shrinkage and warpage, whereas conventional three dimensional optical profiler was employed used for the micro channel measurements. CT based data fusion approach was applied for the holistic part measurements. Moreover, the effect of electron beam alignment was also studied on the CT measurements of micro molded parts.

Fiber-reinforced polymers are commonly used in micro injection applications where higher mechanical properties are desirable e.g. in electronic connectors. Nevertheless, the use of fiber-reinforced polymers affects the desired accuracy, which is attributed mainly to the orientation of fibers in the final part. The non-destructive nature of X-ray CT allows to study the fiber orientation and its effect on the dimensional accuracy of the parts. An experimental investigation was carried out focusing the influence of process parameters (melt temperature, mold temperature, cooling time and packing pressure) on the desired fiber characteristics (orientation, fiber volume content

etc.). A simulation based study was also performed to validate the CT based characterization of fiber reinforced composites.

The last part was focused on a specific micro injection molding application where the internal defects (voids) alter the quality adversely. A series of experimental investigations were made by varying the critical process parameters. X-ray CT was used for the part characterization and quality assessment considering the different quality criteria e.g. total void volume, part volume (shrinkage) etc. Optimal set of process parameters was identified by performing the statistical analysis.

Table of Contents

List of figures

List of tables

List of acronyms

INTERAQCT: International Network for the Training of Early stage Researchers on Advanced Quality control by Computed Tomography

CT: Computed Tomography

iCT: Industrial Computed Tomography

µCT: Micro Computed Tomography

IM: Injection Molding

µIM: Micro Injection Molding

NDT: Non-destructive Techniques

SOD: Source-to-Object Distance

SDD: Source-to-Detector Distance

CAD: Computer-Aided Design

I/2/3D: One/Two/Three Dimensional

SEM: Scanning Electron Microscope

CMM: Coordinate Measuring Machine

XRM: X-ray Microscopes

COC: Cyclic Olefin Copolymer

PC: Polycarbonate

PBT: Polybutylene terephthalate

CHAPTER 1. INTRODUCTION

Chapter 1.
Introduction

This PhD work was performed as a part of a Marie Curie ESR Project INTERAQCT - International Network for the Training of Early stage Researchers on Advanced Quality control by Computed Tomography.

1.1 INTERAQCT

The INTERAQCT project [1] has been conceived as a pan-European industrial-academic initiative that will provide the unique and encompassing training environment required, by bringing together expertise from industry and academia in each of these domains (CT-equipment, CT-software, NDT, dimensional metrology, additive manufacturing, micro-manufacturing, composite manufacturing). INTERAQCT targets quantification and improvement of the reliability of CT measurement results, by determining the probability of detection of material defects as well as by achieving metrological traceability. In addition, CT based quality improvement loops will be targeted for key emerging manufacturing technologies. The details about the project are as follows:

- Project acronym: INTERAQCT
- Project full title: International Network for the Training of Early stage Researchers on Advanced Quality control by Computed Tomography
- Grant agreement no.: 607817
- Grant agreement for: Initial Training Networks
- Funded by: European Union's Seventh Framework Programme (FP7-PEOPLE-2013-ITN)

Fig. 1.1: The logo of the INTERAQCT project

1.1.1 Participants

The INTERAQCT consortium was formed consisting of various academic, industrial, national metrology institutes spread across Europe.

Academic partners

- Katholieke Universiteit Leuven, Mechanical Engineering Department, Belgium
- Fraunhofer Institute for Integrated Circuits - IIS, Germany
- University of Applied Science Upper Austria, Research Group Computed Tomography, Austria
- Universita Degli Studi di Padova, Italy
- Danmarks Tekniske Universitet, Denmark
- RWTH Aachen, Laboratory for Machine Tools and Production Engineering - WZL, Germany

Industrial partners

- X-TEK Systems LTD, U.K.
- Volume Graphics GMBH, Germany
- Materialise NV, Belgium

National metrology institutions

- Physikaltisch-Technische Bundesanstalt - PTB, Germany
- National Physical Laboratory - NPL, U.K.

Associated Partners

- LayerWise, Belgium
- Novo Nordisk A/S, Denmark
- Borealis Polyolefine GMBH, Austria
- Eltek S.P.A., Italy
- Argon Measuring Solutions, Belgium
- Nuovo Pignone S.R.L., Italy
- Kiekert AG, Germany

1.1.2 Objectives

The scientific objectives of the project were mainly divided into four work packages (WP1, WP2, WP3 and WP4). WP1 covers research activities improving the various steps required to obtain a CT voxel model, including the image acquisition on the CT machine

and subsequent voxel model reconstruction and segmentation steps. Subsequently, WP2 covers a series of interrelated challenges that need to be solved in order to guarantee traceable dimensional metrology. This work not only complements, but also supports enhancing material defect analysis in WP3. Both material and geometry aspects merge again in WP4, which makes use of CT for establishing quality control loops for innovative manufacturing technologies (Fig. 1.2). The numbers (1 to 13) indicate the different PhD project defined within these four work packages.

The current PhD project corresponds to number 11 within the work package 4 entitled as: “CT based quality optimization of micro injection molding”.

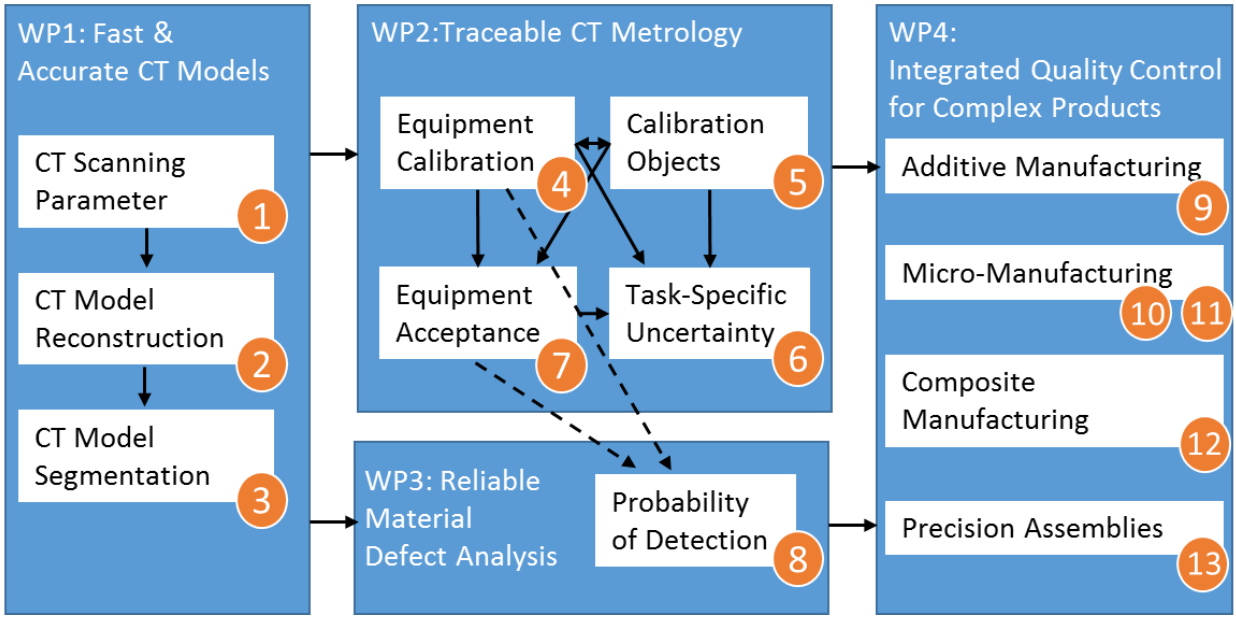

Fig. 1.2: **S**cientific approach of INTERAQCT

1.2 The current PhD project

This part of chapter consists of the introduction about the topic of current research, the objectives and the structure of the thesis.

1.2.1 Introduction

Innovation towards demand-driven customized and high-quality products is a necessity in the competitive market. The Industrial Advisory Group of the Factories of the Future highlighted the key technologies and enablers for this required transition [2]. These comprise manufacturing technologies (e.g. micro injection molding, additive manufacturing etc.), manufacturing with new and advanced materials (e.g. composite materials), and micro-manufacturing including high-precision assemblies. However, the availability of adequate quality control technologies is indispensable for a further breakthrough of these key enabling technologies. Various industries such as medical, aerospace, and automotive require certified reliability and guaranteed technical

performance levels. This implies both accurate dimensional quality control as well as the timely identification of material defects to ensure compliance to customer specifications, to allow manufacturing process parameter adjustments whenever necessary, and to avoid premature catastrophic component failure.

The integrated quality control is a major challenge as the performance of the workpieces depends on internal structures and properties which are difficult to be measured by conventional means. For micro applications, the major challenge concerns the geometric quality control of complex parts, often with critically small internal holes that are inaccessible with conventional means e.g. a touch trigger probe of a coordinate measuring machine. For lightweight composite parts, the performance is dependent on the critical fiber characteristics inside the workpiece e.g. the orientation, length, and distribution of the fibers as well as the quality of the fibre-matrix interface.

For the last few years industrial X-ray Computed Tomography (CT) has been regarded as a promising technology, which can evolve towards integrated quality control of complex workpieces combining dimensional metrology and material defect analysis [3]. However, major challenges remain in order to exploit its full potential for fast and reliable high-end quality control. For micro-parts, challenges evidently relate to the size of the objects: at these sizes, CT equipment limitations including source drift and spot size become important uncertainty contributors. In addition, standard reference objects cannot be used at these sizes, hence conceiving, manufacturing and calibration of micro-reference objects is required. Similarly, fibre-reinforced composite parts are important materials for many industrial branches like the aeronautics, automotive, packing, construction and leisure industries. For characterization of composites, the main limitations are the limited spatial and contrast resolution and lack of CT data evaluation methods that fulfil the need of industry concerning reproducibility and accuracy [4]. With emerging methods like high resolution CT, phase contrast CT, multi-energy CT, and quantitative CT (for evaluation of fibre length, orientation and distribution, as well as for determination of porosity), CT bears the inherent capabilities to replace commonly used non-destructive testing and quality control techniques [5].

Therefore, this PhD project aimed at developing methods for control and optimization of micro injection moulding process using X-ray CT measurements and analyses of micro parts as depicted Fig. 1.3. It further aims at going beyond the state-of-the-art of CT technology for micro measurements by using new methods and approaches. The basic approach of the current research is to identify general critical aspects of quality of micro injection molded parts where X-ray CT can be applied in place of the conventional methods of characterization. At the same time, new approaches are exploited for the enhancement of CT based characterization of micro parts.

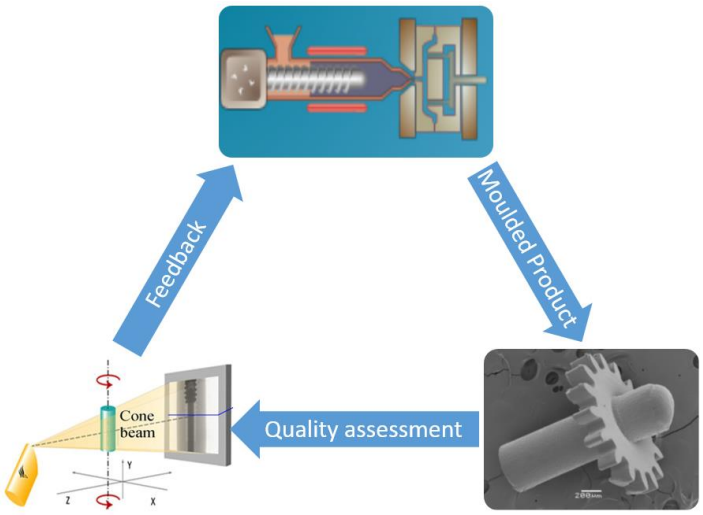

Fig. 1.3: The basic approach for the project

Three most important quality aspects were identify with respect to the micro injection molding process which are:

1. Micro measurements, Fig. 1.4 (a)
2. Fiber characteristics, Fig. 1.4 (b)
3. Defects, Fig. 1.4 (c)

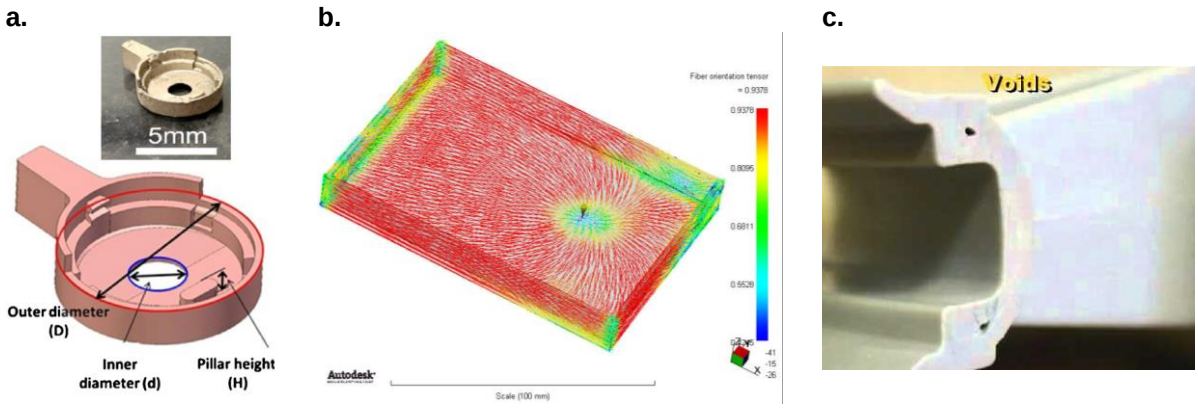

Fig. 1.4: Micro features measurement [6] (a), fiber orientation [7] (b) and void defects [8] (c) in different injection molded parts

Depending on the application, one or more of the above mentioned quality aspects can be applicable. In this project, new product development is source of motivation, thus, each of the quality aspects has been addressed with a dedicated application based product, where the optimization is the major concern.

1.2.2 Structure of thesis

The thesis is divided into seven chapters including this one as depicted in Fig. 1.5

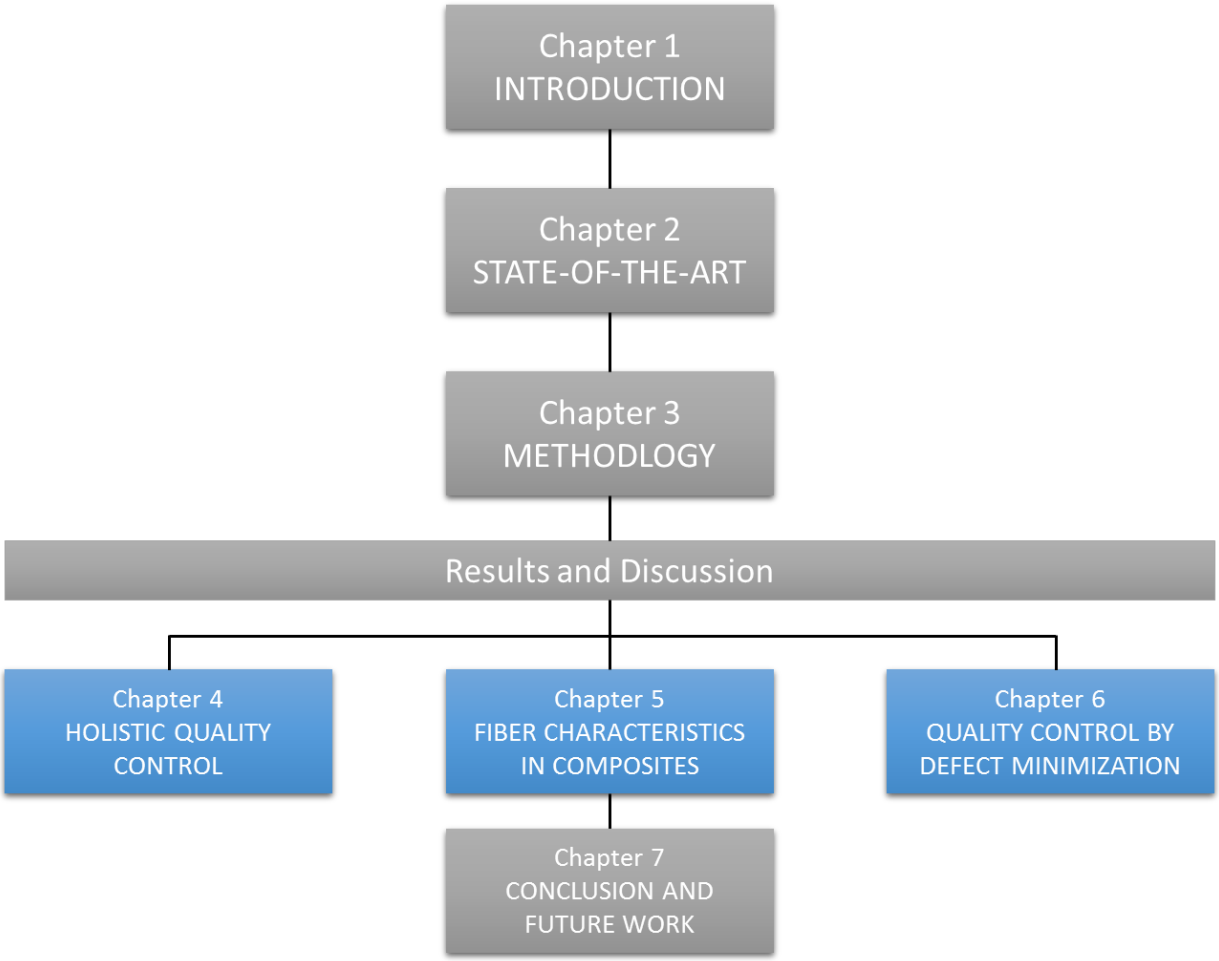

Fig. 1.5: Thesis structure

The first chapter discusses general overview of the project definition and the issues to be addressed in the proposed research work.

The second chapter includes the state-of-the-art review of technological advancements in the field of both micro injection molding and X-ray computed tomography. It also highlights the problems and challenges in the respective fields.

The different methodologies are discussed in third chapter. It includes the state-of-the-art machines used for experimentation, their technical specifications and the different materials used for experimentation. It further adds the design of experiment approach and the various software tools used in this work.

The next three chapters include the main results and discussions:

Chapter 4: This chapter is based on the holistic quality control of microfluidics. It describes the CT based measurements and their enhancement using data fusion approach. In the second part of the chapter, the effect of beam alignment on the measurements of micro molded parts is investigated. Conclusions based on this study have been made at the end of the chapter.

Chapter 5: CT base fiber characterization is the basis of this chapter. In the first part, a simulation based approach is used to investigate the influence CT scanning parameters and resolution on the fiber characterization. The next part, describes the effect of fiber orientation on the dimensional accuracy of the micro molded parts.

Chapter 6: In this chapter the internal defects of micro injection molded parts are highlighted. An application based investigation has been performed to minimize the void defects in molded parts. The various results are included and discussed in this chapter.

The last chapter (Chapter 7) includes general conclusions and the proposed future work.

References

[1] https://www.interaqct.eu/ (Retrieved on October 27, 2017)
[2] European Factories of the Future Research Association, Factories of the Future 2020 Roadmap - Consultation document, Brussels, 2012.
[3] Kruth, J. P., Bartscher, M., Carmignato, S., Schmitt, R., De Chiffre, L., & Weckenmann, A. (2011). Computed tomography for dimensional metrology. CIRP Annals-Manufacturing Technology, 60(2), 821-842.
[4] Salaberger, D., Kannappan, K. A., Kastner, J., Reussner, J., & Auinger, T. (2011). Evaluation of computed tomography data from fibre reinforced polymers to determine fibre length distribution. International Polymer Processing, 26(3), 283-291.
[5] Kastner, J., Plank, B., & Requena, G. (2012). Non-destructive characterisation of polymers and Al-alloys by polychromatic cone-beam phase contrast tomography. Materials characterization, 64, 79-87.
[6] Ontiveros, S., Yagüe-Fabra, J. A., Jiménez, R., Tosello, G., Gasparin, S., Pierobon, A., & Hansen, H. N. (2012). Dimensional measurement of micro-moulded parts by computed tomography. Measurement Science and Technology, 23(12), 125401.
[7] Autodesk® Moldflow® Structural Alliance 2012 Validation Report: Additional Data Mapping to Structural Analysis Packages.
[8] https://www.paulsontraining.com/injection-molding-training/injection-molded-part-problems-solutions/ (Retrieved on October 27, 2017)

CHAPTER 2. STATE-OF-THE-ART

Chapter 2.
State-of-the-art

The chapter includes the introduction about the micro injection molding process, the machinery and challenges. The state-of-the-art techniques for quality assessment of micro parts are also discussed. X-ray computed tomography (CT) is introduced and various aspects have been highlighted.

2.1 Micro injection moulding

Micro injection moulding (also known as Precision Injection Moulding) is a well-established manufacturing process which is used on a large scale for replication of micro-components. It provides additional advantages including design freedom, unique geometrical features and sustainable economic benefits. From the metrological point of view, it can be defined as the production of parts with micro features having dimensions, functional features and tolerance requirements usually in the range of μm (10^{-6} m) down to nm (10^{-9} m) depending on the applications [1].

Today, micro injection moulding is of the key technologies for micro manufacturing due to its mass production capabilities and relatively low production cost. Starting from the conventional injection moulding process, it has undergone major developments especially in terms of machinery over the years. The first phase of development was from mid-80s to mid-90s [2]; in that period, the production of micro features on macro parts started from conventional injection moulding machines. Hydraulically driven modified commercial units with a clamping force of usually 25 up to 50 tons, could be applied for the subtle way of replicating micro structured mould insert with high aspect ratios by injection moulding. In the late 90s, special micro injection units or even completely new machines for the manufacturing of real micro parts were developed. The aim was to reduce the minimal amount of injected resin, which is necessary to guarantee a stable process and increase the replication capabilities of very small features (down to 20 μm).

Currently, there a number of machines equipped with special features for micro injection have been produced by leading manufacturers. Minimum shot weights down to 25 mg are now obtained, micro features can be replicated in a short cycle time. Three-dimensional micro product are produced and have entered in a large number of applications and the demand of miniaturization is growing [3].

As already outlined, the current micro injection moulding machines are very different than to just scaling down the conventional Injection molding process. Giboz et al. [4]

highlighted the differences between micro and conventional injection molding processes, which have been listed in the Table 2.1.

Table 2.1: Comparison between the conventional injection moulding and microinjection moulding

Process component	Injection moulding	Micro injection moulding
Machine	- Hydraulic and electrical machines - Clamping force >15 t	- Electrical or electro-pneumatic machines - Clamping force <15 t
Flow simulation	- 2½D calculation	- 3D calculation required
Mould development	- CAD rules for the part geometry - Injection gate diameter > 1mm	- Simulation for the dimensions and the positioning of feeding channel (Gate diameter <1mm)
Realization	- CNC machining - EDM (Electrical Discharge Machining)	- CNC machining or EDM for base mould - LIGA or LIGA-like, µEDM, ultra-short pulse Electro Chemical Milling (ECM), Laser ablation, Deep Reactive Ion Etching (DRIE)
Plasticization	- Screw (Ø>20mm) + thermal heating - Shear rates < 10^4 s^{-1}	- Plasticization screw (Ø < 20mm) or plunger
Injection		- Injection screw or plunger (Ø < 20mm) - Shear rates > 10^6 s^{-1}
Temperature	- Manufacturer's recommended	- Higher than manufacturer's recommended - Variotherm process for the mould
Holding	- Switchover set as function of the pressure or the course	- Switchover based on the plunger/screw position - Rapid freezing of the injection gate
Cooling	- Generally few tenths of seconds	- Instantaneous cooling
Part control	- Parts masses and dimensions	- Dimensional tolerances, Part functioning

2.1.1 µIM machine

The injection moulding process is a sequential operation that results in the transformation of plastic pellets into a moulded part. The material melted is injected under high pressure into the mould cavity for producing moulded parts. A conventional

injection moulding process consists of three main phases namely plastification; injection, filling and packing phase; and cooling and ejection; this is termed as an injection cycle (see Fig. 2.1).

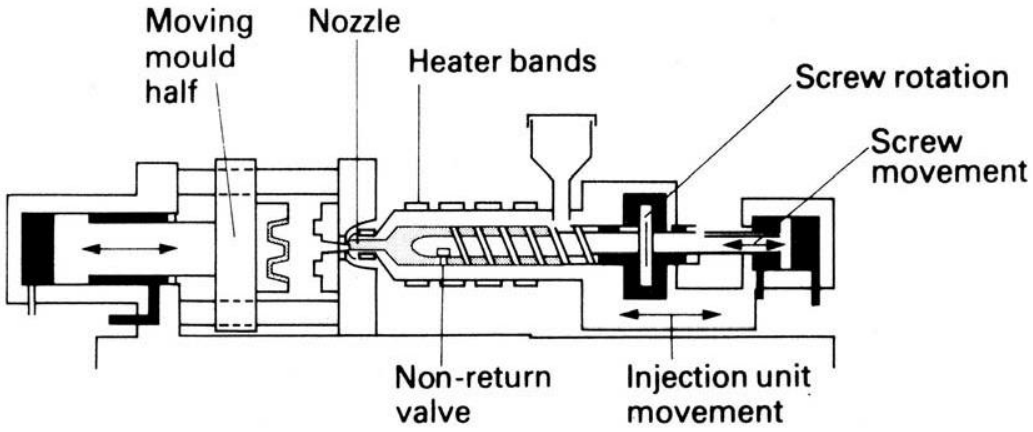

Fig. 2.1: Schematic view of a hydraulic injection moulding machine with its main components [5]

The screw performs four functions in one single unit viz. plastification and homogenization; metering; locking; and injection. When a conventional reciprocating screw is employed on moulding micro parts, it may lead to the following issues [3]:

- it becomes difficult to control the melt metering accuracy as a result of the screw structure and the limitation to reduce screw size.
- there is a melt back-flow when high injection pressure is applied to fill small and micro cavities due to the channel configuration

Fig. 2.2: Screw and injection plungers for µIM [3] (a) and a screw for conventional injection molding [3] (b)

These issues have been taken into account and a new micro molding machine has been developed. It has two different units for plasticizing and homogenizing; and for metering and injection named as screw extruder and plunger injection unit respectively.

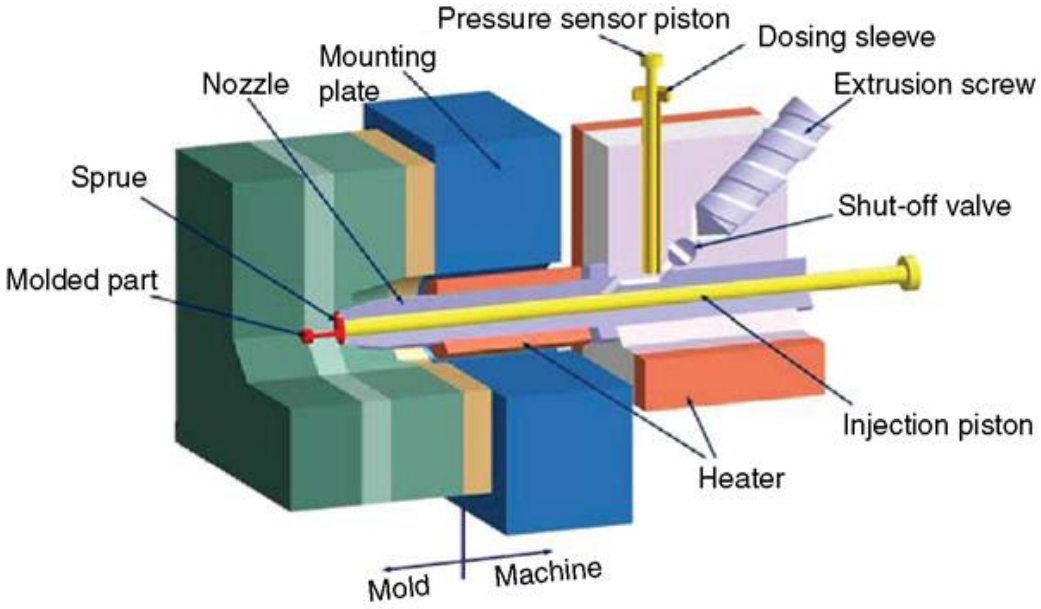

Fig. 2.3: Injection unit of a micro-injection molding machine [6]

The plastification takes place in a dedicated functional part of the machine, which is separated from the injection unit:

- The very small amount of plastics needed is plasticized either by a plasticizing small screw (diameter of 14 mm, see Fig. 2.3) or in an electrically heated cylinder, and then fed into the injection cylinder by a plunger (diameter of 5 mm).

- A second plunger with a diameter of just 5 down to 2 mm, depending on the machine configuration, injects the molten material into the cavity. It is driven by an electric motor and a precise linear drive. Typically, the shot weight can be varied between 5 and 300 mg.

The micro-injection molding process steps are the following (see Fig. 2.4):

a. Plastic pellets are plasticized by the fixed extruder screw and fed into the metering chamber.
b. The shut-off valve closes in order to avoid backflow from the metering chamber.
c. After the set volume has been achieved, the plunger in the dosage barrel delivers the shot volume to the injection barrel.
d. The injection plunger then pushes the melt into the mold.
e. Once the plunger injection movement is completed, a holding pressure may be applied to the melt. This is achieved by a slight forward movement (max. 1 mm) of the injection plunger.

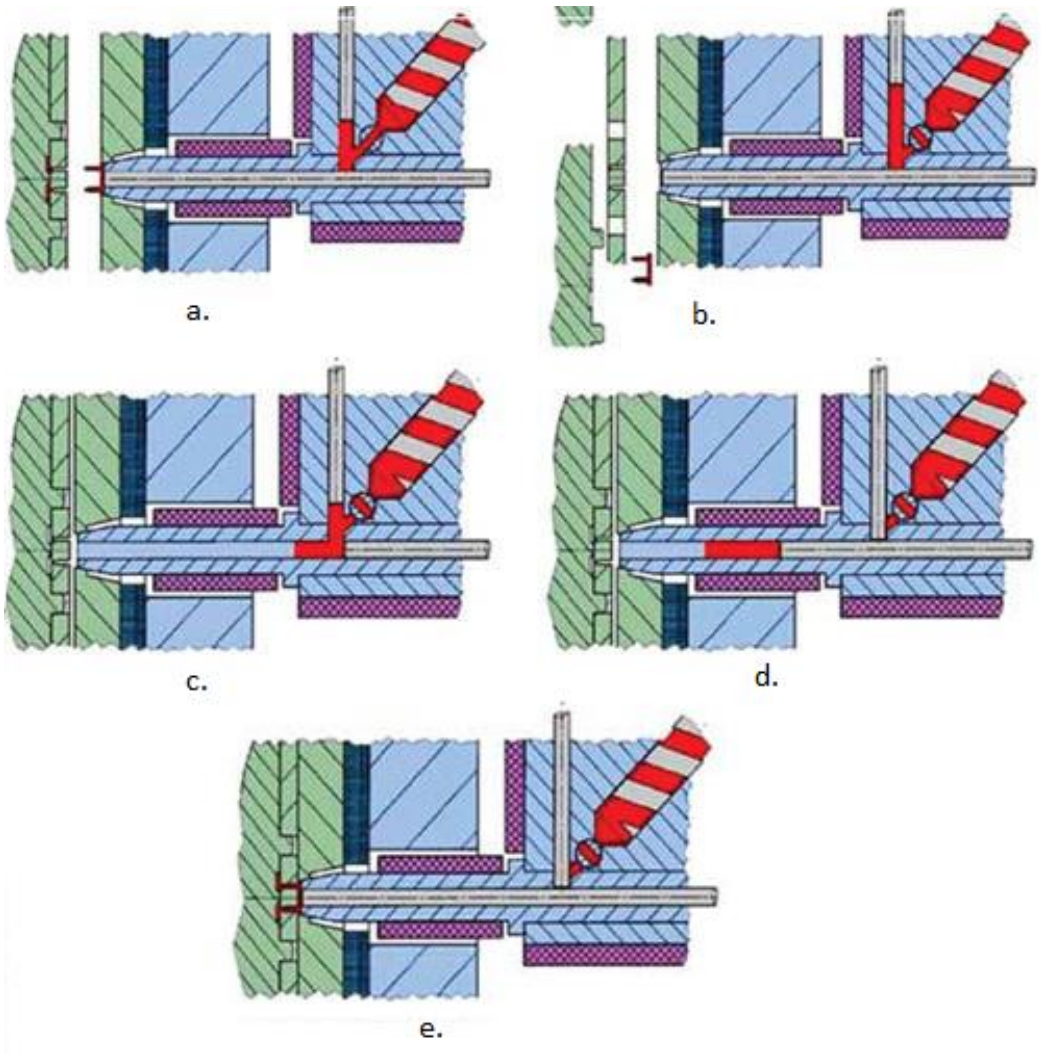

Fig. 2.4: Micro-injection molding steps [6]

2.1.2 Challenges in µIM technology

Injection molding is a complex nonlinear dynamic process during which the machine parameters, material properties, and process variables interact with each other, as depicted in Fig. 2.5. The qualities of the molded part, which can be characterized in terms of dimensions, appearance, and mechanical properties, are strong functions of the processing conditions [7]. There exist a number of challenges for micro injection moulding technology which need to be considered for the improvement of the process. The most important challenges [3] are briefly discussed here:

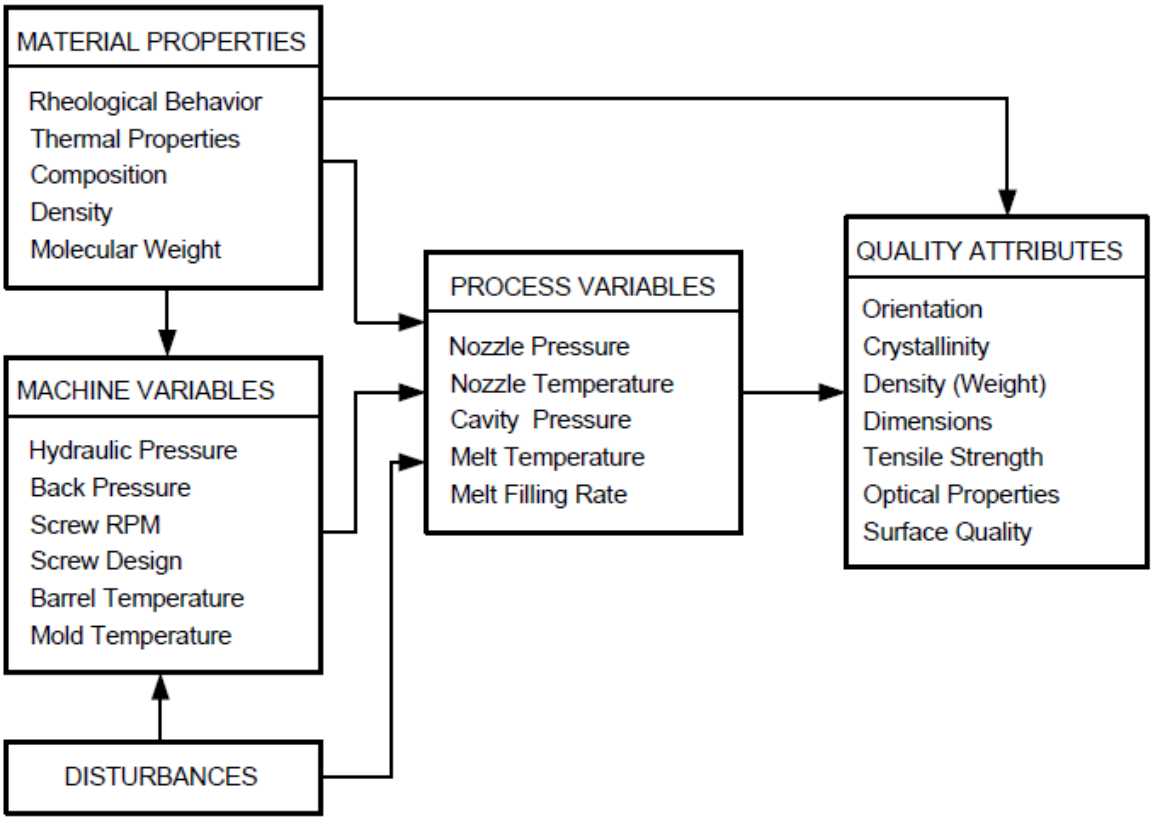

Fig. 2.5: Relationships among the machine, material, process variables and part quality [7]

- *Injection moulding machine*

As already mentioned that a conventional injection moulding machine can also be employed for micro parts but it is neither a technically nor an economically viable alternative. Dedicated machine is required, which should be equipped with special metering and injection ram (pistons, plunger) and screws designs to accurately meter the shot volume and to avoid problems associated with material degradation. Machine requirements further include shut-off nozzle to avoid drooling from the nozzle due to high melt temperature, precise alignment and gentle mould movement to avoid deformation of delicate parts, and local clean room enclosure to avoid contamination of moulded parts. The Variotherm process was introduced to control the mould-wall temperature; which employs two fluid circuits at different temperatures to heat up and cool down the mould at filling and cooling stages respectively.

- *Process*

Process optimization for reliable micro and sub-micro scale replication is still a challenge, hence of utmost importance. There are limitations regarding the achievable aspect ratio of columns, grooves, and walls which depend on the geometry, the polymer type, and the process parameters. As of now the ejection is carried out by suction pads, electrostatic charging, blowing out, or direct handling of the sprue still connected to the actual moulded part. Given the size and the weight of the micro injection moulded parts,

damages are witnessed quite often. To avoid such damages, new ejection techniques are needed.

- *Material characterization*

Several limitations are associated with the determination of rheological properties of polymers using conventional capillary rheometers, as sometimes it is difficult to replicate the exact process (µIM) condition during the test. Also, AFM (atomic force microscopy) and nano-indentation provide limited information about the mechanical properties.

- *Tooling*

Traditional methods of tooling, such as various machining processes (e.g. milling) and electrical discharge machining (EDM) have already reached to saturation with decreasing dimensions of mould inserts and cavities. Mould air evacuation is needed if micro features' thickness is down to 5 µm, the same order as the dimension of vent for air escape. Overall size of sample or batch of micro structures that can be moulded in one step is limited by the shrinkage of the polymer which is a function of the overall size of the parts. The farther a delicate micro structure with high aspect ratio is placed from the centre of shrinkage, the more difficult the demoulding is. Appropriate tooling and part designs are required to overcome and/or compensate shrinkage issues.

- *Simulation*

In order to achieve industrial applications within short development times, simulation of the micro injection moulding process is a valuable tool to be employed. Especially dedicated software for polymer micro replication is not available yet and available packages show limitations in terms of prediction accuracy.

- *Quality control*

Part quality is one of the most challenging aspects of process control. Part quality is assessed mainly by the external quality and internal quality. External quality mainly consists of dimensional accuracy and shrinkage/warpage. Whereas internal quality is assessed by various internal aspects e.g. voids/sink marks and fiber characterization if the composite material is used. The metrological aspect of the quality control is quite a challenging task due to micro and nano range measurements. Furthermore, three dimensional measuring capabilities are required, along with sub-µm or even nanometer accuracy. On the other hand, for internal quality assessment a fully non-destructive technology is needed. The mass production capability of µIM also demands for in-line process control instrumentation.

2.2 Metrology in manufacturing

As defined in [8] Metrology is science of measurement and its application which includes all theoretical and practical aspects of measurement, whatever the measurement uncertainty and field of application.

In the field of industrial manufacturing, metrology plays a significant role especially in the product development and quality control since measurement is the basis for quality control. The process control is achieved based on the measurands either defined on the components or on some specific process characteristic; subsequently the parts are described using absolute values combined with tolerances.

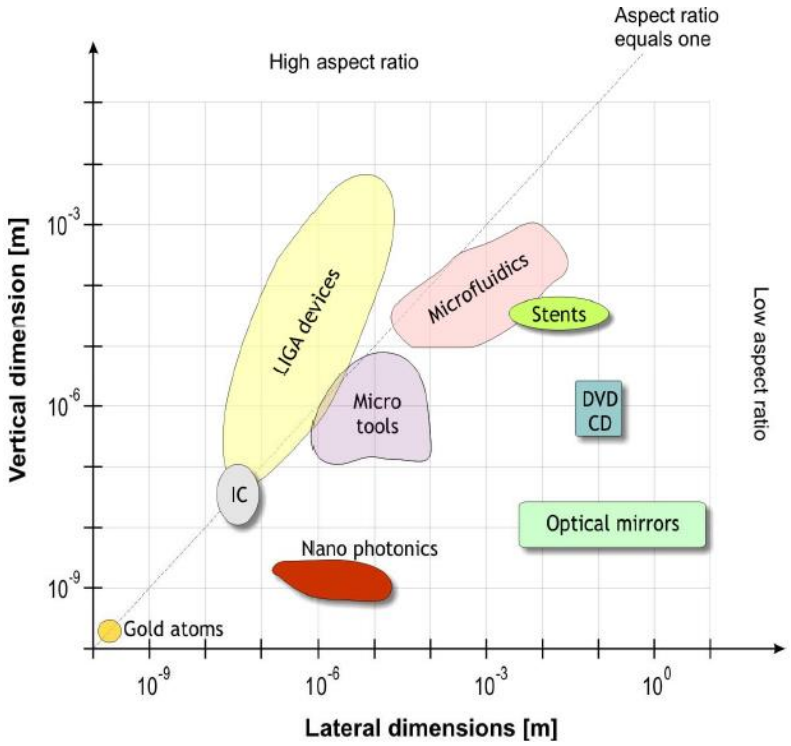

Fig. 2.6: Dimensional variability of different micro and/or nano products [9]

The role of metrology gets bigger when the targeted measurements are in micro or nano range. At the same time, the metrological tasks become quite challenging due to the smaller absolute dimensions and increased complexities. However, nano-sensitive techniques for thickness and surface roughness measurements of components with micro features are available. The real metrological challenges arise for components with high aspect ratios. In other words, when the lateral (x, y) dimensions of components shrinks to micrometers (µm) and the thickness dimension (z) increases and even surpasses the lateral dimensions by large factors [10]. Fig. 2.6 provides basic information of aspect ratios of application based micro/nano products.

2.2.1 Metrological tasks for µ-components

Micro metrology includes measurement and calibration of dimensional features on components with minimum one critical dimension and/or functional feature in µm range. Wilkening et al [11] provided a summarized overview of the typical measurements tasks in concern to micro components. The complete list is provided below:

- Distance is defined as the distance between two surfaces oriented in the same direction, e.g. distance between two lines of a line grating or two planes in a microstructure.
- Width is defined as the distance between two opposing surfaces, e.g. width of a channel.
- Height is defined as distance between two surfaces of same orientation but placed in a vertical direction, e.g. depth of microfluidic channel.
- Geometry/form is defined as the distance between the surface of the object and a predefined reference, e.g. flatness of wafer.
- Texture and roughness is defined as geometries of surface structures whose dimensions are smaller than that of the object under investigation. This poses a particular challenge for micro sized objects because the surface becomes dominant with respect to object volume.
- Thickness of layers
- Aspect ratio as defined by the depth of a structure divided by its width, also mentioned in previous section.

There can be single or a combination of any of the above mentioned tasks in real applications according to the requirements. Some common applications and their metrological tasks are given in Table 2.2.

Table 2.2: Typical micro injection molding applications and corresponding characterization tasks

Application	Basic measurement tasks	Source
Semiconductors	- Critical Dimensions (CD) referring to the width of the smallest structures in an integrated circuit - Overlay referring to precision of mask repositioning - Film thickness and profile - Line width roughness	[12]
Microfluidics	- Width and height of channels - Surface roughness - Alignment accuracy - 2D → 2½D → 3D	
Fiber composite parts e.g. Micro connectors	- Part quality (shrinkage, warpage) - Fiber orientation - Fiber content estimation	
Internal defects	- Vacuum voids - Wall thickness analysis - Part shrinkage	[13]

2.2.2 State-of-the-art techniques

Earlier, there were optical microscope and profile projector for micro-measurements. Then, the emergence of semiconductor technology put high demands on film thickness measurement and lateral resolution in mask fabrication. In 1980, the so-called first nanometer metrology tool (Talystep stylus profilometer equipped with an inductive probe) was developed. It was mainly used for measurement of step heights of thin films using a maximum trace length of 2 mm and maximum height range of 12 µm [14]. Since then, numerous metrological tools and technologies have been developed employing different physical principles. The available tools for micro metrology are roughly divided into the following categories [9]:

- Interferometers
- Surface profilers or topographic instruments
- Microscopy
- Micro and nano coordinate metrology
- Emerging techniques

2.2.2.1 Interferometers

Interferometry has now become a very important metrology tool due to the introduction of modern electronics, computers and software to the basic technique. Scanning interferometry is a very powerful tool for micro and nano surface metrology. It has the ability to obtain step height, roughness and lateral dimension information from a single non-contact measurement.

A schematic of a scanning interferometer system is shown in Fig. 2.7 (a). The upper beam splitter directs light from the light source towards the objective lens. The lower beam splitter in the objective lens splits the light into two separate beams. One beam is directed towards the sample and one beam is directed towards an internal reference mirror. The two beams recombine and the recombined light is sent to the detector. When the path length to the sample and the reference are the same interference is observed. The detector measures the intensity as the interferometric objective is scanned in Z. The detector takes a series of snapshots as the sample is measured. This gives as series of images of the intensity map of the light being reflected from the surface. The area of interest for the measurement is the interference area. These intensity images are used to create a 3D image of the surface being measured. Different techniques are used to control the movement of the interferometer and also to calculate the surface parameters. The accuracy and repeatability of the scanning white light measurement are dependent on the control of the scanning mechanism and the calculation of the surface properties from the interference data.

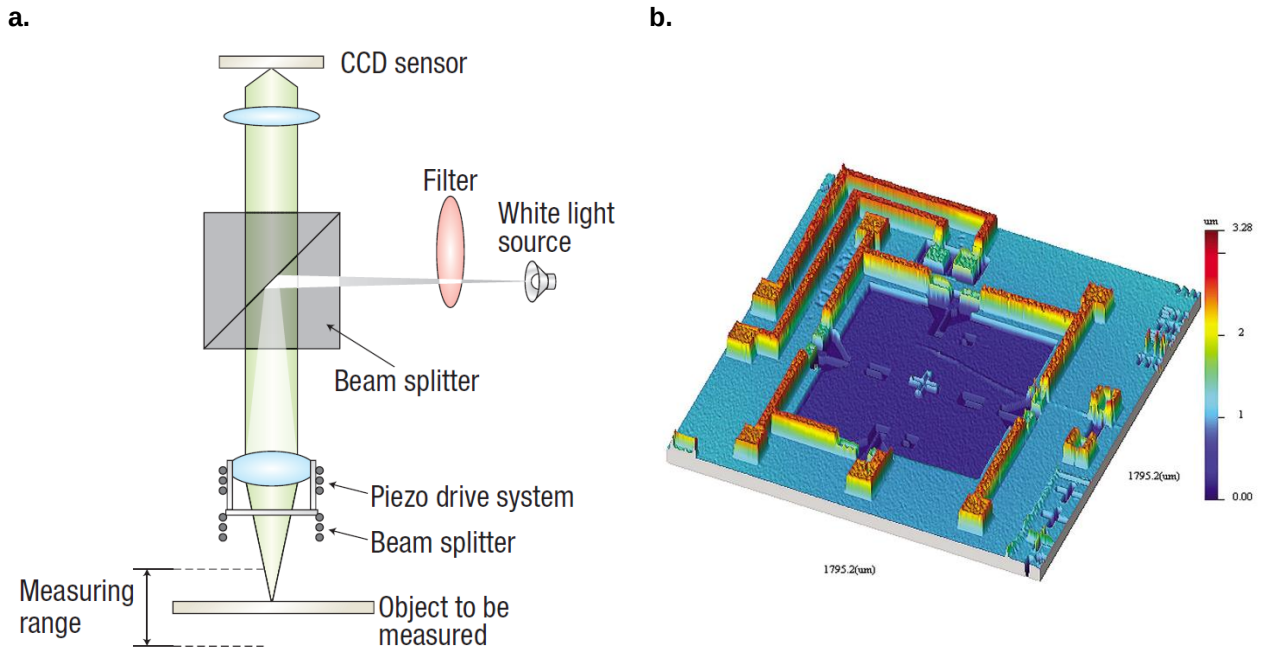

Fig. 2.7: A typical interferometer setup [15] (a) and measurement of a MEMS device [15] (b)

2.2.2.2 Surface profilers

Other than interferometer, the principal methods of surface topography measurement are stylus profilometry, optical scanning techniques, and scanning probe microscopy (SPM). These methods, based on acquisition of topography data from point by point scans, give quantitative information of heights with respect to position [16]; see Fig. 2.8.

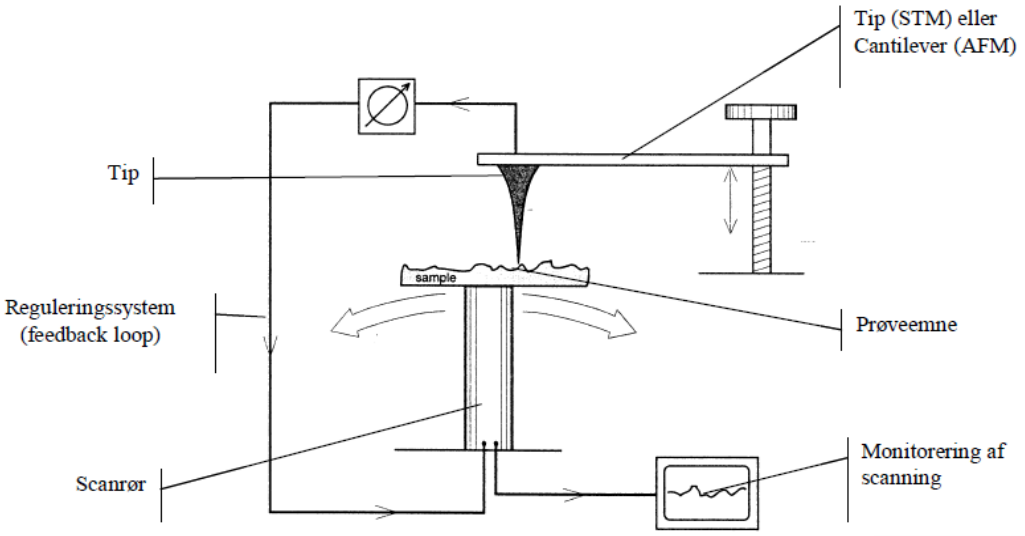

Fig. 2.8: Principle of stylus profilometry [17]

Table 2.3 shows a comparison of various surface measuring instruments.

Table 2.3: Comparison of various surface measurement methods [9]

Principle	Advantages	Drawbacks
Stylus	- Traceability - Large range	- Mechanical contact - Tip geometry
Autofocus	- Point by point probing	- Limited lateral resolution - Max. detectable slope approximately 15º
White light interferometry	- Fast - High vertical resolution	- Limited lateral resolution - Max. detectable slope approximately 30º
Confocal	- High aspect ratio structures - Max. detectable slope approximately 75º	- Limited lateral resolution - Limited vertical resolution
SPM	- nm resolution	- Slow limited range

2.2.2.3 Scanning electron microscopy

Scanning electron microscopy (SEM) provides high-resolution, large depth-of-field imaging of solid materials, allowing visualization and metrology of 3-D features, surfaces and cross-sections. Secondary- and backscattered- electrons are collected to build up images dominated by surface topography- and composition- related contrast respectively. The incident electrons also interact to produce fluorescent X-rays with element specific energies, see Fig. 2.9.

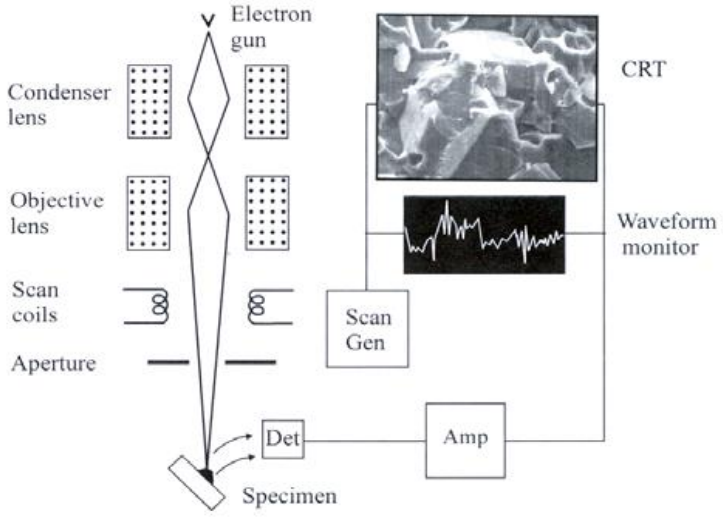

Fig. 2.9: Principle of SEM technique [18]

Table 2.4 contains some advantages offered by SEM over other optical microscope techniques and limitations. The use of SEM for accurate dimensional measurements is

dependent upon the interpretation of the electronic representation of the SEM image (micrograph). Any distortion of the image has a direct influence on the measurement accuracy. For optimization of the measurement accuracy modelling of the electron gun performance as well as the electron beam/sample interaction is required. SEM micrographs are 2D images, therefore, contains no information regarding the 3rd dimension (height). However, SEM in combination of photogrammetry (3D SEM) can be used for the reconstruction of the 3rd dimension [19]. 3D information can be achieved by reconstruction from stereo pairs or triplets of SEM image scan be used for the evaluation of surface topography but is limited by a number of factors [9].

Table 2.4: Advantages and disadvantage of SEM [20]

Advantages	Disadvantages
- magnification levels (100x to 100.000x) - resolution down to 2 nm (for highest magnification) - large depth of field - long working distance (allowing multiple positioning measurement strategies) - Energy Dispersive X-ray Analysis (EDX) for local elemental analysis - minimum diffraction effects	- high vacuum requirement - relatively low throughput - potential for sample charging - electron beam/sample interaction

2.2.2.4 Coordinate measuring machine

Coordinate measuring machine (CMM) is the most versatile and reliable metrological tool. A CMM can efficiently perform very complex measurement tasks. A typical CMM system consists of four main elements:

- *Support system (3D movement)*

The machine incorporates the basic concept of three coordinate axes so that precise movement in x, y, and z directions is possible. Each axis is fitted with a linear measurement transducer. The transducers sense the direction of movement and gives digital display. Accordingly, there may be four types of arrangement namely cantilever, bridge type, column type and gantry.

- *Probing System*

It is the part of a CMM that sense the different parameters required for the calculation. Appropriate probes have to be selected and placed in the spindle of the CMM. Originally, the probes were solid or hard, such as tapered plugs for locating holes. These probes required manual manipulation to establish contact with the work piece, at which time the digital display was read. Nowadays, transmission trigger-probes, optical transmission probes, multiple or cluster probes, and motorized probes are available.

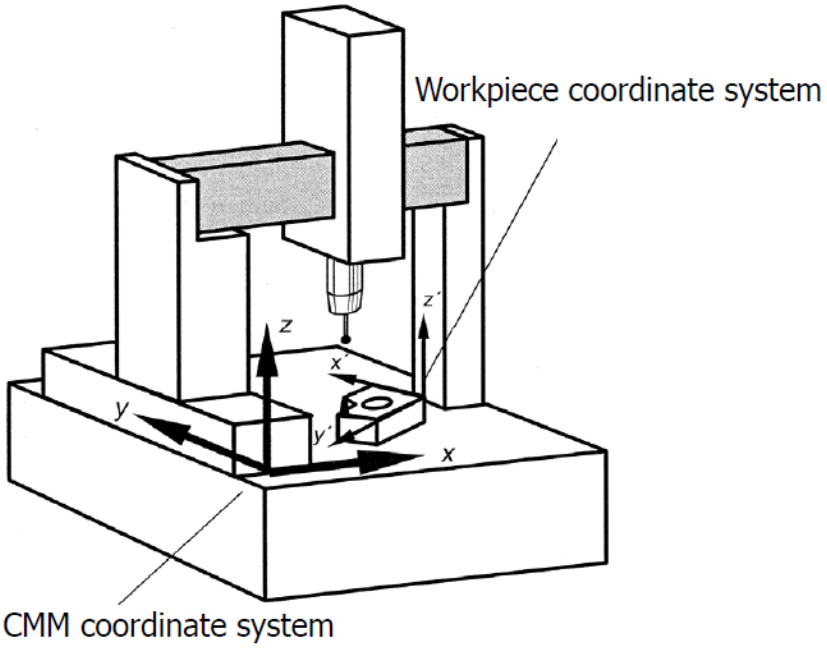

Fig. 2.10: A schematic diagram of a CMM [17]

- *Machine Control and Computer Hardware*

The control unit allows manual measurement and self-teach programming in addition to CNC operation. The control unit is microprocessor controlled. Usually a joystick is provided to activate the drive for manual measurement.

- *Software for 3D geometry analysis*

In a CMM, the computer and the software are an inseparable part. They together represent one system. The efficiency and cost effectiveness of a CMM depend to a large extent on the software.

However, with the continuous miniaturization in mechanical and optical production there is a new demand for highly accurate dimensional measurements on micro parts. The configurational system requirements of a CMM for precise micro measurements are considerably different from a Macro-CMM, see Table 2.5.

Table 2.5: Comparison of Macro and Micro-CMM [21]

Specifications	**Macro-CMM**	**Micro-CMM**
Size of machine, mm^3	1000 × 900 × 1200	300 × 300 × 400
Weight of machine, Kg	1000	40
Measuring range, mm^3	600 × 500 × 400	20 × 20 × 10
Resolution, nm	1000	1
Accuracy, Nm	3000	30
Min. probe diameter, µm	500	50
Min. contact force, mN	100	0.05

2.2.3 Emerging techniques

- *Computed tomography*

Computed tomography is an X-ray 3D imaging technology which is based on the same principle used in medical CT systems (which have resolutions of 1 to 2 mm); rather on a small scale with much increased resolution. The state-of-the-art systems have resolution down to 0.15 µm. It represents true 3D microscopy, where very fine scale internal structure of objects is imaged non-destructively. This NDT technique offers great advantages such as in particular no sampling preparation, fully 3D information, no sectioning etc. In contrast to tactile CMM, a CT scan of an object acquires all surface points simultaneously – including all hidden features like undercuts which are not accessible non-destructively using other methods of measurement; more information can be found in [22, 23]. Within the framework of this project, the main focus is on this technique, therefore, a detailed section is provided in this report.

- *HR 3D X-ray Microscopes*

ZEISS offers 3D X-ray microscopes (XRM) with advanced imaging solutions that have removed major hurdles for 3D imaging by achieving high contrast and submicron resolution imaging even for relatively large samples. These groundbreaking advances in non-destructive, three-dimensional (3D) imaging empower a broad range of technical disciplines. There are two variants: Versa and Ultra which provide true spatial resolution of <700 nm and <50 nm respectively. The minimum voxel sizes are 70 nm and 16 nm for Versa and Ultra respectively [24].

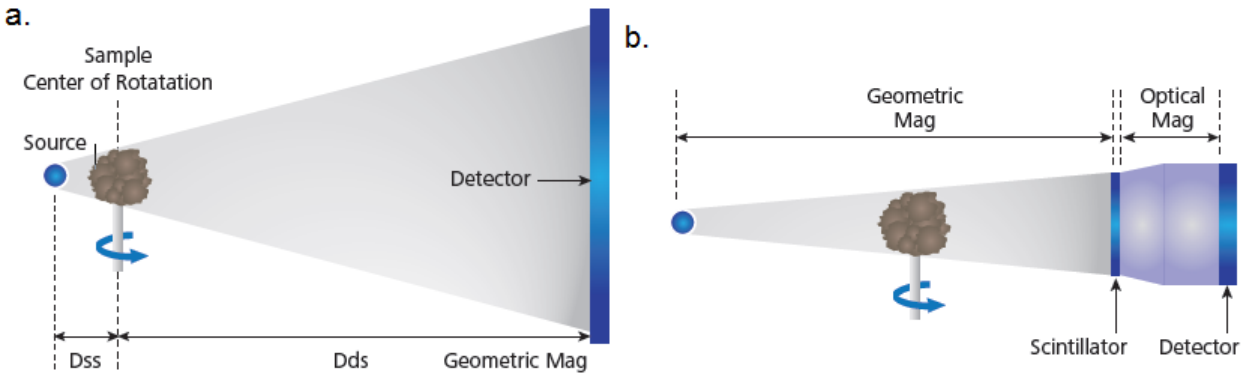

Fig. 2.11: Conventional micro-CT architecture [24] (a) and ZEISS XRM 2 stage magnification architecture [24] (b)

Xradia Versa solutions extend scientific research beyond the limits of projection-based micro- and nano-CT systems. As shown in Fig. 2.11, it uses of a two-stage magnification technique to uniquely achieve resolution at a distance (RaaD); sample images are initially enlarged through geometric magnification similar to conventional micro-CTs. In

the second stage, a scintillator converts X-rays to visible light, which is then optically magnified. Reducing dependence upon geometric magnification enables Xradia Versa solutions to maintain submicron resolution at large working distances. This enables the widest range of sample sizes to be studied effectively, including within in-situ chambers.

2.2.4 Challenges in µ-metrology

In the previous section, an overview of the available instruments for micro and/or nano measurements has been provided. In addition, several emerging technologies have also been discussed in brief. A classification with respect to structural dimensions and complexity can been seen in Fig. 2.12 [25]. However, it is difficult to make a clear contrast among them. The structural complexity termed as 2D, 2½D and 3D are defined as features with aspect ratios <1, aspect ratios ≥1 and with undercuts/ cavities/freeforms respectively. As can be seen from the Fig. 2.12, there is an evident need of instruments and/or technologies for measuring dimensionally small and complex objects. There are several challenges and/or limitations associated with most of the measuring instruments, which further justifies the need of new technologies. Few major challenging issues are discussed here briefly.

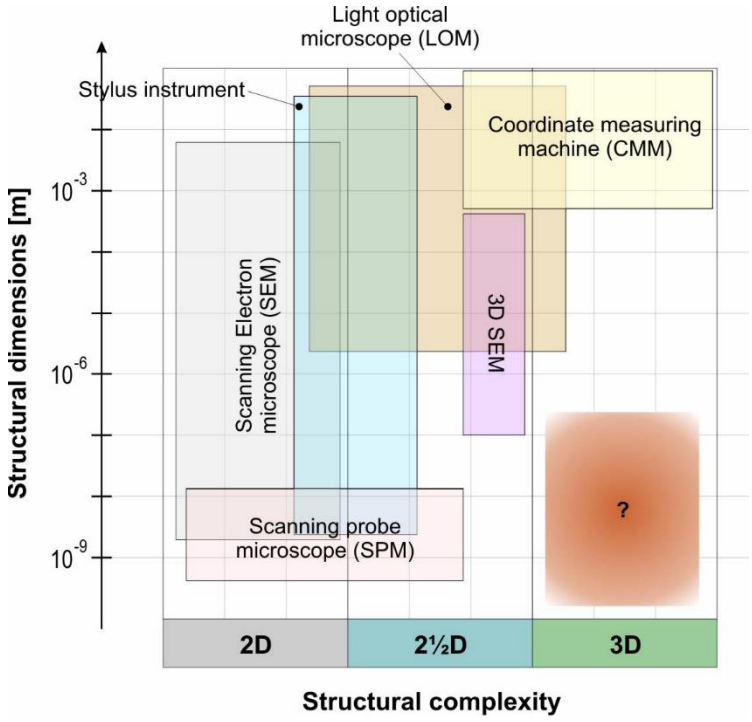

Fig. 2.12: Classification of equipment [25]

2.2.4.1 Measurement force

The force applied by the measuring probe in CMM becomes evident when a micro object is under investigation. As highlighted by Mattsson [10, 26] that there is no way a traditional CMM probing system can be used for the measurement of freestanding

micrometer sized features. His statement is further supported by some calculation; For example, a 100 µm tall pillar with a square section of 50 x 50 μm^2 made of PMMA plastic material. With a standard CMM probe force of 50 mN acting from the side at the top of the pillar, the pillar will bend by approximately 10 µm (see Fig. 2.13), causing very erroneous measurement results. If the pillar is made in silicon the displacement would be about 0.3 µm.

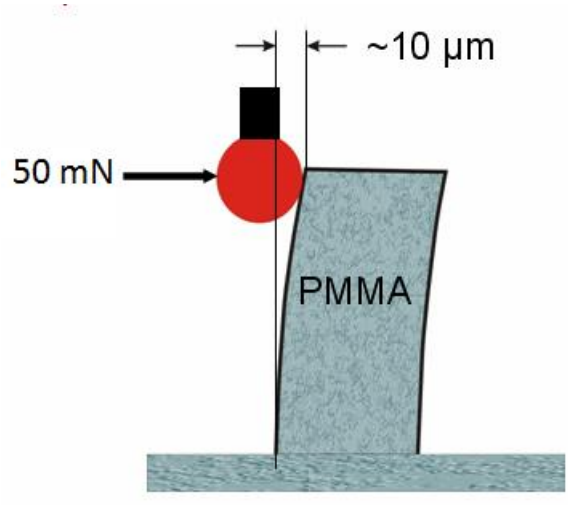

Fig. 2.13: Force applied by a CMM probe [26]

2.2.4.2 Probe access

Further limitation linked to CMM is the probe access, which is a well noticed issue regarding measurement of micro products with CMM. As seen in Fig. 2.14 (a) the top and side surface (A and B) are easily accessible by a contacting probe-tip or a non-contacting optical probe; but inner sidewalls (C) narrow trenches/holes (D) and undercuts in deep narrow trenches (E) are rather difficult or not-possible [26].

From Fig. 2.14 (b) and (c), it is clear that for both types of probing system, several features are difficult to examine. The accessibility can be figured out easily in case of tactile probe; but for optical probes, it is little difficult due to the lack of information regarding their performance when the numerical aperture is strongly reduced in one direction, as will be the case of the deep trench.

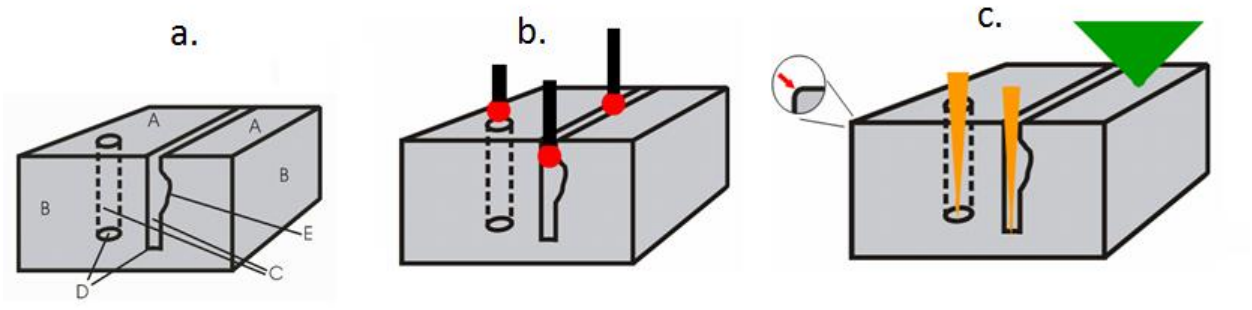

Fig. 2.14: An object with micro features (a) difficult to assess by ball probe (b) and an optical probe (c) [26]

2.2.4.3 Multi material object

It is not only CMM which has limitations, optical profilers based on interferometry also a specific problem when a multi material object has to measurement e.g. metal surfaces and dielectric surfaces. As the analysis programs of interferometers interpret phase changes as height variations; the phase change upon reflection will be different for the two types of materials resulting into an output topographic map showing height variations of up to 50 nm despite being perfectly flat [27]. Optical profilometers relying on surface scattering may have severe problems with locally tilted but smooth surfaces, as they do not back-reflect sufficient amount of light into the microscope objective.

2.2.4.4 Calibration and traceability

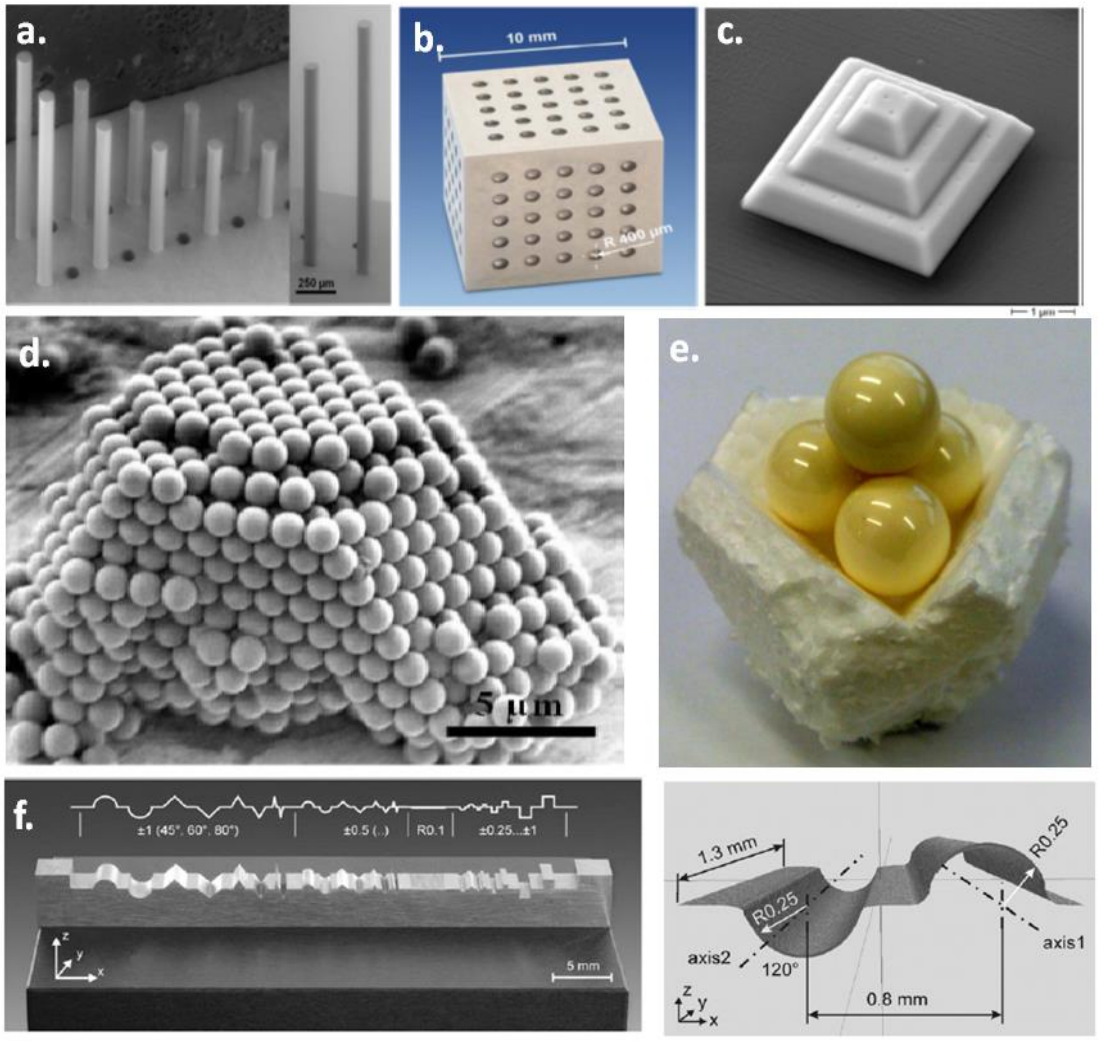

Fig. 2.15: Various reference artifacts available for micro scale measurements (see Table 2.6)

There have been numerous standards for uncertainty and tolerances, when it comes to measurements of macro products. Nevertheless it is also dependent on the measuring instrument. For calibration and traceability, a number of standard artefacts are available: scales, laser interferometers, step-gauges, ball plates, straight edges, optical flats etc.

The scarcity of standards in microscopic world makes the measurement tasks far more challenging. There are some standards available for micro scale measurements which are shown in Fig. 2.15. The first two i.e. the fiber gauge [28] and calotte cube are [29] most widely used reference artifacts for micro measurements, there is very little information available about the other objects. Table 2.6 contains the details of these artifacts. It is important to note that the available standards are applicable mostly for products with low aspect ratios; so theoretically, there is no standard for real 3D micro measurements. Therefore, there is an extreme need of physical standards with nm accuracy as well as standard procedures.

Table 2.6: Specifications of the reference artifacts shown in Fig. 2.15

Object	Specifications	Source
a. Fiber gauge	Nominal Diameter: 125 µm (Tolerance: ±0.3 µm) Non circularity: <0.3% Residual ovality: <0.07% Young modulus: ~67 GPa Non parallelism: <0.3 degs Roughness: R_q-16-142 nm (top); R_q-3.5 nm (flank); R_q-190 nm (base)	[28]
b. Calotte cube	Calottes manufacturing by eroding EDM Cube features 3 facets with 5x5 calottes Calotte: Ø 0.8mm Form deviation: nominal <2µm Used for testing of optical, tactile and µCT sensors	[29]
c. Calibration pyramid	made through gas assisted FIB features steps of ~ 6µm in width and length and 3µm in height	[30]
d. Assembled 1.5 µm silica beads	----------	[17]
e. Tetrahedral of four spheres	Ball grade: Alumina (grade G10) Variation of ball diameter: 0.25 µm Deviation from spherical form: 0.25 µm Surface roughness: 0.02 µm	[31]
f. Micro-contour reference standard	See Fig. 2.15 (d)	[32]

2.2.4.5 Tolerancing and specification

Tolerancing is linked closely together with metrology since a general rule of thumb indicates that the measurement uncertainty should be 1/10 of the specified tolerance. It is very hard to comply with this rule when the absolute dimensions are in the µm range, and therefore exact knowledge about the measurement uncertainty is crucial. As

discussed previously very few calibration artefacts and methods exist at this scale and therefore a sound evaluation of measurement uncertainty is difficult. However, a prerequisite is that it is possible to specify a tolerance, and there still is a long way to go with respect to this issue. The ISO GPS-system is set-up with the traditional workshop dimensional metrology in mind. This means that at many places measuring elements are defined as mm sized, so measuring smaller sizes is not directly possible when interpreting these standards strictly. This goes for surface roughness as well as for dimension, position and form. Some attempts to introduce a function-oriented tolerancing concept for monolithic integrated systems (e.g. MEMS) is given in [33, 34]. This concept is however based on the fact that a layer-by-layer manufacturing methodology is applied. If micro mechanical systems are considered within the usual 4M domain, then a complete lack of guidelines exists.

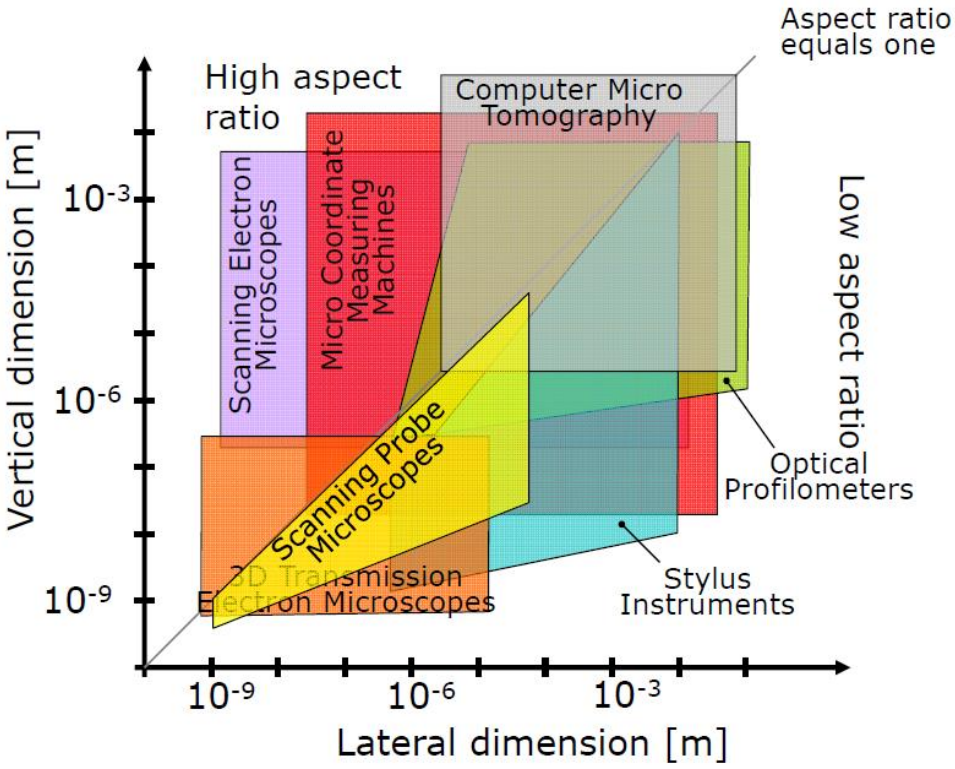

Fig. 2.16: Measurement instruments for dimensional micro and nano metrology [35]

In a summarized way the challenges discussed above can be concluded as follows:

- Probe manufacturing and probe-sample interaction need further improvement for micro parts.
- Micro scaled components constitute a very heterogenic group including a large range of different materials, different measurands and of course a large dimensional span. New measuring devices are needed that integrate different measuring principles.

- High aspect ratio applications do exist, but many applications are still with aspect ratios below 2. Nevertheless, small absolute dimensions (< 1 µm) pose difficulties for dimensional metrology also with aspect ratios around 1.
- The need for 3D analysis exists and is increasing.
- No real solutions exist for rendering 3D results in a scale below 1-10 µm.
- In-process capability of the measuring equipment will become extremely important as micro manufacturing is being industrialized.

Another simple comparison of measuring instruments with dependence on aspect ratio was made by De Chiffre et al [35] in a Stedman-like diagram, see Fig. 2.16. Industrial computed tomography is one such technique which could be foreseen as an effective solution. The next is focused on industrial CT.

2.3 Industrial Computed Tomography

The first CT scanner was invented by Hounsfield in 1969; for which he received a Nobel. The term CT remained associated only with medical field till the early 80s and then it found applications in material analysis and non-destructive testing (NDT) [36]. CT further widened its scope in 90s when it entered the field of dimensional metrology [37, 38]. Today, CT is an established technology which is widely used in manufacturing industries for non-destructive 3D analysis of defects and dimensional measuring of samples which accelerate development cycles leading to control and optimization of production processes.

2.3.1 Basic principle

Industrial CT utilizes the same principle as medical CT, with the following basic differences:

- X-ray source and detector are stationary in the industrial CT system unlike medical CT
- Object rotates whereas in medical CT patient is kept stationary during scanning
- Rotational axis is vertical in industrial CT
- 2D flat panel detector or 1D linear detector
- Industrial CT system has considerably higher power/voltage compared to the one in medical

X-rays are emitted when the electron beam hits the target material. The x-rays or emitted photons pass through the object, reach the detector and create cross sectional image through one plane from a defined angle position. Multiple images are taken at different angle positions, performing one full revolution of the object; which is achieved with the help of the rotating table. A fraction of x-rays is also scattered and absorbed while

passing through the object, which results in a reduced intensity termed as attenuation. Only the transmitted photons are collected on the detector.

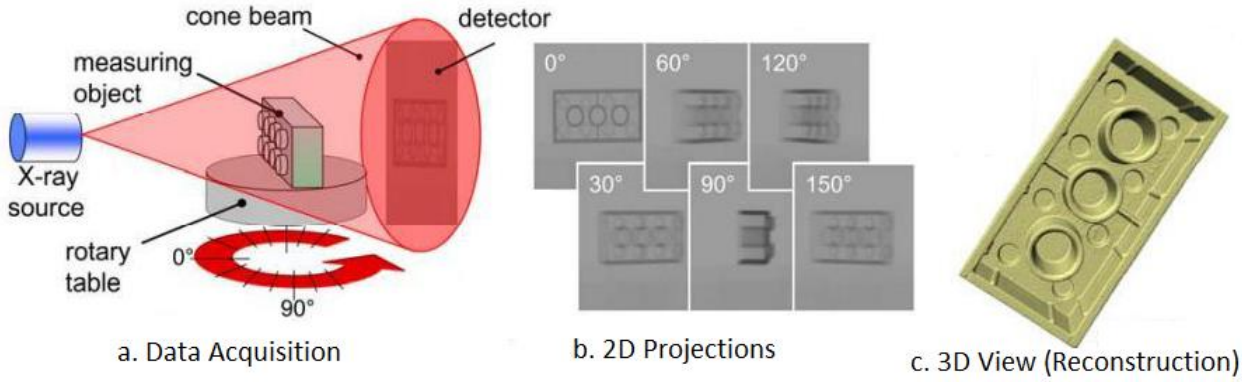

Fig. 2.17: CT reconstruction [21, 33]

The basic approach of producing a 3D image of an object with the help of an infinite number of projections, led Radon to develop the mathematical model used for reconstruction in CT in 1917; also known as 'filtered back-projection. However, the mathematical part is out of the scope of this work. The reconstruction, based on the 2D projections, is carried out using the mathematical algorithms. A schematic diagram of the work flow is shown in Fig. 2.17.

In order to perform dimensional analyses with the help of CT, some additional steps are required; Fig. 2.18 shows a flow chart of measurements via CT. The different steps are discussed in the subsequent sections.

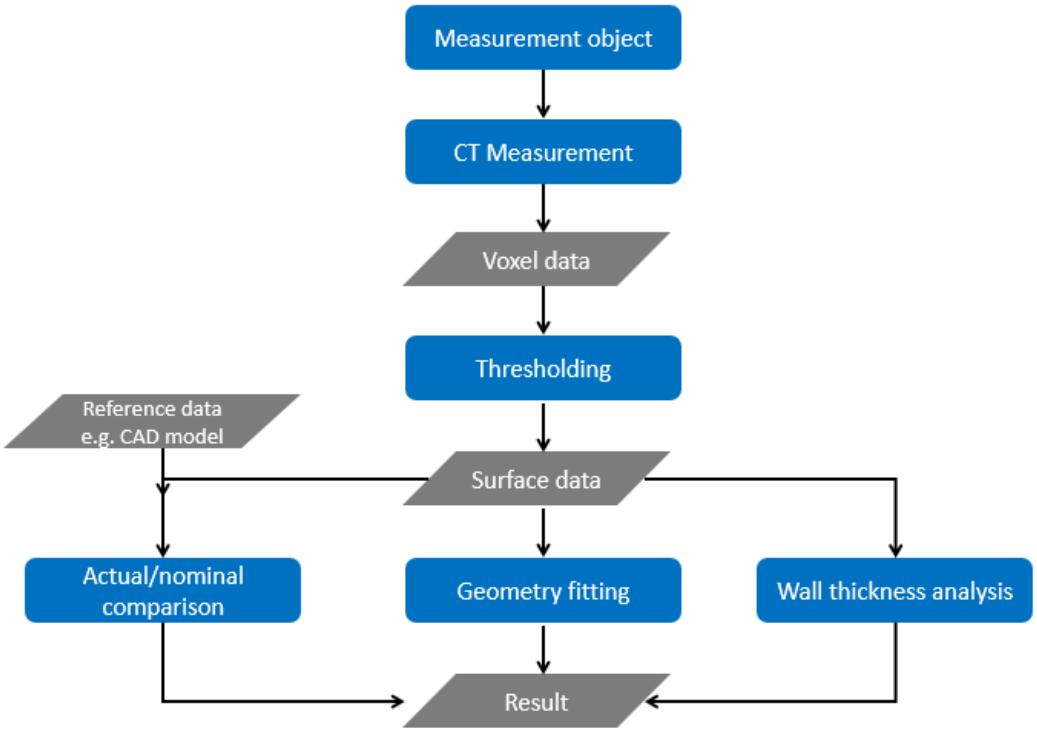

Fig. 2.18: Dimensional CT measurement process

2.3.2 Type of industrial CT systems

Based on the detector section, two types of CT systems are available:

- 2D-CT system (fan beam)
- 3D-CT system (cone beam)

As shown in the Fig. 2.19 (a) and (b), a 2D-CT system has an x-ray fan beam which is achieved with a use of line detector; whereas a cone beam is attributed with an array or a flat panel detector. Line detector is considered to be of better accuracy than that of flat panel/array detector due to the fact that it uses collimated X-rays, which yields to less scattering and pixels interaction. The better signal to noise is due the fact that line detectors make use of thicker scintillators, which allows them to detect more X-rays. Line detectors are more resistant, which enables the operator to use more power, therefore, allows to scan thicker objects. Despite the advantage of better accuracy than that of flat panel; line detectors are not commonly used in industrial CT systems which can be attributed by the higher scanning time [22, 39].

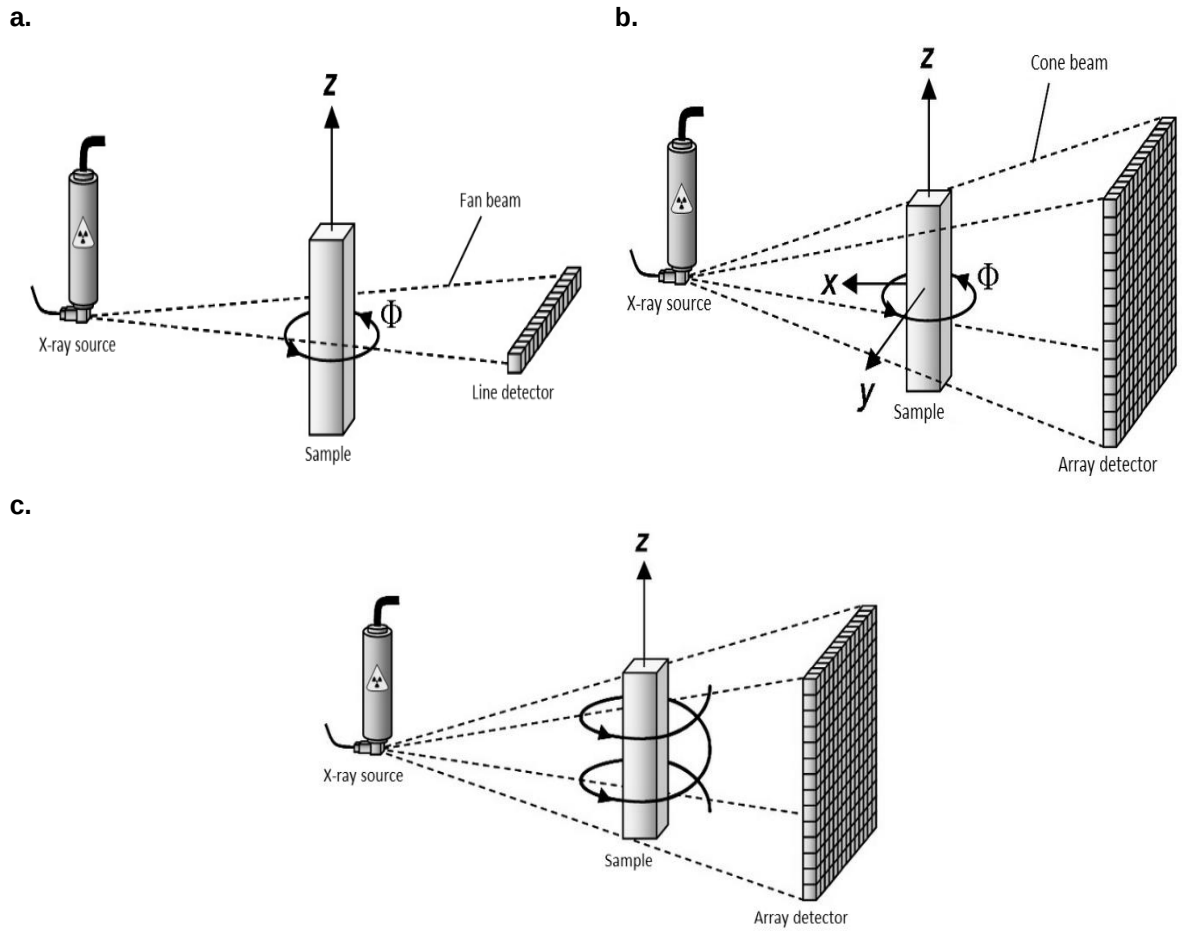

Fig. 2.19: Line detector (a), array detector (b) and helical scanning (c) [40]

The helical scanning approach is the most recent development and it offers the biggest advantage in terms of length of the objects. Theoretically, any length object can be scanned along the rotational axis, Fig. 2.19 (c).

Another way of classifying industrial CT systems is on the basis of their achievable resolution, measuring range and spot size. These are: macro, micro, nano and Synchrotron. As the name suggests, macro and micro CT systems are used for large objects and objects with micro features respectively. Macro or conventional CT system typically has a focal spot size ≥ 0.1 mm. Micro CT is attributed by a small focal spot size (down to 1 or few µm) and by positioning the object close to the focus. In this way a higher geometrical magnification is achieved. It is important to note that higher magnification is combined with an undesirable effect which causes blurring; will be discussed later in this report. Nano-CT system should have a focal spot size typically < 1µm. e.g. 0.4 µm has been achieved in [41]. Synchrotron CT (sCT) can reach 0.2 µm resolution; can go down further to 0.04 µm with the application of Kirkpatrick–Baez (KB) optics [42].The achievable resolution is plotted against measuring range in the Fig. 2.20. It is clear that scanning smaller parts enhances to achieve smaller resolution.

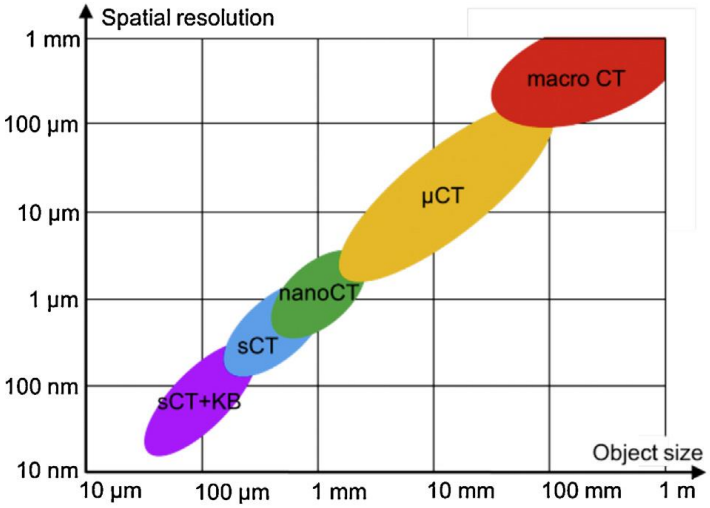

Fig. 2.20: Typical spatial resolutions and object sizes (diameter) for macro, micro, nano, synchrotron and synchrotron CT with KB mirrors (sCT + KB) [23, 41]

2.3.3 Influencing factors

It has been outlined earlier that the industrial CT has two major application: non-destructive testing and dimensional metrology. The typical tasks performed under these application areas are given in Table 2.7.

In comparison to the medical and material analysis applications, CT has additional system requirements. Depending of the size and material characteristics of the object, the penetration power (voltage) is needed e.g. metal generally need higher power due to large attenuation. In addition to 3D reconstruction software, it needs additional software

tools for various analyses. Typically, extraction of geometrical features and calculation of geometrical data (e.g. position, orientation, dimension, length, diameter, angle, form errors, measurement uncertainty, etc.) are the tasks to be performed by the software tool [22].

Table 2.7: CT capabilities

Non-destructive testing	Dimensional metrology
- Defect/failure analysis - Crack detection and measurement - Assembly inspection - Porosity and void detection and analysis - Density discrimination- material composition	- CAD comparison - Inner and outer measurements - Reverse engineering - 3D volume analysis - First-Article Inspection

Measurement uncertainty and traceability have always been a matter of concern in the field of dimensional metrology. The concern gets bigger when the system is not tactile including CT. There are set of guidelines and standards for uncertainty measurement [43, 44] and for achieving traceability; but it is sometimes difficult to identify the sources of uncertainty and subsequent quantification. In case of CT, there is still a lack of international standards and only available set of guidelines national from VDI (Verein Deutscher Ingenieure) is VDI/VDE 2630. However, a significant progress has made towards international standards (ISO) in the last few years. The part two of VDI/VDE 2630 describes the influencing factors and recommendations for dimensional measurements in CT [45]. The sources of uncertainty are broadly categorized as: the system (hardware, software), surroundings, the work piece and the operator. Table 2.8 contains information about the possible error sources during measurements through CT. The important factors have been discussed in details in the next section.

Table 2.8: Sources of uncertainty during measurements via CT [45]

System	**Hardware**	- X-ray source: spectrum, focus properties, stability - Detector: stability/thermal drift, dynamics, scattering, contrast sensitivity, pixel variance, noise, lateral resolution - Mechanical axis: geometrical errors, mechanical stability
	Software	- 3D reconstruction - Threshold determination and surface generation - Data reduction - Data corrections: scale errors
Surroundings		- Temperature - Vibrations - Humidity
Work-piece		- Surface roughness - Penetration depth (attenuation), dimension and geometry - Beam hardening - Scattered radiation - Material composition
Operator		- X-ray source current - Acceleration voltage - Magnification - Object placement and orientation - Number of views/projections - Spatial resolution: relative distance between source, object and detector - Detector exposure time

2.3.3.1 X-ray source

The most important variables which determine the quality of X-ray emission spectrum are: focal spot size; spectrum of generated x-ray energies and x-ray intensity. Among all, the focal spot size plays an important role in quality of the projections; which becomes more significant in during micro measurements. The focal spot is basically the spot where the electron beam hits the target material and generates x-ray photons (Fig. 2.21).

- *Focal spot size*

The focal spot should be as small as possible, ideally approaching zero. As the spot size increases the sharpness/blurriness of edges decreases/increases. This effect of blurring is termed as penumbra effect. This effect gets more prominent with increasing magnification; Fig. 2.22 (a) makes it clear. For micro measurements, this contributes towards considerably bigger errors. The spot size is connected with the power/voltage in an inverse proportion; which is limited due to system specification. The disadvantage associated with smaller spot (or higher voltage) is the concentrated heat produced at the spot on the target inside the X-ray tube, requiring cooled targets and limiting the maximum applicable voltage [46].

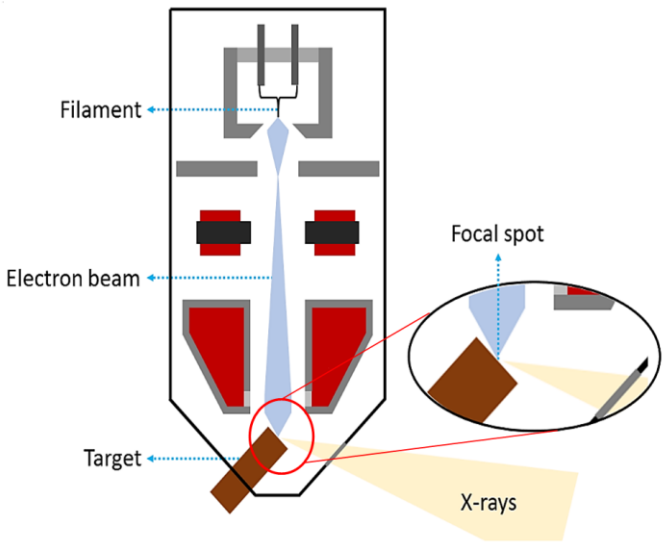

Fig. 2.21: Schematic of an x-ray tube and focal spot [22]

- *Focal drift*

The increased temperature due to high voltage in the X-ray tube further causes a drift in the electron beam; and it results into a local shifting of the focal spot. The whole phenomenon is called as focal drift. Weiss et al [47] reported that a focal drift is responsible for a scaling error or a geometrical form error depending on the drift direction. Drift perpendicular to the detector plane causes a scaling error (voxel size error) in the reconstructed volume, whereas a drift parallel to the detector plane causes geometrical form errors in the calculated CT model. Fig. 2.22 (b) depicts the drift of the electron beam due to the increase of temperature [47].

a. **b.**

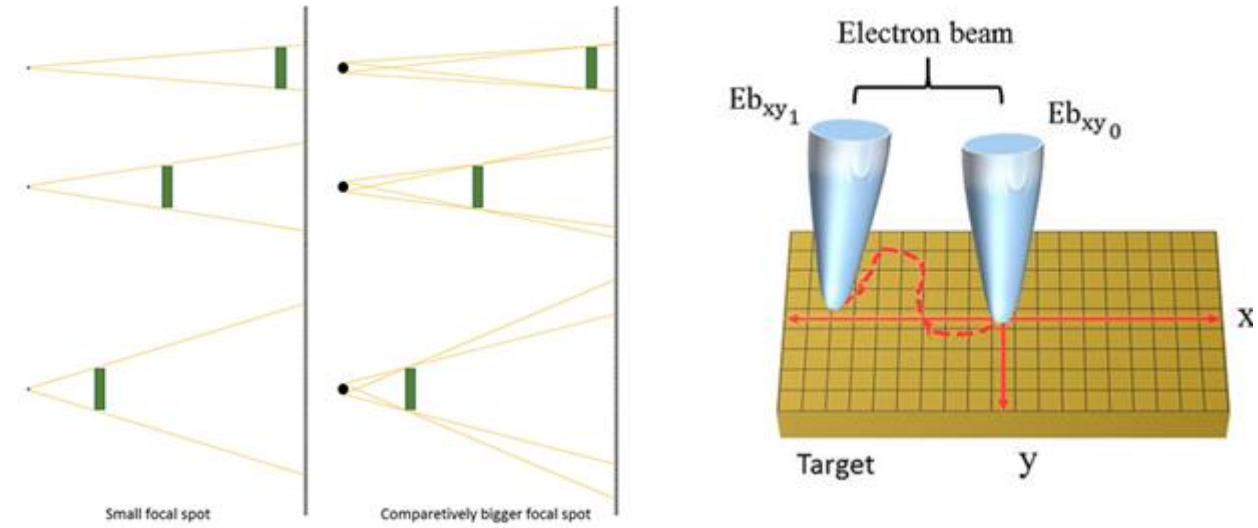

Fig. 2.22: Penumbra effect due to increase of the focal spot (a) and focal spot drift due to the increase of temperature (b) [47]

In his works, Hiller [48] stated that a focus drift can be seen as a (dynamic) misalignment problem. The drift effect can be compensated by either of the following:

- application of a mean scaling factor for the CT dataset [47] or,
- by determining the specific focus position (in x, y, z) for each single projection image

This information can be incorporated in the reconstruction algorithm for the drift compensation.

2.3.3.2 Rotary table and Detector

During the scan, the object is temporarily fixed on a table which is mounted on the rotating platform. An ideal alignment is when the central ray intersect the center of the detector (point O); the rotation axis is perpendicular to the mid-plane and the mid-plane cuts the detector in the central row (Fig. 2.23) and any deviations from the ideal (misalignment of one or more of the detector, X-ray source and rotary table) can introduce artefacts in the scanned data. The results obtained from Sun et al [49] are shown in Fig. 2.24 and 2.25.

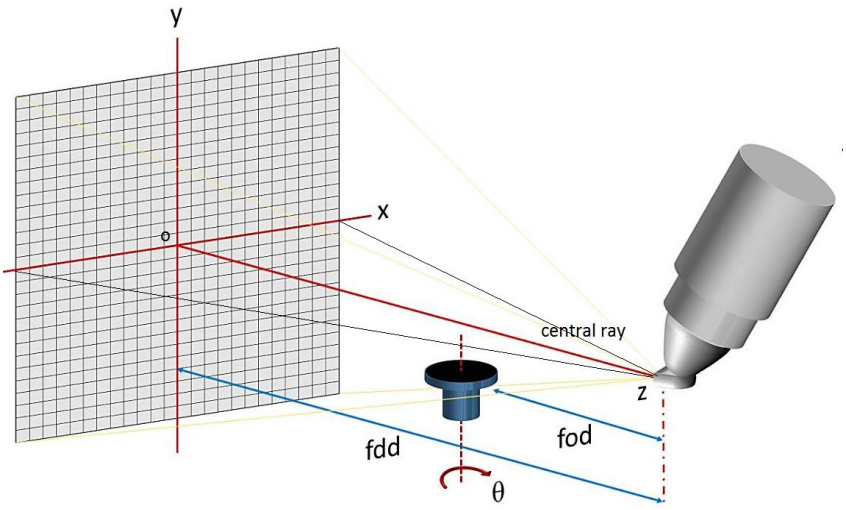

Fig. 2.23: Ideal system alignment [49]

Fig. 2.24 shows artefacts in the image arising when the detector shifts along the horizontal transverse direction (X axis); while Fig. 2.25 shows examples of artefacts caused by a tilt of the detector around its central row (X axis), a twist of the detector around its central column (Y axis) and a skew of the detector around the central ray.

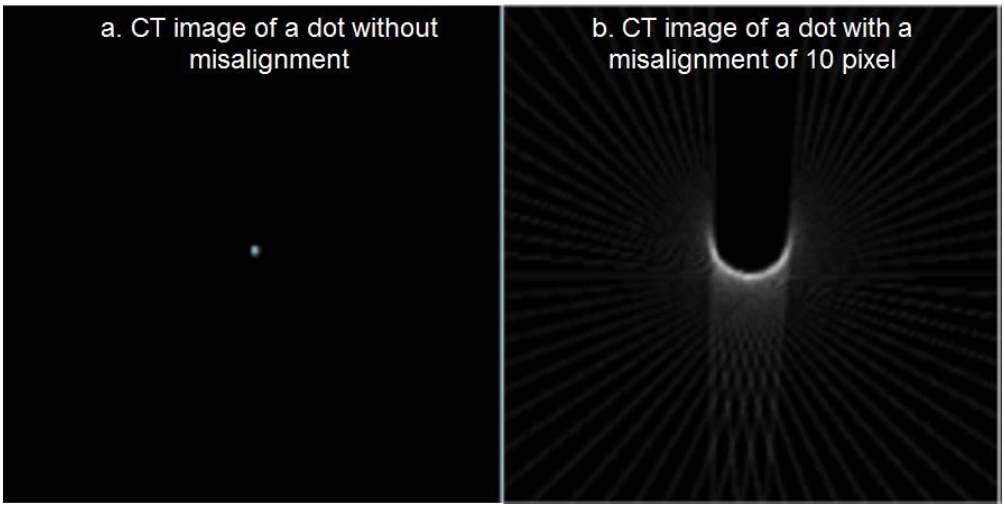

Fig. 2.24: Misalignment effect due to horizontal transversal off-center shift along the detector column direction [49]

Sun et al [49] further concluded that the worst among all is skewed alignment of detector from the central ray in Fig. 2.25 (d), as effective width and height of the detector used in the reconstruction algorithm becomes smaller, which makes the reconstructed images get flattened. It is possible to compute CT system misalignment parameters through a calibration of the system; details about the calibration method can be found in.

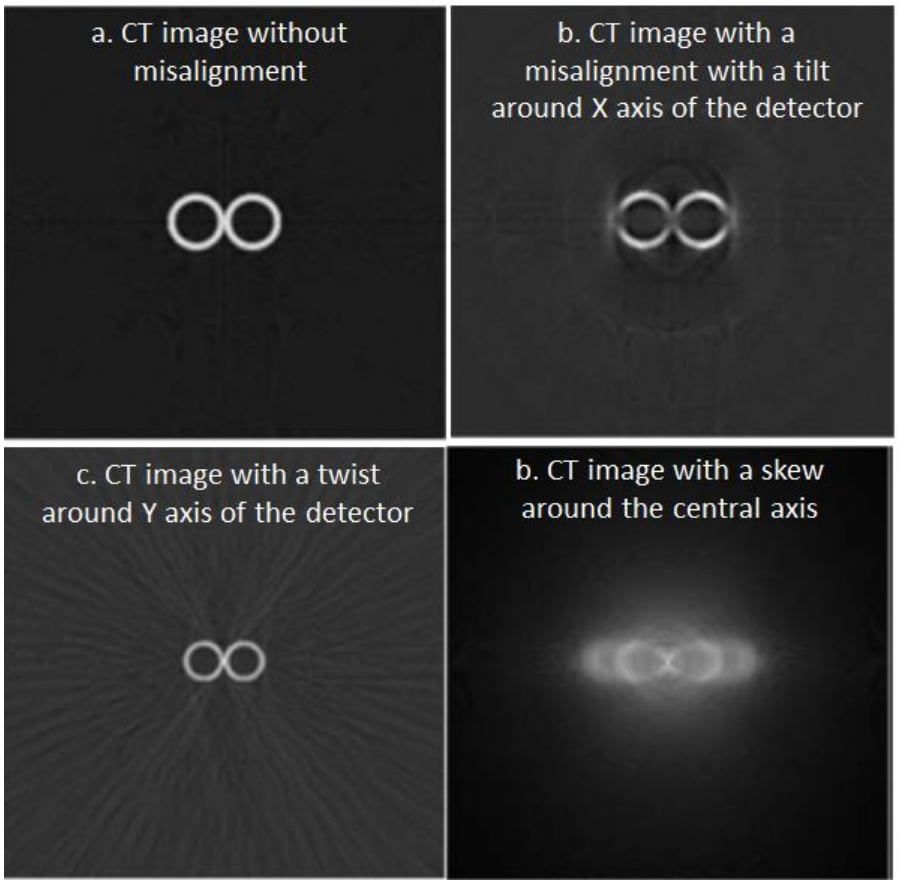

Fig. 2.25: Misalignment effect due to horizontal transversal off-center shift along the detector column direction [49]

2.3.3.3 Software related issues

The following two steps are the major contributors towards accurate measurements, therefore, care has to be taken while performing these actions.

- *3D reconstruction*

The output of the reconstruction step is a 3D volume of grey value integers that describe the material distribution of the scanned workpiece; the relative spacing of volume-elements (voxels) is termed voxel size and influences all dimensional information evaluated from a CT data-set. The size of the voxel is a function of the pixel size and the distance between the source-object and source-detector. However, the voxel size is corrected by measuring rather a simple calibrated object e.g. two sphere on a bar/plate, a gauge block or stepped pyramid etc. This procedure helps in identifying a global correction factor which links the voxel size to the unit of length [22].

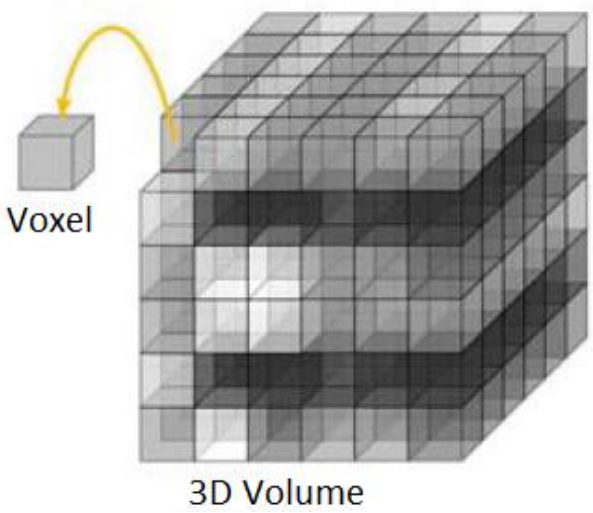

Fig. 2.26: Definition of voxel [22]

Other than voxel size, reconstruction algorithm, identification of the rotational axis, beam hardening and surface detection are the influencing factors towards an accurate reconstruction. Details can be found in the subsequent sections.

- *Thresholding and surface determination*

Surface determination is one of the most critical factor in consideration to the measurement accuracy and traceability. Thresholding is used for accurate image segmentation and surface data determination which influence the resulting reconstructed geometry of the scanned object [50]. Threshold converts a gray value image into a binary one; it determines the boundary between the object and the air and assigns a surface to the scanned object. The determination of the threshold takes place within each of the voxels the 3D model consists of, see a green line in Fig 2.27.The resulting image is a compromise between the background (e.g. black) and the object (e.g. white).

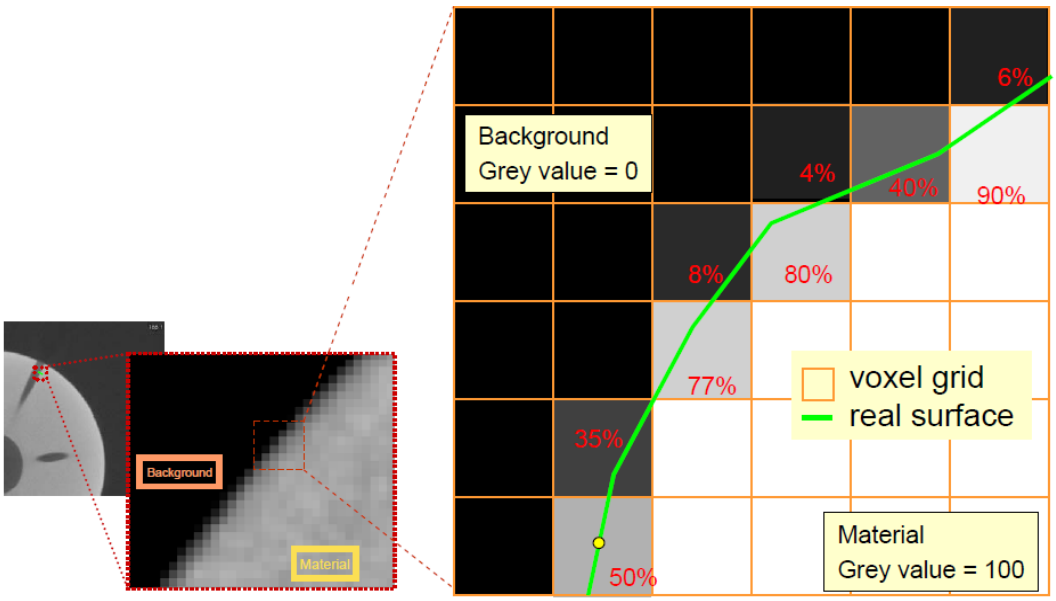

Fig. 2.27: Thresholding and edge detection [51]

It is evident from the procedure of surface detection that it may influence the measurement results drastically, if the selection of threshold is erroneous as presented in Fig. 2.28, the influence of threshold selection on measured results [52]. The diameter is calculated by Gaussian fitting of an ideal cylindrical surface to the resulting CT point cloud. He also showed in his results that with the use of a reference object (e.g. hole-bar) and calibrated values obtained from CMM, the accuracy of threshold determination can be increased.

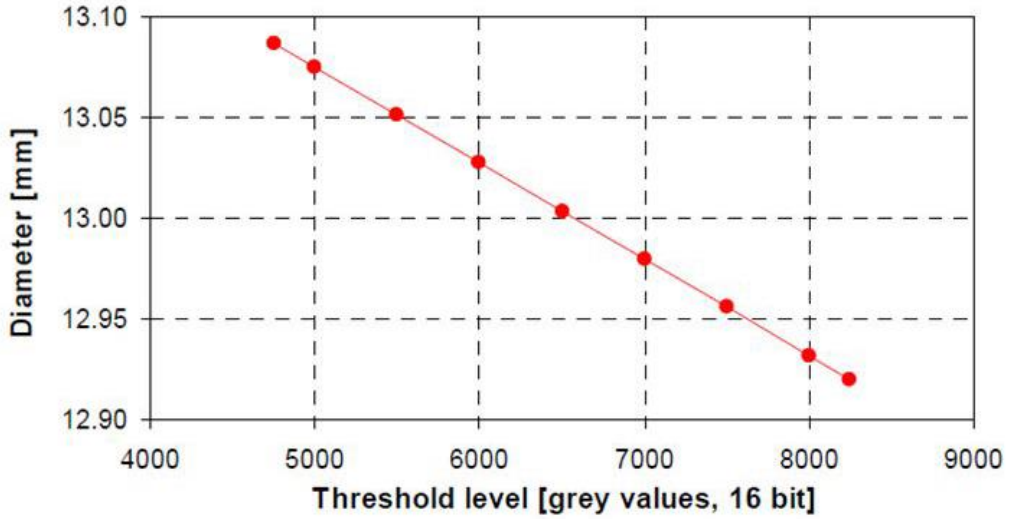

Fig. 2.28: Variation in diameter measurements of a cylindrical part for different threshold values [52]

2.3.3.4 Object characteristics

As previously mentioned, when a beam of X-rays passes through homogeneous material, the intensity of the rays is decreased due to attenuation i.e. scattering and absorption. According to the Lambert–Beer's law, the attenuated intensity (I) is defined as a function of the incident intensity (I_0) for monochromatic radiation and sample of thickness (s).

$$I = I_o e^{-\mu s} \qquad \textbf{(2.1)}$$

where, μ is the linear attenuation coefficient (units 1/length).

The number of photons transmitted through a material, corresponding to the linear attenuation coefficient, depends on the thickness, density and atomic number of the material and the energy of the individual photons. The attenuation is basically loss of intensity, thus minimized. As presented in Fig. 2.29, in case of smaller atoms, (b) and/or low density, (c) the penetration/attenuation will be increased/decreased. In addition, penetration is also dependent on the dimensions (thickness) and geometry of the object. However, any complex geometry can be scanned but the thickness poses certain limitations. Nevertheless, care should be taken during the placement on the object on rotary table. In particular, some calibrated objects can also be used for analyzing material specific attenuation [39].

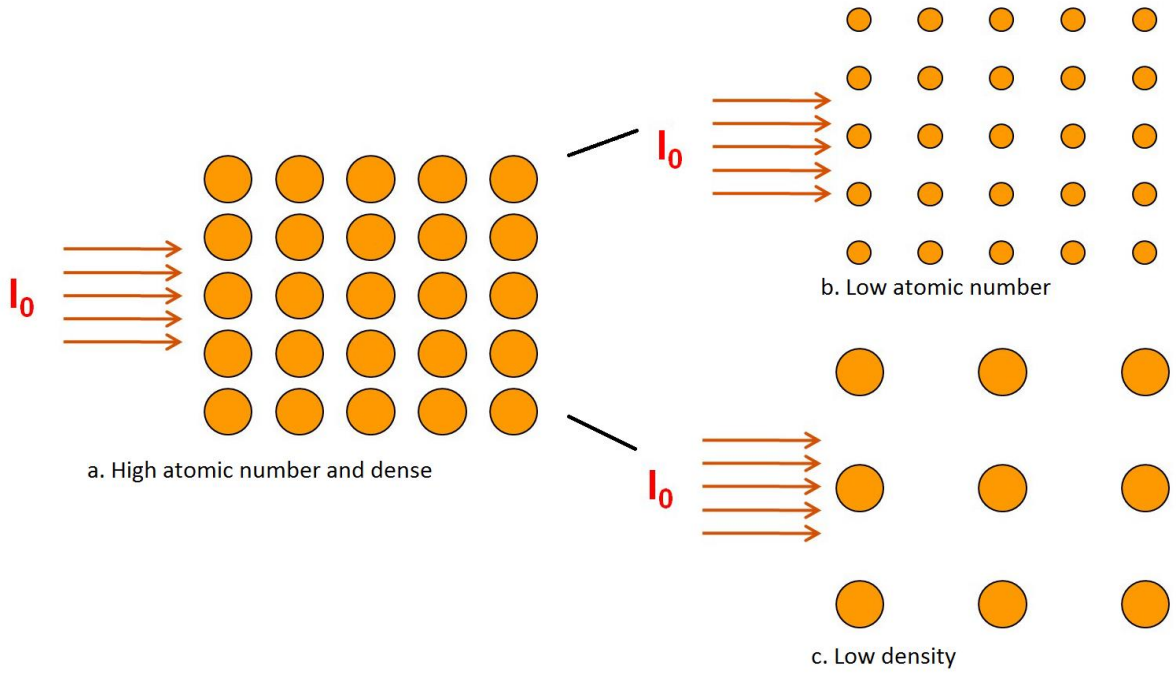

Fig. 2.29: A schematic view of influence of material characteristics on attenuation [39]

Other than the material's atomic structure the composition also affect the CT results, especially in concern to the beam hardening effect. Multi material measurements often exhibit problems related to artifacts, noise, surface determination, and measuring strategy.

2.3.3.5 Beam hardening

Polychromatic x-ray sources are used universally in CT to obtain adequate intensity of photons. While travelling through the object, the low energies' x-ray beams are preferentially attenuated and the higher energies x-rays undergo full penetration and reach the detector. This effect is termed as beam hardening which is due to the fact that only high energies' photons or hard x-rays are able to penetrate the object. Object with higher penetrating thickness are more prone to this effect. Beam-hardening results into an artifact, which produces false line integrals due the photon-energy dependence of the attenuation co-efficient. The threshold determination and the measurements of density and resolution are further affected by the beam hardening. Consequently, higher measurement errors are witnessed in lack of beam hardening correction. Fortunately, methods are available for reduction and/or elimination of the beam hardening artifacts.

- *Use of filters*

With the use of specially designed filters made up of Al/Cu/brass, the of low energies' photons are eliminated before reaching the object thus only high energies' x-ray beams are allowed to penetrate the object. The following figure shows the improved results by using physical filtering.

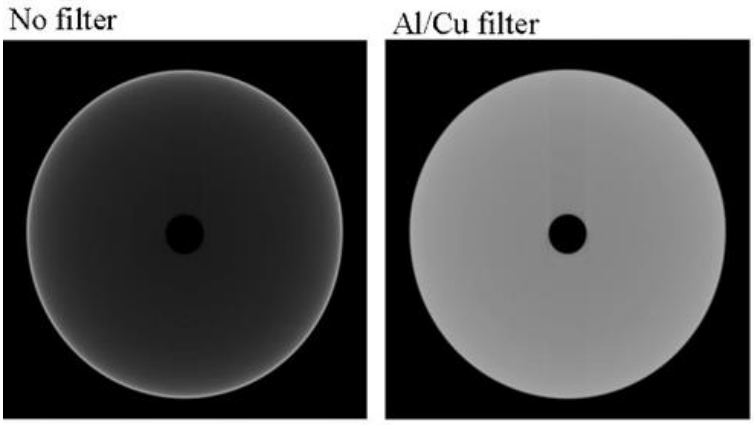

Fig. 2.30: Physical filtering applied for minimizing beam hardening effect (Hollow cylinder: outer ø 6, inner ø 0.6 mm) [22, 53]

- *Linearization*

Herman [54] provided another technique for correction of beam hardening which is limited to single material objects. It requires a reference object of the same material as

object's e.g. step wedge. The basic approach is establishing a relation between a propagated path length within the work-piece and the lowered intensity by means of various estimation algorithms. A characteristic line is determined by using the reference and subsequently, used to compute corrected intensity due to beam hardening. The characteristic line can also be determined from the reconstructed CT image. A binarization has to be performed for this purpose; the details can be found elsewhere [36].

The other possibilities for beam hardening correction is an iterative artifact reduction (IAR) method [55]; and use of different reconstruction algorithms (software) to numerically correct the bear hardening [22].

2.3.3.6 Surface roughness

In general, material surfaces are not perfect. The roughness of the surface causes difficulties in determining threshold during edge detection. Schmitt et al [56] in their work used the following equation for the assessment of uncertainty due to surface roughness. It is important to note that this is just preliminary form of as it is still under investigation [39].

$$u_{wi} = \sqrt{\left(\frac{b.Rz_{mean}}{2}\right)^2} \qquad \textbf{(2.2)}$$

where, Rz_{mean} is the mean value of surface roughness measurements taken at various spots on the workpiece surface and b is assumed as 0.6 for the standard uncertainty based on error margins a rectangular distribution.

2.3.3.7 Operator

Measuring strategy plays a crucial role in any kind of measurement irrespective of the applied method. There is no procedure to quantify the error related to measurement strategy (operator) and the best approach is to minimize it as much as possible. There is nothing like "the best strategy"; only based on the skills and experience of the operator a task based strategy is designed. During CT measurements, several steps are taken by the operator which may have an influence on the final results. The steps susceptible to measurement strategy are:

- selection of magnification,
- placement and orientation of the object on the rotary in order to avoid any vibrations the whole scan,
- determination of voxel size and correction using reference artifact,
- optimizing the source current and voltage,
- decision about number of projections.

The post processing of the CT data may also have an influence from the operator. Thresholding and beam hardening correction are the most prone step.

2.4 Conclusions

The first part of the chapter reviews micro injection moulding, need of metrology in micro-manufacturing and the available technologies and accompanying limitations/challenges. From the perspective of micro metrology, tolerances are being scaled down whereas the geometrical complexities of objects are being increased; therefore, the available measurement technologies seem to be insufficient. New technologies are welcomed and computed tomography is one such technology.

Therefore, the next part is focused on computed tomography consisting basic principle, applications, metrology via CT and hurdles in measurement accuracy. CT is gaining popularity due to its non-destructive way to assess the internal features and intricacies of micro parts. This project aims to utilize the potential of CT in order to develop controlling strategies with respect to the process variables for the micro injection moulding process. CT will be applied to micro moulded parts. Nevertheless, CT has its own limitations, which become more visible when the measurements are of micro scale, therefore, new strategies and approaches are required which can enhance the CT based quality control of micro molded parts.

References

[1] Tosello, G., & Hansen, H. N. (2015). Chapter 6-Micro-Injection-Molding. Micromanufacturing Engineering and Technology, 90-113.

[2] Piotter, V., Bauer, W., Benzler, T., & Emde, A. (2001). Injection molding of components for microsystems. *Microsystem Technologies*, *7*(3), 99-102.

[3] Tosello, G. (2008). Precision moulding of polymer micro components, Ph.D. thesis, Department of Manufacturing Engineering and Management, Technical University of Denmark.

[4] Giboz, J., Copponnex, T., & Mélé, P. (2007). Microinjection molding of thermoplastic polymers: a review. *Journal of micromechanics and microengineering*, *17*(6), R96.

[5] Mills, N.J. (2005). Plastics – Microstructure and engineering applications, Arnold, 3rd edition.

[6] Ganz, M., 2005, Micro Injection Moulding and Compression Moulding, Workshop at the 1st International Conference on Multi-Material Micro Manufacture (4M): Polymer Technology toward Nano, future technology for Europe, Karslruhe (Germany).

[7] Yang, Y., Chen, X., Lu, N., & Gao, F. (2016). *Injection Molding Process Control, Monitoring, and Optimization*. Carl Hanser Verlag GmbH Co KG.

[8] Vim, I. S. O. (2004). International vocabulary of basic and general terms in metrology (VIM). International Organization, 2004, 09-14.

[9] Hansen, H. N., Carneiro, K., Haitjema, H., & De Chiffre, L. (2006). Dimensional micro and nano metrology. CIRP Annals-Manufacturing Technology, 55(2), 721-743.

[10] Mattsson, L. (2006). Metrology of micro-components–a real challenge for the future. In Proc. of the 5th International Seminar on Intelligent Computation in Manufacturing Engineering (CIRP ISME'06) (pp. 547-552). CIRP.

[11] Wilkening, G., & Bosse H. (2005). Nano- and micrometrology – State-of-the-art and future challenges, Journal of Metrology Society of India, Vol. 20, No. 2, p. 125-151.

[12] International technology roadmap for semiconductors - metrology, 2005, http://public.itrs.net/ (January 2006).

[13] Bissacco, G. (2005). Surface generation and optimization in micro milling, Ph.D. thesis, Department of Manufacturing Engineering and Management, Technical University of Denmark.

[14] Dagnall, H. (1980). Exploring surface texture. Rank Taylor Hobson.

[15] Conroy, M., & Mansfield, D. (2008). Scanning interferometry: Measuring microscale devices. Nature Photonics, 2(11), 661-663.

[16] Hocken, R. J., Chakraborty, N., & Brown, C. (2005). Optical metrology of surfaces. CIRP Annals-Manufacturing Technology, 54 (2), 169-183.

[17] Hansen, H., N.; Dimensional Metrology for Micro Manufacturing, PhD Summer School at Denmark Technical University 2013.

[18] Goodhew, P. J., Humphreys, J., & Beanland, R. (2000). Electron microscopy and analysis. CRC Press.

[19] Boyde, A. (1973). Quantitative photogrammetric analysis and qualitative stereoscopic analysis of SEM images. Journal of Microscopy, 98 (3), 452-471.

[20] Rai-Choudhury (ed.), 1997, Handbook of microlithography, micromachining and micro fabrication, Vol 1: Microlithography, SPIE Optical Engineering Press, Washington, USA. ISBN 0852969066.

[21] Wang, L., & Xi, J. (2008). Smart devices and machines for advanced manufacturing. Springer.

[22] Kruth, J. P., Bartscher, M., Carmignato, S., Schmitt, R., De Chiffre, L., & Weckenmann, A. (2011). Computed tomography for dimensional metrology. CIRP Annals-Manufacturing Technology, 60 (2), 821-842.
[23] De Chiffre, L., Carmignato, S., Kruth, J. P., Schmitt, R., & Weckenmann, A. (2014). Industrial applications of computed tomography. CIRP Annals-Manufacturing Technology, 63(2), 655-677.
[24] Carl Zeiss Web Portal: www.xradia.com (Retrieved on October 10, 2017).
[25] Bariani, P. (2005). Dimensional metrology for micro technology, Ph.D. thesis, Department of Manufacturing Engineering and Management, Technical University of Denmark.
[26] Mattssona, L. (2007). The Challenge of Dimensional Metrology on High Aspect Ratio Micro Structures.
[27] Bennett, J.M., & Mattsson, L. (1999). Introduction to Surface Roughness and Scattering, 2nd ed., Optical Society of America.
[28] Marinello, F., Savio, E., Carmignato, S., & De Chiffre, L. (2008). Calibration artefact for the microscale with high aspect ratio: The fiber gauge. CIRP Annals-Manufacturing Technology, 57 (1), 497-500.
[29] Neuschaefer-Rube, U., Neugebauer, M., Ehrig, W., Bartscher, M., & Hilpert, U. (2008). Tactile and optical microsensors: test procedures and standards. Measurement Science and Technology, 19(8), 084010.
[30] Ritter, M., Hemmleb, M., Sinram, O., Albertz, J., Hohenberg, H. (2004). A versatile 3D calibration object for various micro-range measurement methods, In Proc. ISPRS 2004, Istanbul, Turkey.
[31] Léonard, F., Brown, S. B., Withers, P. J., Mummery, P. M., & McCarthy, M. B. (2014). A new method of performance verification for x-ray computed tomography measurements. Measurement Science and Technology, 25(6), 065401.
[32] Neugebauer, M., & Neuschaefer-Rube, U. (2005). A new micro artefact for testing of optical and tactile sensors. In Proc. 5th EUSPEN Int. Conf. (Montpellier, France, 8–11 May 2005) ed F Chevrier vol 1 pp 201–4.
[33] Sun, W.,Brows, S.B., & Leanch, R.K. (2012). An overview of industrial X-ray computed tomography, National Physical Laboratory, Teddington, Middlesex.
[34] Theilade, U.R.A. (2005). Surface micro topography replication in injection moulding, Ph.D. thesis, Department of Manufacturing Engineering and Management, Technical University of Denmark.
[35] De Chiffre, L., Carmignato, S., Kruth, J. P., Schmitt, R., & Weckenmann, A. (2014). Industrial applications of computed tomography. CIRP Annals-Manufacturing Technology, 63(2), 655-677.
[36] Reimers, P., & Goebbels, J. (1983). New Possibilities of Non-Destructive Evaluation by X-ray Computed Tomography. Materials Evaluation 41:732–737.
[37] Mitchell, K.W. (1989). A Generalized Approach to Wall Thickness Measurements in CT Images. Topical Proc. Industrial Computerized Tomography, ASNT, 120–124. ISBN 0-931403-89-8.
[38] Wiacker H (1991) Dimensionsanalyse mit der Computertomografie am Beispiel Turbinenschaufel vermessung. 2. Seminar Computertomografie, DGZfP BB 22, 86–93.
[39] Cantatore, A., & Muller, P. (2011). A report on "Introduction to computed tomography", Department of Mechanical Engineering – DTU.
[40] FRANZ, M., FUNK, C., HILLER, J., KASPERL, S., Krumm, M., Schröpfer, S., & Ezrt, F. (2009). Reliability of Dimensional Measurements by Computed Tomography for Industrial Applications. In Fourth European–American Workshop on Reliability of NDE.

[41] Kastner, J. (2011). X-ray Computed Tomography for the Development of Materials and Components, (Habilitation thesis) Vienna University of Technology, Vienna.

[42] Requena, G., Cloetens, P., Altendorfer, W., Poletti, C., Tolnai, D., & Warchomicka, F. (2009). Submicrometer Synchrotron Tomography of Multiphase Metals Using Kirkpatrick–Baez Optics. Scripta Materialia 61:760–763.

[43] BIPM, I., IFCC, I., & ISO, I. (2008). IUPAP and OIML JCGM-100: 2008 Evaluation of Measurement Data–Guide to the Expression of Uncertainty in Measurement. International Organization for Standardization, Geneva, Switzerland.

[44] ISO, I. (1998). 14253-1: geometrical product specifications (GPS)–inspection by measurement of workpieces and measuring equipment–part 1: decision rules for proving conformance or nonconformance with specifications. International Organization for Standardization, Geneva, Switzerland.

[45] VDI/VDE 2630-1.2 - Computed tomography in dimensional measurement - Influencing variables on measurement results and recommendations for computed tomography dimensional measurements, VDI/VDE Society for Metrology and Automation Engineering (GMA) (2010).

[46] Welkenhuyzen, F., Kiekens, K., Pierlet, M., Dewulf, W., Bleys, P., Kruth, J. P., & Voet, A. (2009). Industrial computer tomography for dimensional metrology: overview of influence factors and improvement strategies. In Proc. of the 4th International Conference on Optical Measurement Techniques for Structures and Systems: Optimess 2009.

[47] Weiss, D., Deffner, A., & Kuhn, C. (2010). Proc. Industrielle Computertomografie Tagung (in German).

[48] Hiller, J. (2011). Estimation of Uncertainties at Dimensional Measuring with Industrial X-ray Computed Tomography by Simulation (in German), Ph.D. Thesis, University of Freiburg.

[49] Sun, Y., Hou, Y., Zhao, F., & Hu, J. (2006). A calibration method for misaligned scanner geometry in cone-beam computed tomography. NDT & E International, 39 (6), 499-513.

[50] Carmignato, S., Dreossi, D., Mancini, L., Marinello, F., Tromba, G. and Savio, E., 2009. Testing of x-ray microtomography systems using a traceable geometrical standard. Measurement Science and Technology, 20(8), p.084021.

[51] Reinhart, C. (2008). Industrial computer tomography - A universal inspection tool, 17th World Conference on Nondestructive Testing (WCNDT2008), Shanghai, China (2008) 10.

[52] Carmignato, S. (2007). Traceability of dimensional measurements in computed tomography, In: Proceedings of 8th A.I.Te.M. Conference (2007) 11.

[53] Kerckhofs, G., Schrooten, J., Wevers, M., Van Marcke, P., & Van Cleynenbreugel, T. (2006, September). Standardisation and Validation of Micro-CT for the Morphological Characterisation of Porous Structures. In Proc. 9th Eur. Conf. Non-Destructive Testing (ECNDT), Berlin, 25-29.

[54] Herman, G. T. (1979). Correction for beam hardening in computed tomography. Physics in Medicine and Biology, 24(1), 81.

[55] Kasperl, S., Hiller, J., & Krumm, M. (2009). Computed tomography metrology in industrial research and development. Materials Testing, 51 (6), 405-411.

[56] Schmitt, R., & Niggemann, C. (2010). Uncertainty in measurement for x-ray-computed tomography using calibrated work pieces. Measurement Science and Technology, 21 (5), 054008.

CHAPTER 3. METHODOLOGY

Chapter 3.
Methodology

This chapter includes the different methodologies employed during the work. The details about the micro injection molding machine and various materials used for experimentation are provided. The various technologies used for characterization are briefly explained including CT. In addition, the statistical approach of experiments is also included.

3.1 Micro injection molding machine

In this work, a state-of-the-art micro-injection moulding machine (MicroPower 15 from Wittmann-Battenfeld) was used for most of the moulding experiments. The machine is characterized by a maximum clamping force of 150 kN and a maximum injection speed of 750 mm/s. The plasticizing screw has a diameter of 14 mm and the injection plunger has a diameter of 5 mm (Fig. 3.1). A state-of-the-art Wittman-Battenfeld MicroPower *15* micro injection moulding machine was used to mould the test specimens. As previously mentioned, this machine uses a screw to meld and mix the polymer and a separate plunger to inject it into the mould cavity. Both the injection unit and the clamping unit are electrical. The main characteristics of the machine can be seen in table 5.3.

Fig. 3.1: Micro injection molding machine: MicroPower 15 from Wittmann-Battenfeld (Source: Wittmann-Battenfeld)

Table 3.1: Wittmann-Battenfeld Micropower 15 technical data sheet

Properties	Unit	Value
Clamping unit		
Clamping force	kN	150
Opening stroke / Opening force	mm/kN	100/15
Ejector stroke / Ejector force	mm/kN	40/5
Injection unit		
Dosing screw diameter	mm	14
Dosing screw stroke	mm	26
Screw L/D ratio		20
Injection plunger diameter	mm	8
Max injection volume	cm^3	1
Specific injection pressure	bar	2500
Max. screw speed	min^{-1}	200
Max. plasticizing rate	g/s	1.7
Max. screw torque	Nm	90
Nozzle stroke b / Contact force	mm/kN	230/40
Injection speed	mm/s	750
Injection rate into air	cm^3/s	38
Barrel heating power, nozzle inc.	kW	2.45
Drive		
Electrical power supply	kVA	9

3.2 Materials

The polymeric materials used for injection molding experiments are available in the form of pallets. Depending on the application, a specific polymer/composite material was used. The following four materials were used for the task specific experimentation:

a. **COC**: Cyclic Olefin Copolymer (TOPAS® 5013L-10)
b. **PC**: Polycarbonate (Makrolon® Rx2530)
c. **PBT**: Polybutylene terephthalate reinforced with short glass fibers (10% in weight) (BASF, Ultradur B4300 G2)

The material undergoes drying operation according to the supplier's specifications before starting the experiments. More details about the materials are included in the specific chapters.

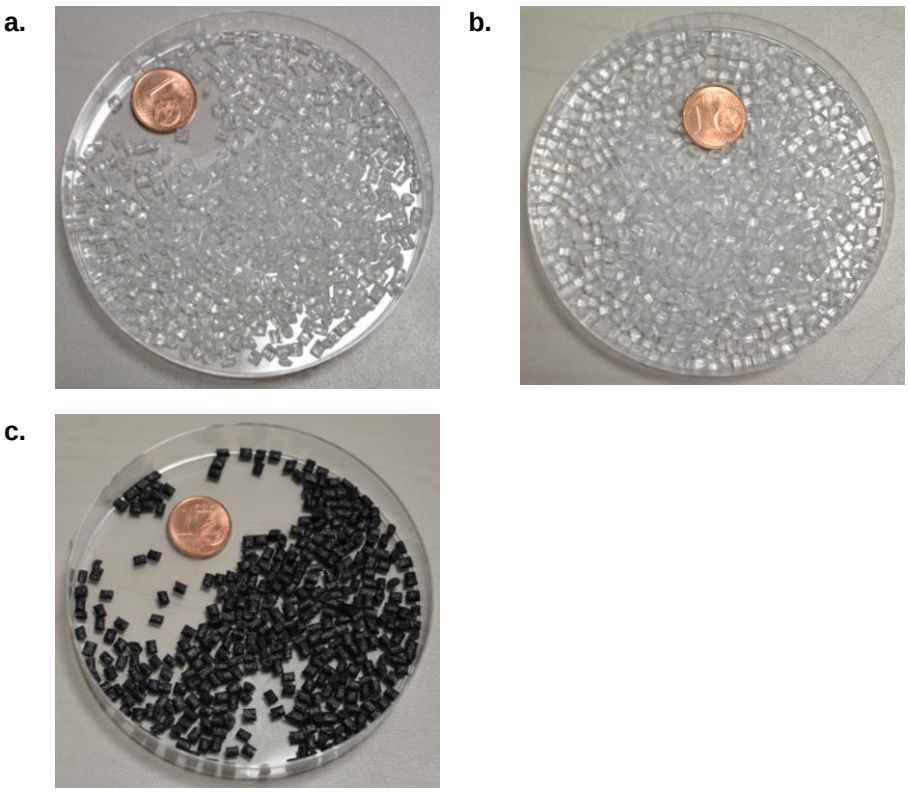

Fig. 3.2: Different polymeric material in the form of pallets: COC (a), PC (b) and PBT (c)

3.3 Design of experiment approach

Design of experiments (DoE) is an approach used in numerous industries for conducting experiments to develop new products and processes faster, and to improve existing products and processes. When applied correctly, it can decrease time to market, development and production costs, and improve quality and reliability [1]. There are several DoE strategies, the most commonly used are:

- One factor-at-a-time approach;
- Factorial experiments.

The one factor-at-a-time approach consists of selecting a starting point or baseline set of levels for each factor, then successively varying each factor over its range with the other factors kept constant at the base level. After all the tests are performed, a series of graphs are usually constructed showing how the response variables are affected by varying each factor with all other factors held constant. The major disadvantage of this strategy is that it fails to consider any possible interaction between the factors. An interaction is the failure of the one factor to produce the same effect on the response at different levels of another factor. Interactions between factors are very common, and if

they occur, the one-factor-at-a-time strategy will usually produce poor results. The correct approach to dealing with several factors is to conduct a factorial experiment. This is an experimental strategy in which factors are varied together, instead of one at a time. This experimental design helps in investigating the individual effects of each factor (or the main effects) and to determine whether the factors interact. One very important feature of the factorial design is that it makes the most efficient use of the experimental data.

3.4 X-ray computed tomography

A metrological micro CT system (Nikon Metrology, MCT225) was used for all the CT analyses carried out during this work, see Fig. 3.3. The system features a micro-focus X-ray source, a temperature controlled enclosure, laser corrected linear and rotary guides and high resolution detector as the main components.

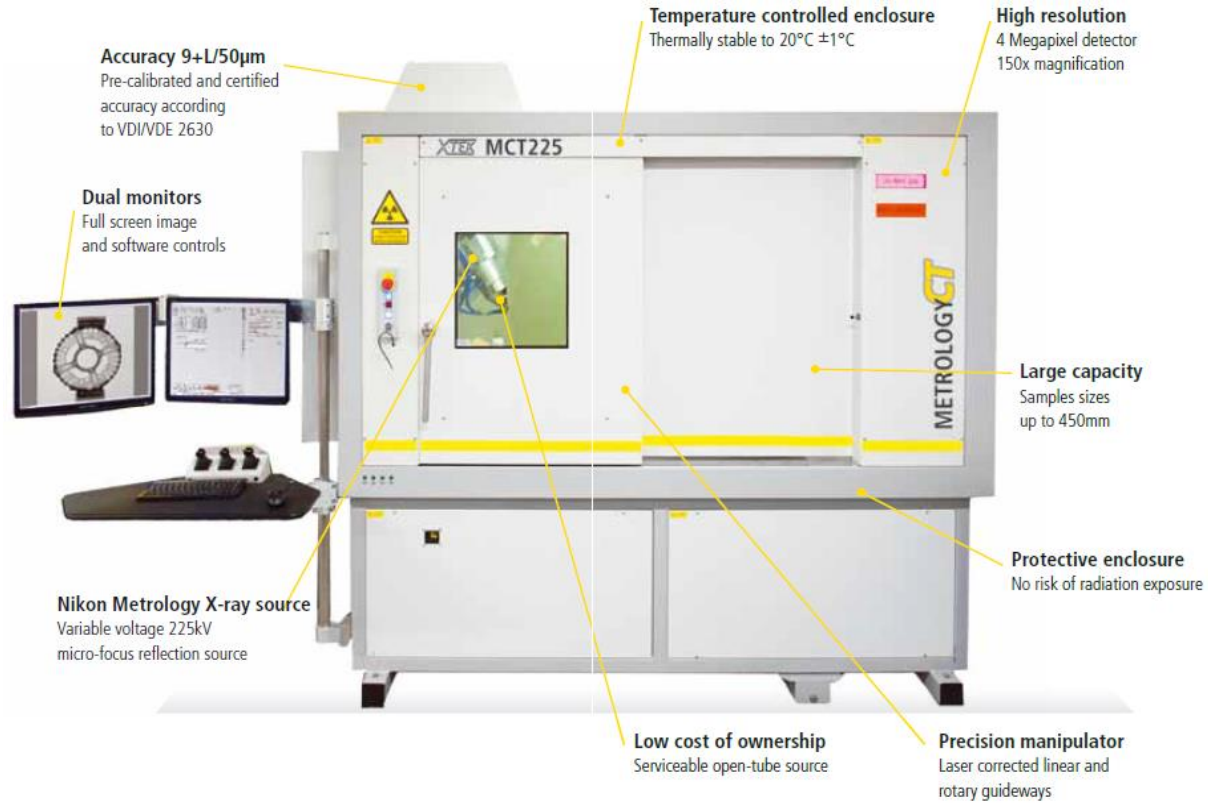

Fig. 3.3: X-ray CT system from Nikon (Source: Nikon Metrology)

MCT225 is pre-calibrated using accuracy standards traceable to the UK's national measurement institute (NPL) and verified using VDI/VDE 2630 guidelines for Computed Tomography in Dimensional Measurement. Absolute Accuracy guarantees measurement accuracy without time consuming comparative scans or reference measurements, samples are simply placed on a rotary table inside the enclosure and measured. Several key metrology features provide long term stability and enable the MCT225 to achieve an impressive accuracy specification of (9+L/50) µm:

- Nikon Metrology developed micro-focus X-ray source.
- Temperature controlled enclosure.
- High precision linear guide ways.
- Axis travels error corrected.
- Liquid cooled X-ray source.
- High resolution optical encoders.
- High resolution 4Megapixel detector.
- Finite Element Analysis (FEA) optimized manipulator.

The technical specifications of MCT225 are listed in Table 3.2.

Table 3.2: Nikon Metrology MCT225 system specifications

Properties	Value
Max. permissible error (MPE)	9+L/50 µm (L in mm)
Sample size (maximum)	Diameter 250 mm Height 450 mm
Sample weight (maximum)	50 kg (Max) 5 kg (for metrology applications)
Manipulator travel	(X) 400 mm x (Y) 300 mm x (Z) 730 mm x R 360° continuous
Source to detector	1175 mm
Detector	16 bit 4 Mpixels (2000 x 2000 pixel)
Magnification	1.6x to 150x
X-ray source	X-ray source
X-ray spot	3µm micro-focus
Enclosure temperature	19 to 21° C
Radiation protection (DIN 54113-2, IRR99)	< 1 µSv/hr
Material penetration	Plastics: 170 mm; Aluminum: 75 mm; Iron: 15 mm
Cabinet dimensions (WxDxH)	2414 mm x 1275 mm x 2205 mm

3.5 3D optical profiler

The 3D optical profiler uses both confocal microscopy and interferometry to measure the surface topography of a workpiece. The instrument is installed on an isolated table (no vibration of the workpiece and the instrument) and there's also a motorized and tiltable clamping system for the workpiece as shown in Fig. 3.4 (a).

a. **b.**

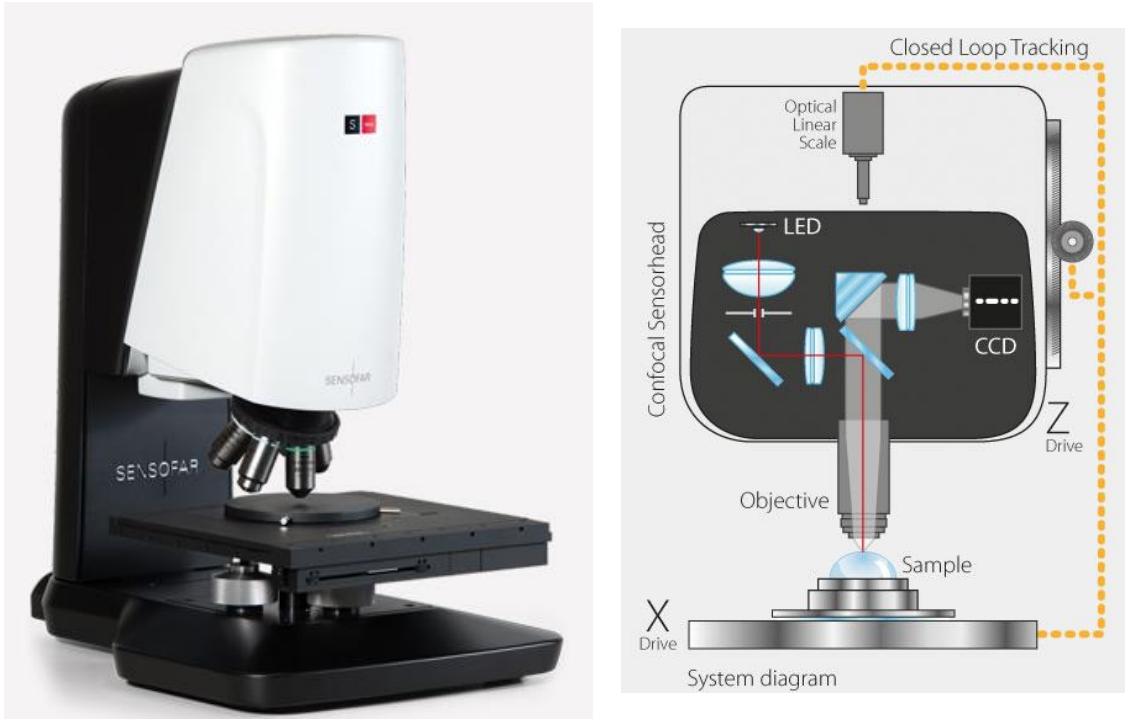

Fig. 3.4: S neox optical profiler Sensofar (a) and principle of confocal microscopy (b) (Source: Sensofar)

Confocal microscopy is an optical imaging technique for increasing optical resolution and contrast of a micrograph by means of adding a spatial pinhole placed at the confocal plane of the lens to eliminate out-of-focus light. It enables the reconstruction of three-dimensional structures from sets of images obtained at different depths (a process known as optical sectioning) within a thick object. Different light sources have different wave lengths, e.g. red 630 nm, green 530 nm and blue 460. The shorter is the wavelength the higher is the achieved lateral resolution[1]. For this reason, the blue light is suited for those applications where the highest lateral resolution is required.

Technical characteristics of the instrument depends in particular on:

- Movement of the z axes
- Installed optics

The instrument is scanning along the z axis using a piezoelectric system: in this way the vertical positioning accuracy is very high however with limited vertical range. A “linear stage” is available to enlarge it, however with decreased positioning accuracy. In the Table 3.3 below main technical characteristics of the instrument are reported. These characteristics depends on different optics.

Table 3.3: Technical characteristics of the profiler

	5X Interferometry	2.5X Confocal	20X Confocal	100X Confocal
Working Distance (mm)	9.3	6.5	4.5	1.0
NA[2]	0.15	0.075	0.45	0.9
FOV[3] (µm)	2546x1909	7016x5280	636x477	127x95
Spatial Sampling[4] (µm)	3.32	5.16	0.83	0.17
Optical Resolution[5] (µm)	0.93 – 1.11	1.87	0.31	0.15
Maximum Slope	8°	3°	21°	51°
Vertical Resolution[6] (nm)	<0.1 - 1	300	8	2

[1]Lateral resolution is defined as the ability of the system to distinguish two points in the direction perpendicular to the direction of the beam.

[2]The numerical aperture (NA) indicated the angular aperture of a microscope and is a measure of its ability to gather light and resolve fine specimen detail at a fixed object distance.

[3]Maximum field of view (FOV)

[4]Spatial sampling = Pixel size on the surface

[5]Optical resolution = half of the diffraction limit according to the Raleigh criterion (Values for blue light)

[6]Vertical resolution = system noise measured as the difference between two consecutive measures on a calibration mirror placed perpendicular to the optical axis.

3.6 Software tools

A number of software tools were used for various data analysis and simulations during the work. The most commonly used software tools are briefly described here:

Autodesk Moldflow

Moldflow is commercial software which provides simulation tools for injection mold design, plastic part design, and the injection molding design process. It helps in reducing the need for costly physical prototypes, avoids potential manufacturing defects, and helps bring innovative products to market faster. Within this, it has been used for different simulation studies according to the needs. More information can be found in [2].

VGStudio MAX

It is the high-end software for the visualization and analysis of industrial CT data. It provides a number of tools for measurement and analysis e.g. porosity, fiber characteristics and CAD comparison etc. It has been used for processing CT data and subsequent analyses performed within this framework. More information can be found in [3].

Minitab 17

It is a statistical program designed for data analysis. It is used for the design of experiment and statistical analysis. More details about the software can be accessed in [4]

aRTist

(Analytical RT Inspection Simulation Tool) for CT simulations It is software tool for simulation CT acquisition process, which generates realistic radiographs on the basis of virtual part representations and well defined radiological parameters [5].

In addition, several other tools e.g. GOM Inspect, SPIP were also used for some task specific needs.

References

[1] Montgomery, D. C. (1997). Design and Analysis of Experiments, 5th Ed., John Wiley & Sons.

[2] https://www.autodesk.com/products/moldflow/ (Retrieved on October 10, 2017)

[3] https://www.volumegraphics.com/en/products/vgstudio-max.html (Retrieved on October 10, 2017)

[4] http://www.minitab.com/ (Retrieved on October 10, 2017)

[5] Bellon, C., & Jaenisch, G. R. (2007, June). aRTist–analytical RT inspection simulation tool. In Proc DIR (pp. 25-27).

CHAPTER 4. HOLISTIC QUALITY CONTROL

Chapter 4.
Holistic quality control

This chapter consists of two parts. In the first part, a microfluidic based study has been carried out which includes micro molding of the parts, their subsequent characterization using X-ray CT and microscopy. A data fusion approach is used for the holistic measurement of such microfluidics. In the second part of the chapter, influence of electron beam alignment is studied of the CT measurements of the micro molded parts.

4.1 Holistic quality control of microfluidics

In last decade, there have been significant developments to make micro-injection moulding a stable high-volume process for manufacturing disposable microfluidic devices. Several problems have been successfully overcome by improvements made to the process or to the equipment. Micro-injection moulding is currently used for commercial microfluidic applications; however, there a number of challenges, which require further investigation and research. One of the most important challenges is acquiring holistic and accurate 3D measurements which is needed during the process optimization stage before the mass replication. The increasing complexity of features and miniaturization make the task of holistic 3D data acquisition difficult. For the last few years, industrial computed tomography (CT) has emerged as a promising coordinate measuring technology, which enables integrated quality control of complex workpieces combining dimensional metrology and material defects analysis. In this work, CT is used for macro measurement and combined with other sensor data to provide a complete quality information.

4.1.1 Introduction

Microfluidic devices have wide number of applications, the majority of which are for medical diagnostics. Some of the common examples of polymeric microfluidics are components for micropumps, which are used for medical, chemical and environmental technology [1, 2]. The function of such micropumps is the delivery of small amount of fluids for different applications, such as point-of-care platforms or small fuel cells; they are designed to be low in cost and disposable. Other commonly used microfluidic systems are reaction vessels and mixing structures which are currently being produced by micro-injection moulding [3, 4]. Lab-on-a-chip system for blood diagnostics is widely used which includes functions such as sample absorption, separation, mixing with reagents, analysis and waste absorption. The ‘‘Snake’’ mixer slide is also a type of

microfluidic system comprising of a plastic chip with meander-shaped mixers, which mixes fluids possessing a range of viscosities and at different flow rates [5]. DNA analysis systems (bio-MEMS, l-TAS and Integrated LOC) which are typically manufactured of glass, are currently being manufactured in polymers. Such integrated systems usually combine an entire process chain, such as storage and waste vessels, transport channels, filters, mixing and separating structures, reaction chambers and detection points on a plastic substrate [2, 4, 6, 7].

Mass-producing such integrated systems in polymers rather than glass would decrease their cost; therefore, polymeric microfluidic systems have very popular in last decade. Although several polymeric microfluidic systems have been made available commercially, it should be noted that due to process limitations, the process is not fully implemented for relatively complex microfluidic systems. Integration of external elements, such as electrodes or micro-heaters, within a mass production technique such as micro-injection moulding, still poses a major challenge for the technology.

Micro-injection moulding has become one of the main fabrication techniques used to produce polymeric microfluidics due to several advantages that makes it commercially applicable with potential for further developments in the future. The various advantages include:

- Wide range of thermoplastics available and the potential for full-automation with short cycle times [6, 8, 9];
- Cost-effectiveness for mass-production process, especially for disposable products [7,10],
- very accurate shape replication and good dimension control [8,11];
- Low maintenance costs of capital equipment as compared to lithographic methods [9] and
- Applicability of the strong ‘know-how’ available from conventional injection moulding. Within certain limitations, this may be scaled down to micro-injection moulding.

In addition to the knowledge transfer from conventional injection molding to micro injection molding; it also require very dedicated control procedures for micro molding machines. Micro-features have always been a challenge for injection machines, because of the requirement to completely fill cavities in the micro-range before the material starts to solidify. This is specifically critical for microfluidic devices where there is a large change in thickness between the substrate and the micro features. There is an evident need of process optimization with respect to the desired part quality. Common processing parameters are melt temperature, mould temperature, injection speed, and injection pressure, holding pressure, injection profile controlled either by speed or pressure and cooling time, in addition to the possibility of changing the material type. The

part quality can be measured in terms of complete filling, dimension stability, mechanical properties or any other parameter depending on the product.

The technique for evaluating the quality of the part varies according to the specific application of the part. The quality parameters for microfluidic applications can be the micro-channel width, the tolerances or the filled aspect ratio. Inspection can also take place as a part of the process by using in-line video cameras. However, in-line quality control may not be enough for some purposes, such as surface finish or material morphology within the component [12, 13] and in this case further inspection has to be done with specialized equipment. Inspection techniques for measuring small micro moulded parts may require additional customized vices, tweezers and fixturing [14]. Quality assurance with regard to specific processing issues may require the use of specialized equipment. Weber et al [3] reported the use of a laser profilometer to check warpage by measuring deviation in the flat surface of the part. A 3D measurement for the geometric dimensions of the part can be made by using a confocal microscope with suitable image-processing software [15]. In addition, atomic force microscopy (AFM) has been used for surface inspection and characterization, and scanning electron microscope (SEM) for observing 3D details and evaluating dimensions [13, 16]. Although SEM is a standard imaging technique, it is not the best method for the measurement of 3D features. Contact-probe methods, such as micro coordinate measurement machines (CMM) have been commercially developed for 3D dimensional metrology. A classification with respect to structural dimensions and complexity was introduced by Bariani [17], which was modified by Hansen et al [18]. As shown in Fig. 1, the structural complexity termed as 2D, 2½D and 3D are defined as features with aspect ratios <1, aspect ratios ≥1 and with undercuts/cavities/freeforms respectively. As the structural dimension is lowered and the complexity is increased there is a lack of instrument/technology which can provide a measuring solution singlehandedly. Multisensor data fusion could be a step towards filling the void to some extent [19].

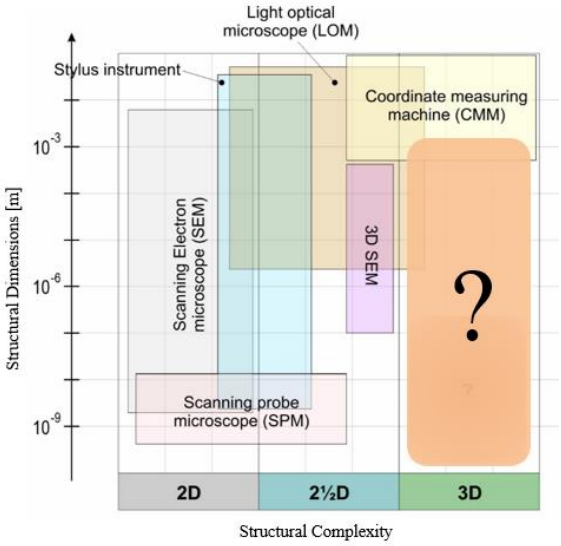

Fig. 4.1: Classification of dimensional measuring equipment, adapted from [19]

As already highlighted, X-ray computed tomography has been proposed as a successful non-destructive technique for dimensional metrology in recent years. Nevertheless, measurement traceability is still challenging and there exist several influencing factors contributing to the measurement uncertainty, which are difficult to quantify [20]. When it comes to measurements of micro features, the resolution becomes significantly a limiting factor for typical industrial CT systems with micro- or nanofocus tubes. Using data from other sensors in addition to CT data can provide holistic geometrical measurement information, even for complex objects, thus complementing the CT data set.

The term data fusion is quite broad in itself and used in different fields, more information can be found in [19, 21, 22]. As defined by Weckenmann et al [20] “Multisensor data fusion in dimensional metrology can be defined as the process of combining data from several information sources (sensors) into a common representational format in order that the metrological evaluation can benefit from all available sensor information and data. This means that measurement results can be determined, which could not – or only with worse accuracy – be determined solely on the basis of data from an individual source (sensor) only.” For example, Bartscher et al [23, 24] used multisensor data fusion for measuring a cast cylinder segment. The outer and inner geometries were measured with fringe projection system and 2D-CT system respectively. Both the data sets were fused together and the results were compared with tactile measurements; the reported deviations were less than ± 0.38 mm (of the order of voxel size of CT measurement). In this study, the potential of CT is utilized for quality assessment of a microfluidics; in addition, data from confocal microscopy is used for enhancement of the CT result by data fusion.

4.1.1.1 Examples of microfluidics

Microfluidics are used wide range of applications and thus manufactured accordingly with desired features. Metallic mold inserts are designed depending on the applications, which are used for the mass replication of that specific design. A number of different microfluidic designs have been tested within this work, which are shown in Fig. 4.2. They contain different type of micro channels, which have different critical aspects such as channel height, channel width, spacing etc. The feature details shown in Fig. 4.2 have been obtained from confocal microscopy. The part shown in Fig 4.2 (a) has been used for this current study.

a.

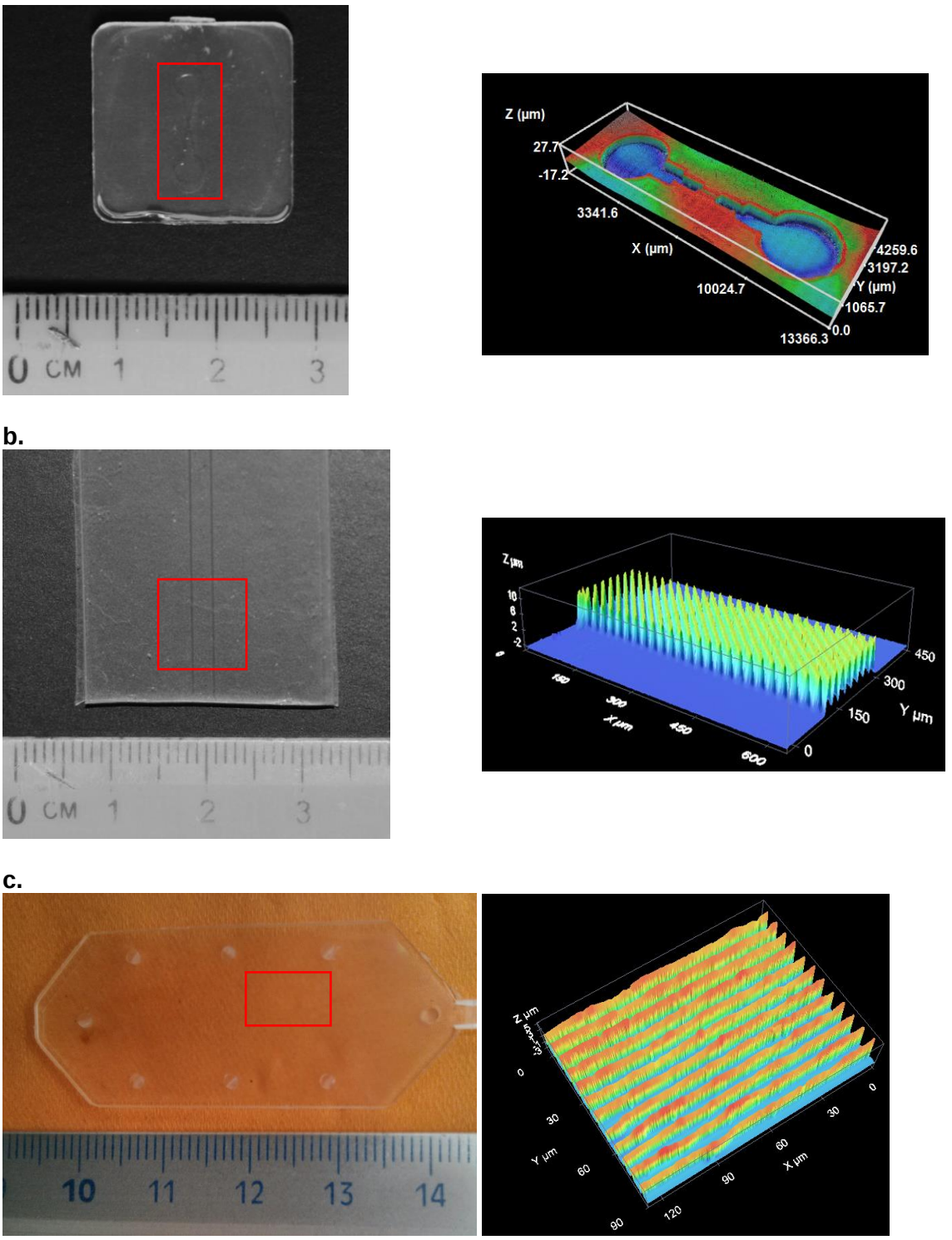

Fig. 4.2: Examples of microfluidics

4.1.2 Materials and methods

This section contains the details of the part geometry, different materials used, the micro injection molding machine and molds. The CT scanning set up and parameters are also included.

4.1.2.1 Experimentation

As shown in Fig. 4.3, the part is squared shape (20 mm × 20 mm) with a width of 2 mm. It contains a micro channel which has a height of 20 µm and smallest width of 30 µm at the centre, the other dimensions are provided in Fig. 4.3 (b). Two different materials: Cyclic Olefin Copolymers (COC) and Polycarbonate (PC), have been used for manufacturing. They are used in the form of pallets as shown in Section 3.2. It is of interest to see which material produces better replication quality.

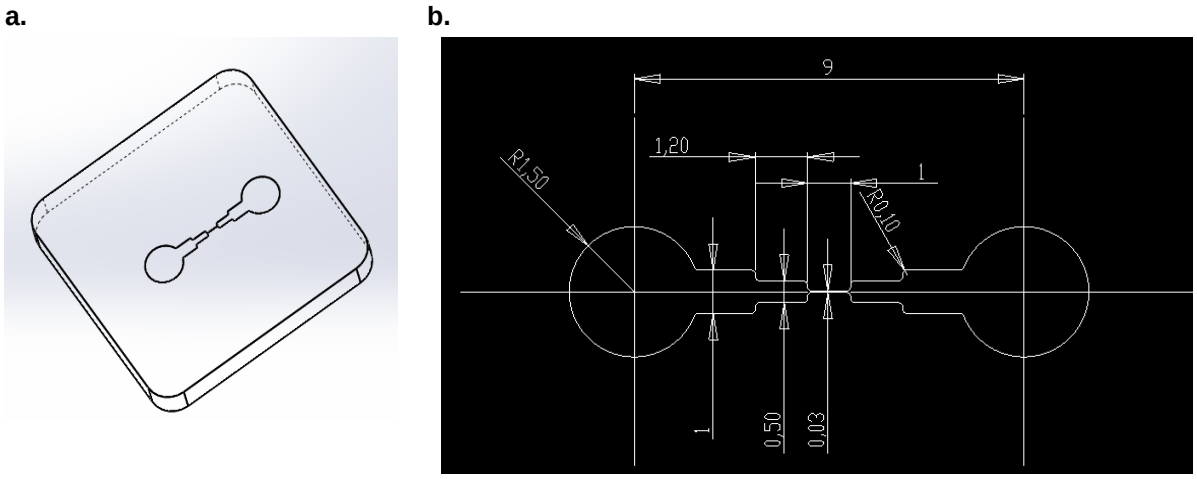

Fig. 4.3: Nominal part geometry (a) and micro channel dimensions (b) [25]

Table 4.1: Material properties

	Cyclic Olefin Copolymer (COC)	Polycarbonate (PC)
Grade name	TOPAS® 5013L-10	Makrolon® Rx2530
Melt temp., °C	240 - 300	280 - 320
Mold temp., °C	95 - 125	80 -100
Injection speed, mm/s	50 - 150	200
Drying temperature, °C	100	120
Drying time, h	4 - 6	2 - 4
Packing pressure, bar	500 -1100	

The material properties are listed in Table 4.1. The machine used for these experiments is Arburg 270 M (350-90); which is characterized by a Clamping force: 350 kN and screw diameter: 25 mm. The mold assembly is presented in Fig. 4.4, a two plate mould was used in this work. The cavity was located on the moving half of the mould, whereas the fixed half was flat to close the cavity. The mold insert plate was produced from lithography, which is shown in Fig. 4.5 (a). Since the mold contains the features, it will be interesting to measure the mold insert.

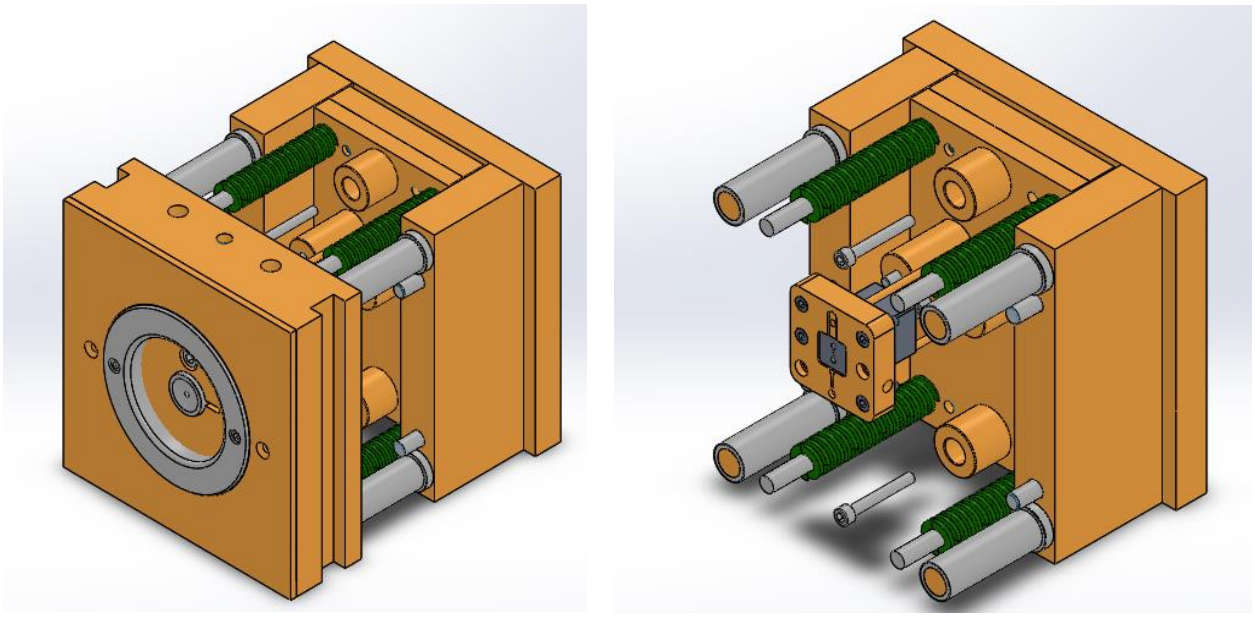

Fig. 4.4: Mold assembly for the experimentation

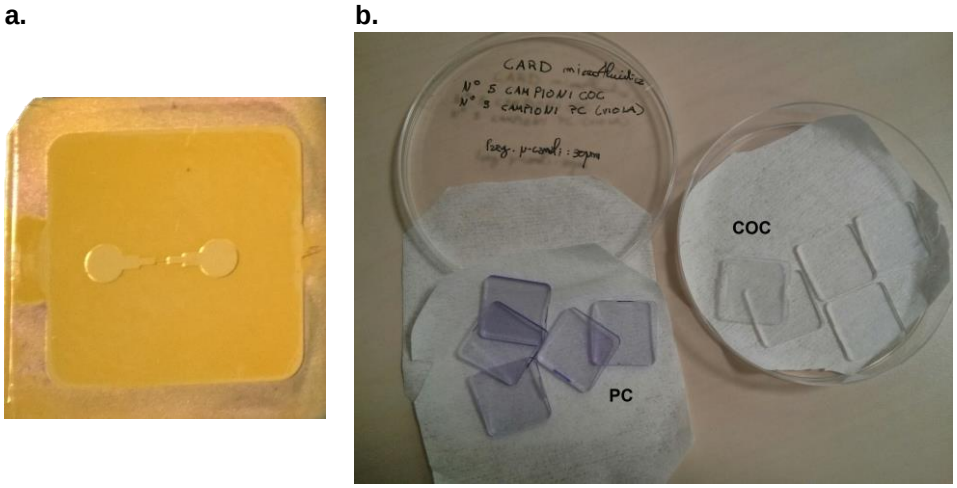

Fig. 4.5: Mold insert (a) and manufactured parts with a channel width of 30 µm (b)

Multiple test specimens were moulded for each of the materials. When changing from one material to another, the first few test specimens were discarded to stabilize the process. As shown in Fig. 4.5 (b), the parts look different in appearance due to the light

violet color of polycarbonate; which also makes it easier to identify. For each of the materials, two randomly selected parts were used for the measurements.

4.1.2.2 X-ray CT scanning

Nikon MCT 225 x-ray computed tomography system was used for scanning the micro molded part. The aspect ratio of the part and the micro details make the CT scanning a challenging task. In order to optimize the CT measurement results, several preliminary scans were performed varying the parameters: mainly the voltage, current and exposure time. The set of optimal scanning parameters is provided in Table 4.2. The magnification achieved for the complete part scan was 15x; in addition a partial scan (only the micro channel) was made at a magnification of 20x. The placement of part for CT scanning is shown in Fig. 4.6.

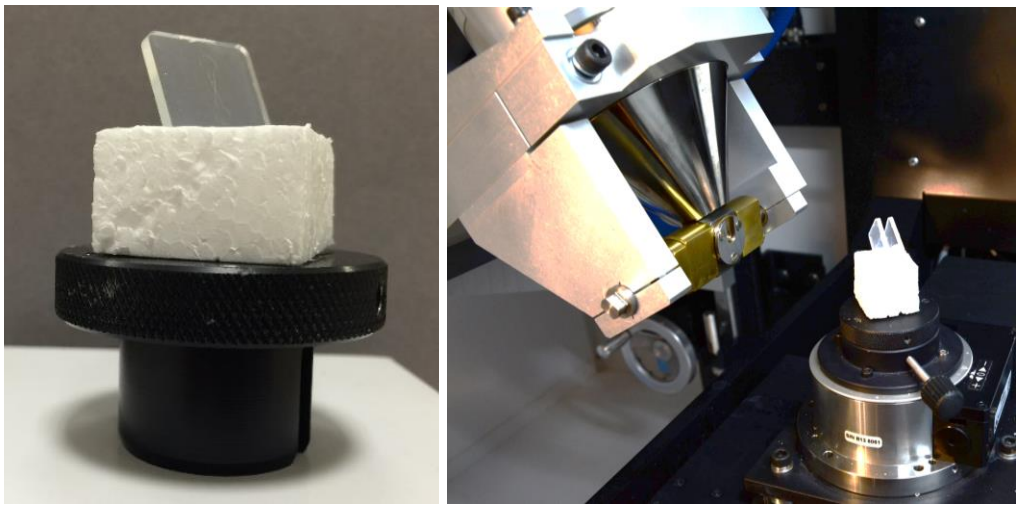

Fig. 4.6: Part placement inside the CT system

Table 4.2: CT scanning parameters

Parameter	Value
Voltage, kV	90
Current, µA	56
Exposure time, s	4
Number of Projections	2000
Magnification	15x (full scan) 20x (partial scan)
Voxel size, µm	~14 (15x) ~10 (20x)
Repetitions	3

4.1.2.3 Confocal microscopy

In order to measure the micro channel with sufficient resolution, another non-contact measuring technique is needed, such as confocal microscopy as described in Section 3.5. In order to have a larger area scan, extended topography measurement was performed, by stitching a number of single small areas to cover the desired measuring area with a specified overlap (default overlap is 10%). The drawbacks of this procedure for extended topography measurement are the long scanning time, stitching errors and the limited z-range; for instance, one extended topographic measurement was over 4 hours long. Due to these drawbacks, measurement of the entire surface of the part (20 x 20 mm) is not feasible by extended topography using confocal microscopy only (in particular, stitching errors on such large areas would increase to values that are not acceptable for accurate evaluation of overall part geometry).

a.

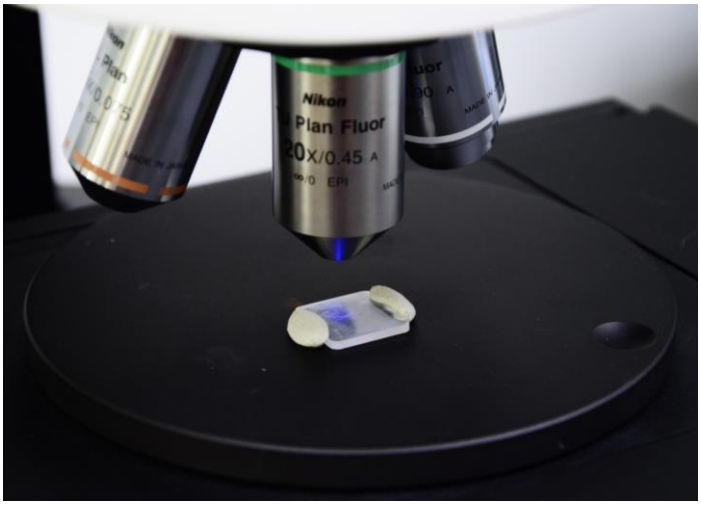

b.

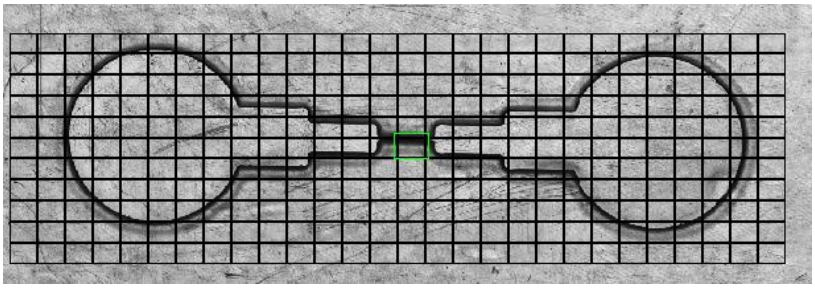

Fig. 4.7: The specimen measurement (a) and the stitching procedure with extended topography (b)

Table 4.3: Acquisition settings

Parameter	Value
Objective	20x
Optical resolution, µm	0.31
Stitching overlap, %	25 %
Correlation	XYZ (slower)
Field of view (FOV), µm²	636 x 477
Acquired area, mm²	15.94 x 4.58
Stitching Grid	29 x 11

4.1.2.4 Moldflow simulation

In injection molding process simulation is widely used for predictions. Autodesk® Moldflow Insight 2013 was used for simulation in the current work. The part geometry along with the feeding system (STEP or IGES format) was imported. Meshing is the most crucial aspects of the simulation which affects the accuracy of prediction. Solid 3D mesh usually gives better results when the part is free-shaped and has changes in thickness, though it takes more computational time. Dual domain mesh is better suited for parts with 2D geometry (i.e. with two dimensions significantly bigger than the third, thickness). Dual domain meshing consists of dividing the surfaces of the part in finite triangular elements. It is important that triangles on the two surfaces match in order to give accurate simulation. For good warp results at least 90% match is required.

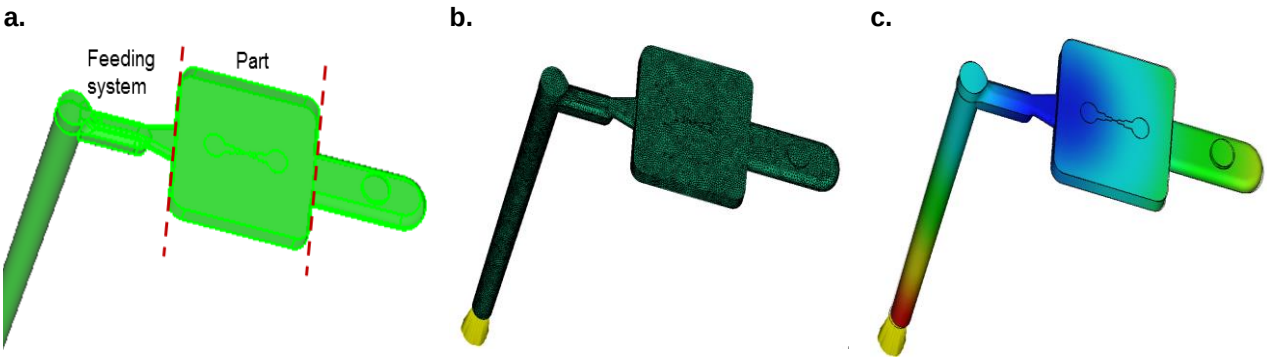

Fig. 4.8: Moldflow simulation procedure model of the mold cavity and feeding system (a), meshing (b) and analysis (c)

The analysis type is then chosen. A cool + fill + pack + warp analysis was selected in this work. The injection location is set accordingly to the mould design. It is important to cover the whole area by setting multiple injection locations, see Fig. 4.8 (b). The material was selected from the in-built database and the process setting were incorporated. The cooling channels were according to the actual injection moulding process.

4.1.3 Results and discussion

In this section, the results obtained from both the methods i.e. CT and confocal microscopy are reported and discussed. The simulation results are also discussed in comparison to CT from the point of view of warpage of the final part. Lastly, the data fusion results have been presented and discussed.

4.1.3.1 Scan quality and shrinkage measurement

The projections obtained from the CT scanning are reconstructed into a 3D volume for performing measurements and analyses. Subsequently the volumetric data is imported into VG StudioMax. The next step is the surface determination using ISO-50 [21]; followed by the desired measurements. The scan obtained at 15x contains the entire part while the scan at 20x contains only the central part with the micro channel due to the limited field of view (cone beam CT) [21]; the voxel sizes are 14 and 10 µm respectively. The results for the both the scans are provided in Fig. 4.9.

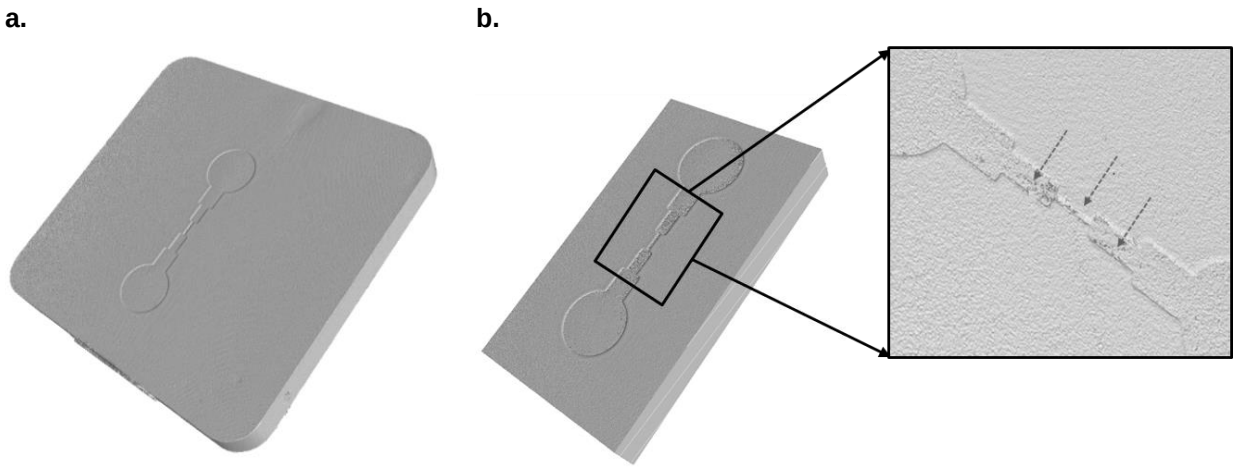

Fig. 4.9: Reconstructed volumes at a magnification of 15x (a) and 20x (b)

While the overall scan quality is good, the quality at the micro channel region is affected by the noise and the limited resolution especially, as visible in Fig. 4.9 (b). The arrows show the areas of the CT data at the micro channel region that are more affected these limitations. For better resolution, the magnification can be increased but it introduces negative effects, e.g. blurring depending on the X-ray spot size [21].

As explained in Fig. 4.10, the linear shrinkage was measured on the volumetric data in X, Y and Z directions around the centre and the measured values are D_x, D_y and D_z respectively. The measurement was performed on all three repetition scans for two parts of each material and the corresponding values are reported in Table 4.4 and 4.5.

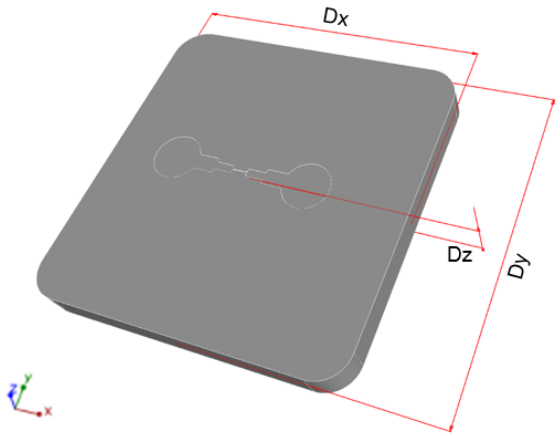

Fig. 4.10: Linear shrinkage measurement on CT volumetric data [25]

The measurements of two parts for each material are very similar, which shows uniform behavior of that material. The variations in the measurements of the two parts are less than 0.02 mm for both COC and PC except for a variation of around 0.04 mm for D_y for PC. The standard deviation of the three scans is also very low, which shows a good repeatability of scanning.

Table 4.4: Shrinkage measurement results COC

		Scan-1	Scan-2	Scan-3	Mean	Std. Dev.
	Part-1	19.9270	19.9320	19.9240	19.9277	0.0033
D_x [mm]	Part-2	19.9190	19.9220	19.9080	19.9163	0.0060
	Variation	0.0080	0.0100	0.0160	0.0113	
	Part-1	19.9530	19.9540	19.9530	19.9533	0.0005
D_y [mm]	Part-2	19.9490	19.9580	19.9470	19.9513	0.0048
	Variation	0.0040	-0.0040	0.0060	0.0020	
	Part-1	1.9403	1.9402	1.9400	1.9402	0.0001
D_z [mm]	Part-2	1.9403	1.9400	1.9399	1.9401	0.0002
	Variation	0.0000	0.0002	0.0001	0.0001	

Table 4.5: Shrinkage measurement results PC

		Scan-1	Scan-2	Scan-3	Mean	Std. Dev.
	Part-1	19.8700	19.8670	19.8610	19.8660	0.0037
D_x [mm]	Part-2	19.8630	19.8640	19.8640	19.8637	0.0005
	Variation	0.0070	0.0030	-0.0030	0.0023	
	Part-1	19.9280	19.9280	19.9280	19.9280	0.0000
D_y [mm]	Part-2	19.8890	19.8890	19.8880	19.8887	0.0005
	Variation	0.0390	0.0390	0.0400	0.0393	
	Part-1	1.9287	1.9298	1.9297	1.9294	0.0005
D_z [mm]	Part-2	1.9263	1.9298	1.9290	1.9284	0.0015
	Variation	0.0024	0.0000	0.0007	0.0010	

The shrinkage percentage from the nominal values was calculated using the mean values of three scans. The results are plotted in the Fig. 4.11.

It can also be seen in Fig. 4.11, that the two part of the same material underwent almost similar amount of shrinkage is each of three directions; which indicates the process was stable. The shrinkage is x and y directions is lower than 0.5% for COC and slightly higher than 0.5% for PC. In z direction, the COC part exhibits 3% shrinkage whereas PC exhibits 3.5%. Therefore, it can also be concluded that the part with PC witnesses more shrinkage compared to the COC. It is also evident that the shrinkage is not uniform in all the directions. The differential shrinkage results into the warpage of part, which is discussed later is this chapter.

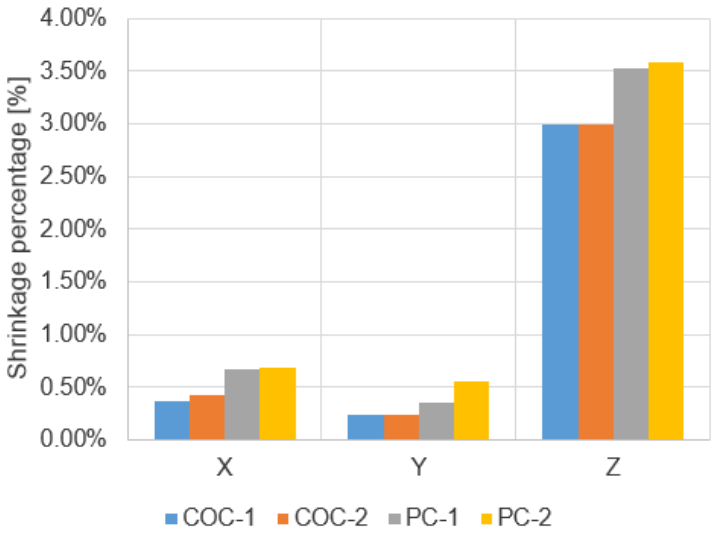

Fig. 4.11: Average linear shrinkage of the part

The CT results are advantageous for the macro quality assessment of the part but the resolution and noise limit the reliability of the CT data for micro measurements of this particular case. There arises a need of other measuring instrument/technology for the micro channel quality assessment; therefore, confocal microscopy was used for this purpose.

4.1.3.2 Warpage/geometry deviation

- *Simulation*

The warpage results of the simulation is in the form of deflection considering all the effects e.g. the shape of part, packing pressure, cooling etc., shown in Fig. 4.12. The simulation results very almost identical for both the materials, therefore, only one of them is presented here. The Fig. 4.12 (a) and (b) show the deflection in x and y components and Fig. 4.12 (b) shows in z component alone. The section in yellow/red shows the highest warpage defect corresponding to the high deflection. The scale factor used here is 10 for better visualization. The results are useful for observing the warpage behavior of the part.

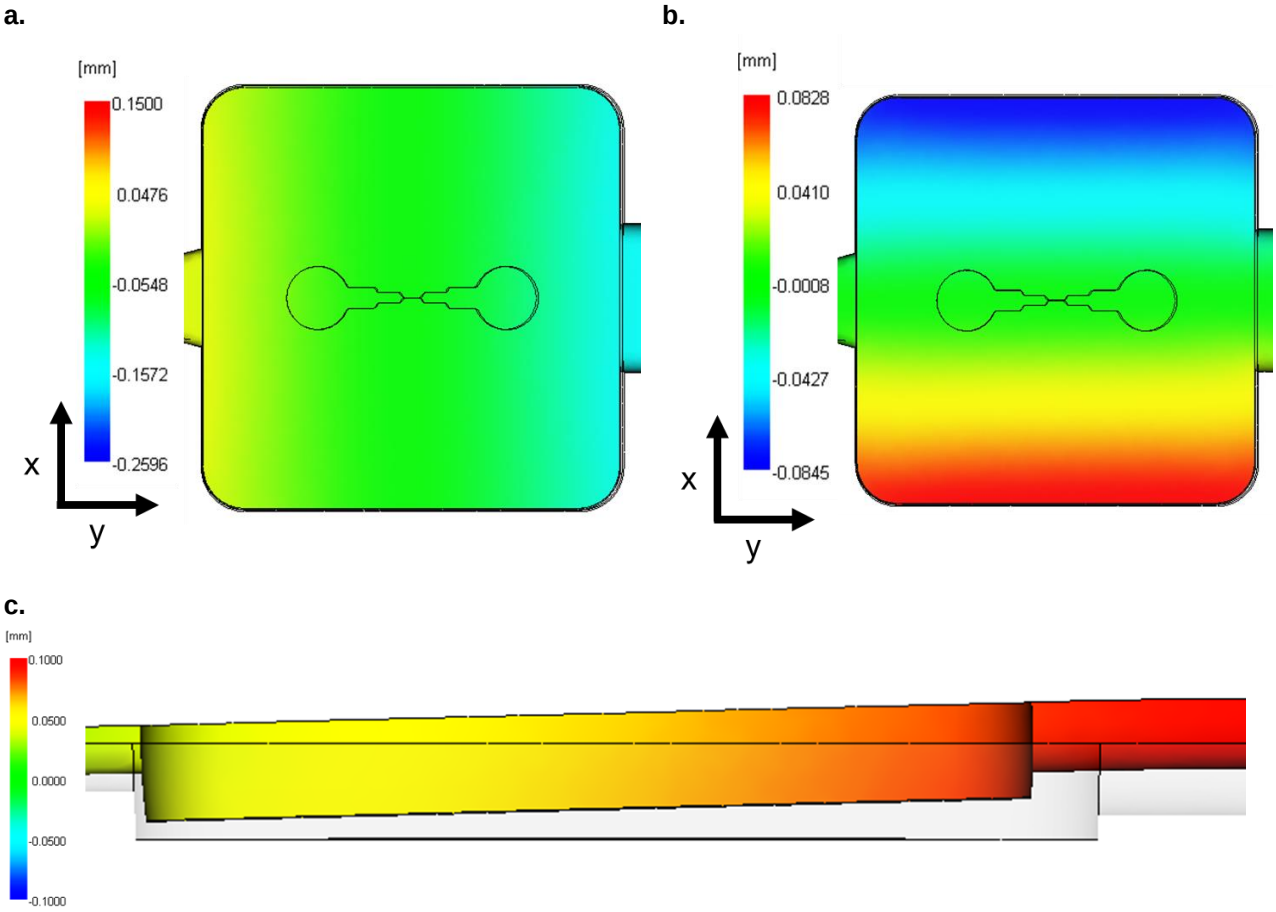

Fig. 4.12: Representative deflections for warpage considering all effects in x-direction (a), y-direction (b) and z-direction (c) (for better visualization, a scale factor of 10 is used here) [25]

- *From CT data*

The simulation results are just the initial predication which may not hold accurate especially for micro injection molding parts. It was possible to utilize the CT volumetric data to perform geometry deviations from the CAD model or the nominal geometry. The nominal-actual comparison was used in VGStudio Max. The best fit alignment was performed; the results are provided in Fig. 4.13 for both COC and PC parts. The part with PC material shows larger deviations than that of COC part; which could also be interpreted from the quantitative shrinkage results.

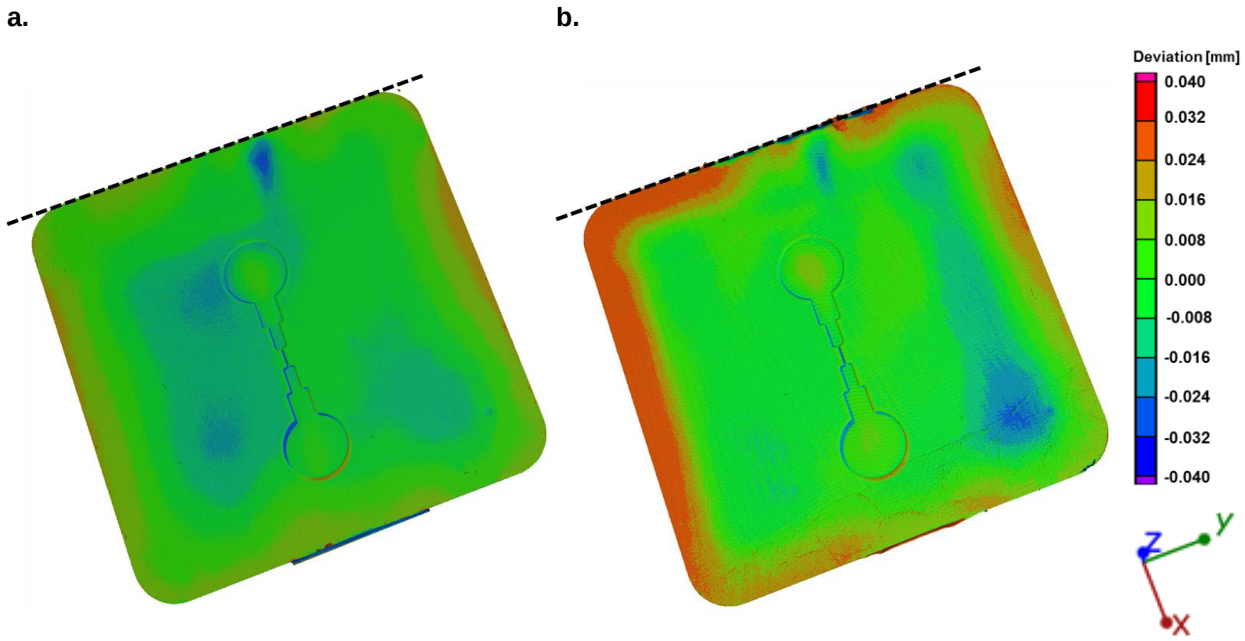

Fig. 4.13: Nominal-actual comparison performed on CT data for COC (a) and PC (b) [25]

It should be noted that the comparison has been performed with respect to the injection plane (dotted black line) as the part shows tendency to shrink towards that direction which is clearly visible from the simulation results in Fig. 4.12.

4.1.3.3 Micro-channel measurements

In addition to the specimen, the mold insert (Fig. 4.5 (a)) was also measured with confocal microscopy to compare the quality of replication. A plane form removal operator was used to level out a tilt (linear form), an inherent spherical component, or that exhibit or possess an unwanted polynomial term. The obtained extended topographies along with the 2D views are shown in Fig. 4.14.

The topographies are basically high density point clouds which are plotted with respect to the x, y and z coordinates, where z coordinate shows the height/depth of the micro channel. In general, the surfaces of both COC and PC appear to be similar qualitatively

with significant local height variations especially at the two circular regions. There is a strong curvature at the circular region where the height variation are huge. Bending is also visible in the mold insert (Fig. 4.14 (a)); which could be due to the fact that it was measured in the released state. The most insert is thin metallic plate which is fitted against the fixed half of the mold; therefore, it possess a slight bending even visible with naked eyes. More detailed information about the height variations can be acquired from the linear profiles along the axes.

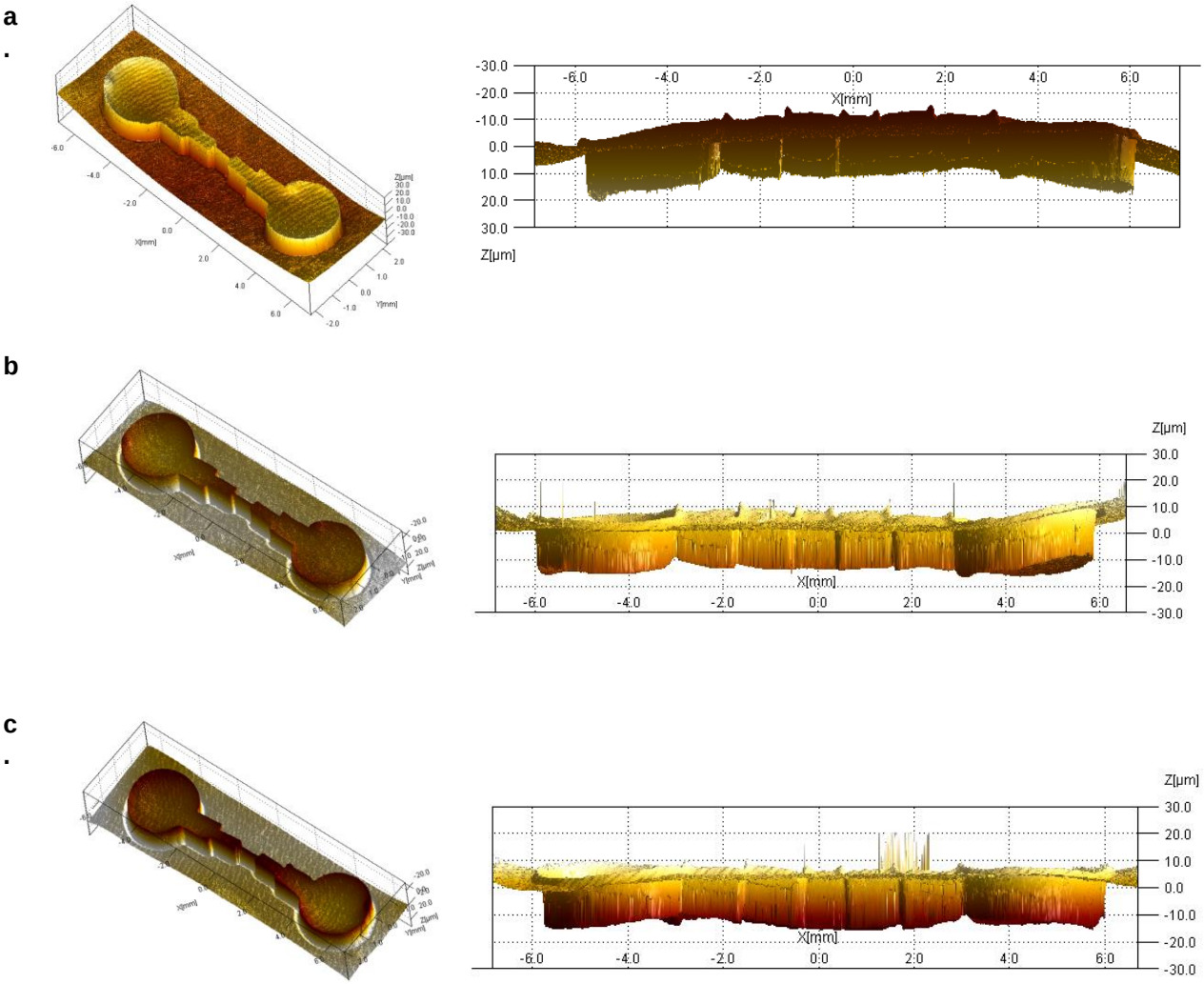

Fig. 4.14: Surface data obtained from 3D optical profiler: mold insert (a), COC (b) and PC (c)

As explained in Fig. 4.15, four profiles (A, B, C and D) were obtained along the y axis for estimating the channel width. Furthermore, another profile in the along the x axis was acquired to see the curvature which results into a large variation in the channel height.

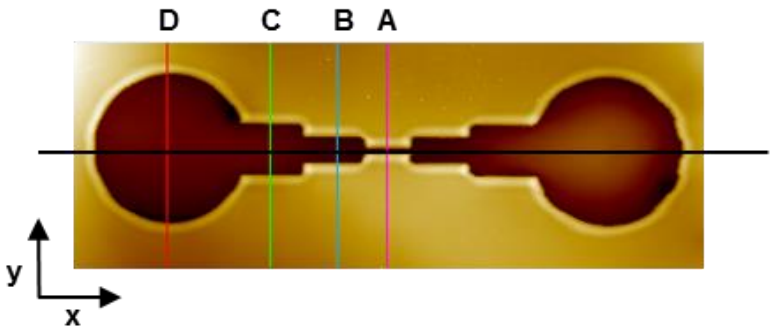

Fig. 4.15: Different profile selection along the x and y axes

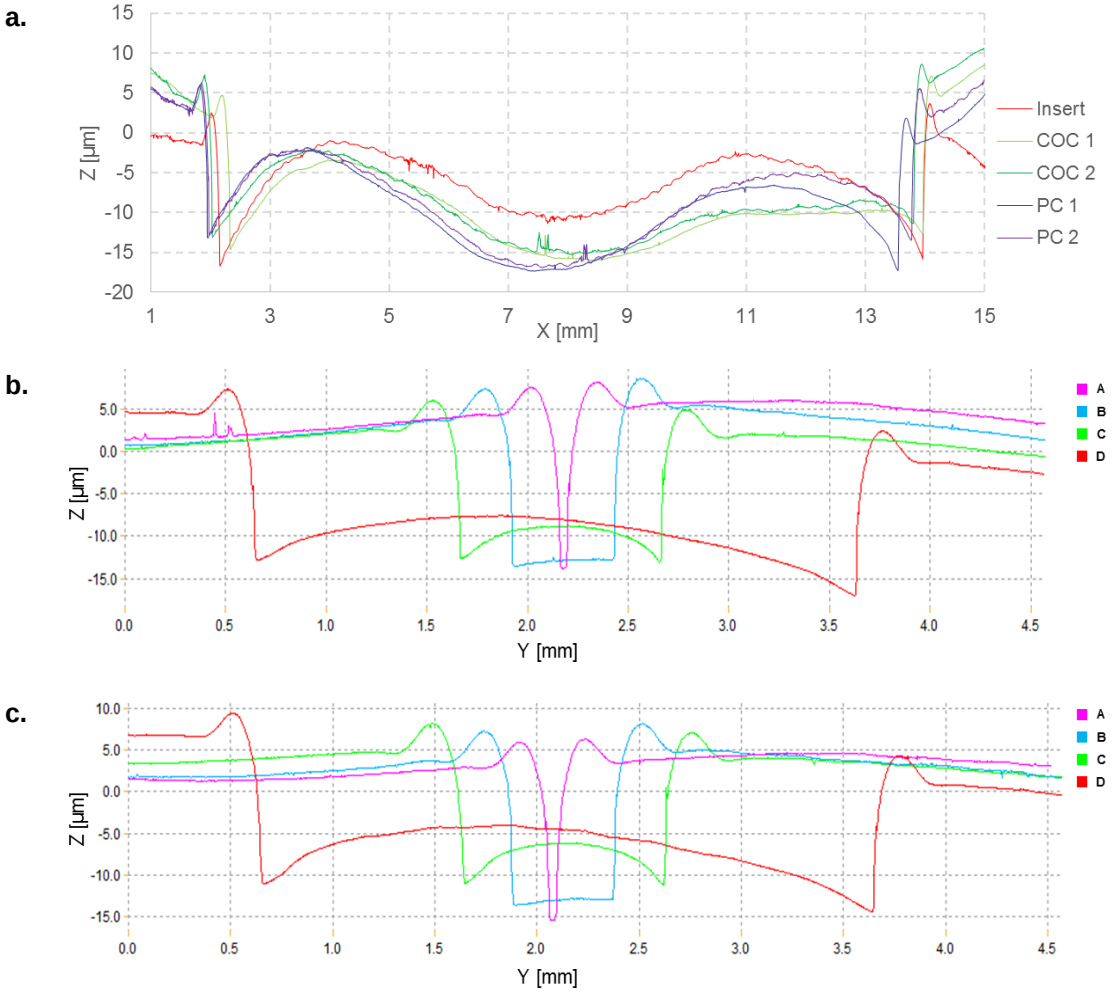

Fig. 4.16: Linear profiles obtained along the x axis (a) and y axis for COC (b) and PC (c)

From Fig. 4.16 (a), the 2D profiles along the x axis show a large curvature; which shows a local height variation of as big as 10-12 µm. Nevertheless, the curvature is replicated from the mold insert. In comparison to PC, COC has a bit falter profile. The curvature is also present along the y axis; the wider the channel the bigger the curvature is. Important

to note that the height varies roughly within a range of 10 to 20 µm; which makes CT data quite unreliable for measuring the micro channel features, as the CT resolution is also of the same order.

The measured average heights for mold insert, COC part and PC part are 18.17, 17.88 and 17.93 µm respectively; and the average widths are 30, 28.5 and 30.7 µm respectively; as presented in Fig. 4.17.

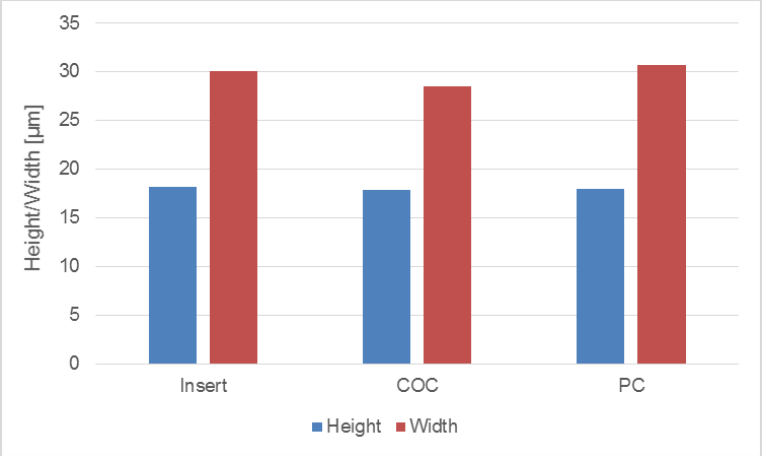

Fig. 4.17: Measured height and width of the channel

4.1.3.4 Data fusion

The data obtained from the each of sensors/techniques (CT and confocal microscopy) can be represented in the form of point cloud (defined by X, Y, and Z coordinates representing the external surface of an object). The density of the point differs according to the settings and resolution. When extracting the point cloud from CT data, the density can be varied according to the requirements. High density point clouds contain more details about the part surface. As shown in Fig. 4.17, the point density is considerably higher for the confocal microscopy data (the best point density was selected for CT data). For this comparison only a small ROI was used. The quality of the point cloud is the most important factor for data fusion techniques.

a. **b.** **c.**

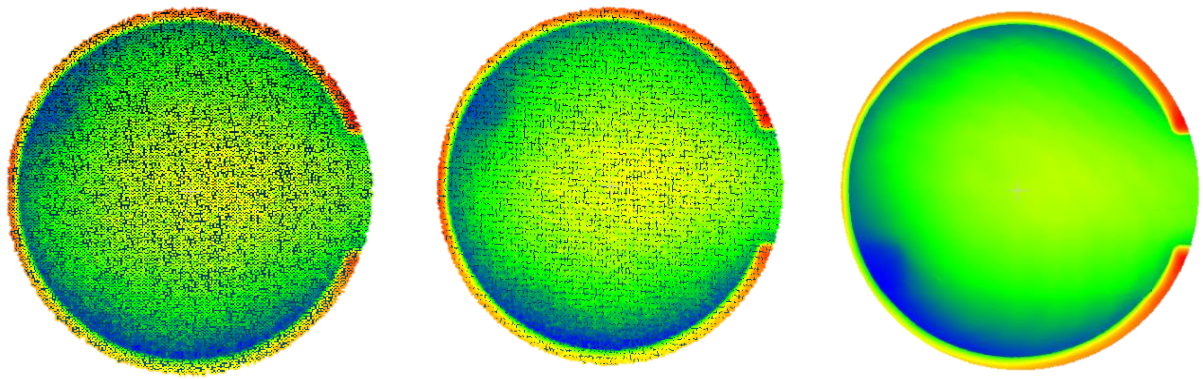

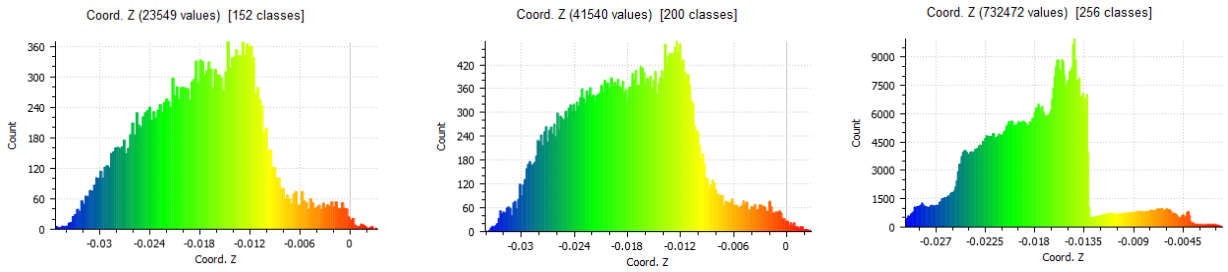

Fig. 4.18: Point cloud density of the data from CT at magnification of 15x (a), 20x (b) and confocal microscopy (c)

The purpose of using data fusion here is to combine the individual information (point clouds) and merge them together in a single dataset including both the complete geometry scanned by CT and the high density data for the micro channel area scanned by confocal microscopy. State-of-the-art ICP (Iterative Closest Point) algorithm was used for registration of 3D point clouds. This standard approach performs a fine registration of two overlapping point clouds by iteratively estimating the transformation parameters, and assuming that good a priori alignment is provided. A data fusion procedure was implemented using the software package GOM Inspect V8.

As already highlighted the goal of this activity is to have a single data set with the best information in terms of point cloud which can be utilized for the holistic quality assessment of such parts where both macro and micro details are important. The full part CT scan at the magnification of 15x was used at the base model. Although the density of points is lower here, but for the macro analysis it is significantly good. Therefore, the area containing micro channel is replaced with a high resolution data (i.e. CT partial scan at 20x and optical profiler scan). Thus, there are two possibility to employ the data fusion procedure:

- F1: Low resolution CT scan (CT15x) + high resolution CT scan (CT20x);
- F2: Low resolution CT scan (CT15x) + high resolution profiler scan (Pro).

The original CT dataset (CT15x) and the fused datasets, i.e. F1 and F2, are then compared with the CAD and the results are provided in Fig. 4.19 (a), (b) and (c) respectively. F1 does not show significant changes in the results as compared to the **CT15x** which is due to the fact the resolutions for both datasets were limited by CT constraints. F2 shows improvements at the micro channel region in the local height distribution compared to the **CT15x**.

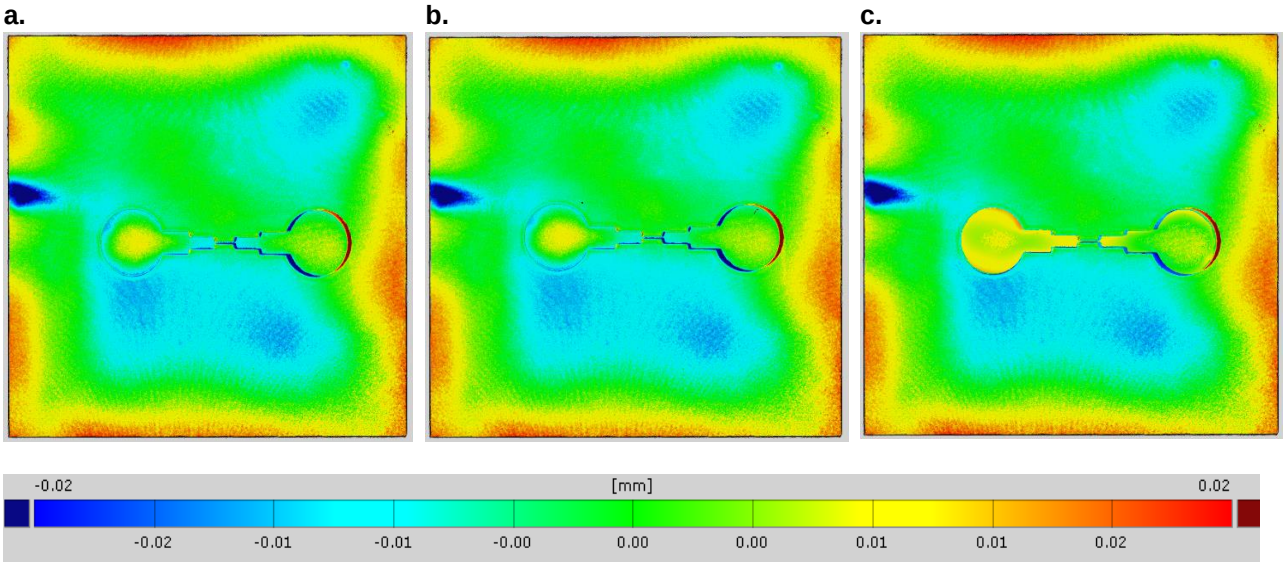

Fig. 4.19: CAD comparison obtained for CT15x (a), CT15x + CT20x (b) and CT15x + Pro (c) [25]

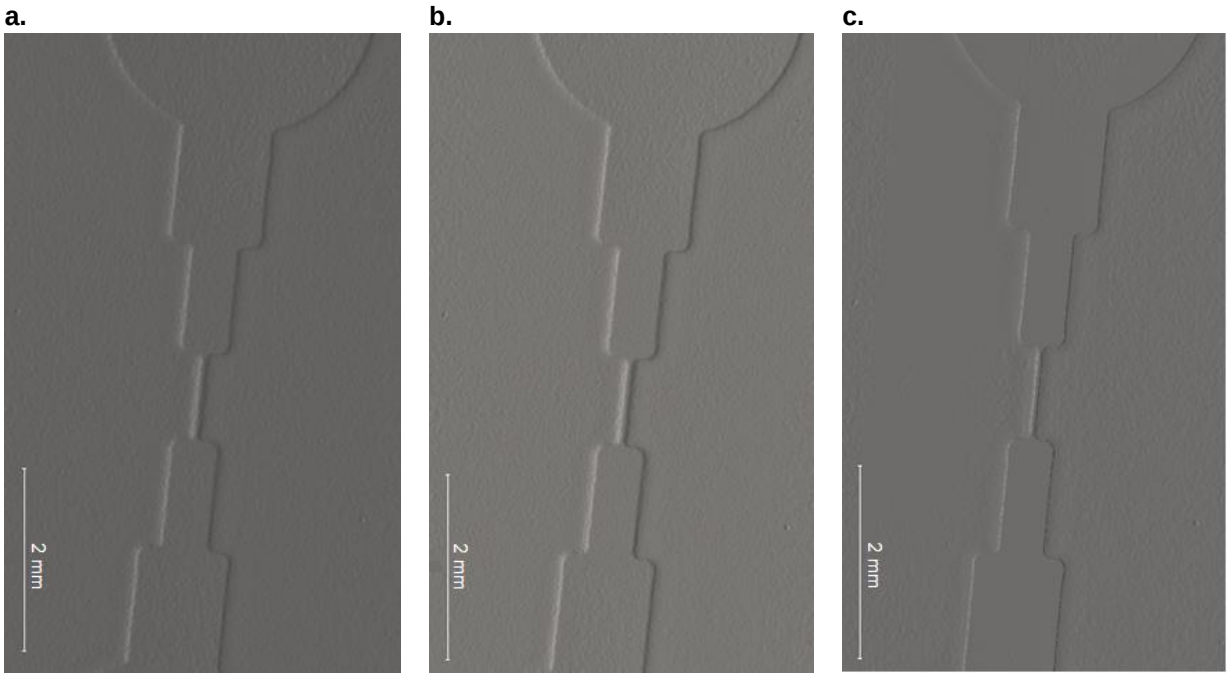

Fig. 4.20: Surface quality as resulted from the fused datasets CT15x (a), CT15x + CT20x (b) and CT15x + Pro (c)

The results were also compared qualitatively from the obtained single raw datasets as presented in Fig. 4.20. It can be seen in Fig. 4.20 (a) that the first fusion result (F1) show small improvement in the surface quality at the micro channel region as compared to original CT data, which is due to the fact that the difference in the resolution/point density is not really considerable. On the other hand, the second set of fused data (F2) shows

significant improvement at micro channel region owing to the higher resolution of the profiler data.

4.1.4 Conclusions

One of the most important applications of micro injection molding is microfluidics, which demands for holistic quality control for mass replication. X-ray CT as an emerging technology provides a significant improvement in quality control and reverse engineering due to its non-destructive nature. Within this work, a specific microfluidic system was selected as a case study which was manufactured with two materials: COC and PC. X-ray CT provided significantly important results as far as the part quality is concerned. The CT based measurement of the overall linear shrinkage of part revealed that the shrinkage is x and y directions is lower than 0.5% for COC and slightly higher than 0.5% for PC. In z direction, the COC part exhibits 3% shrinkage whereas PC exhibits 3.5%. Therefore, it can also be concluded that the part with PC witnesses more shrinkage compared to the COC. The non-uniform shrinkage resulted into warpage of the part, which was also possible to quantify from the CT results.

When it comes to the measurement of the micro channel, the resolution became the limiting factor of CT, therefore, confocal microscopy was used for this task. Thanks to the high resolution data, the local variations in the channel height were examined. The height varies from 5 µm to 20 µm resulting into a curvature along that plane.

To overcome the limitation (mainly resolution) of CT, data fusion was implemented by merging CT data with high density point cloud data obtained from confocal microscopy (profiler). To summarize, it was desirable to have a single raw point cloud dataset in several applications (e.g. microfluidics) to communicate measurement results in a robust way. At the same time, it allows the users to perform other analyses and/or measurements without compromising the quality of data since it is impractical to use high resolution scans for the entire part. Therefore, the fusion procedure provides the possibility to improve the resolution of regions of interest (ROIs) within the same dataset.

Future work can be done on the quantitative ways to assess the fusion procedure. In addition, the current research opened two points of concern which are: the accuracy of the stitching procedure from the confocal microscopy and the fusion procedures. Further investigation may be required on these issues.

4.2 Influence of Electron Beam Alignment

4.2.1 Introduction

The necessity of miniaturization arose during the second industrial revolution boosted by revolutionary developments of computer-based systems. Initially, it was restricted to 2D electronic circuits, but this scenario is slowly changing and miniaturization of 3D devices and systems which can physically interact with objects in the surrounding is being recognized as a potential way of bringing revolutionary changes to our society. Examples are: micro gears, injection nozzles and fiber optic components. Where dimensional tolerances are demands which have to be met in the micrometer down to the sub-micrometer range [26, 27]. Dimensional metrology is trying to meet these demands.

Nowadays, several technologies/equipment are available with microsensors, which are able to measure and provide accuracy in the micro range scale. Most common technologies/equipment are: tactile and tactile-optical probes, ultrasonic probes, optical sensors and micro computed tomography. As already discussed in the first part of the chapter, CT has the advantage of being a non-contact technique capable of acquiring a high density point cloud, of both internal and external geometries, of the object being measured [20, 28]. Due to its complex measurement chain, containing a vast number of influencing factors leading to a still high measurement uncertainty, CT has not yet being established as a reliable metrological technique since, so far, there are no standards which can deal with the system uncertainty and traceability to the internal standard of length [20, 29, 30].

This work was coordinated by KU Leuven and the findings have been published by Probst et al in [31]. The entire work can be divided in three separate parts focusing of three different case studies which are:

- The first consisting of the measurement of two ruby spheres (at KU Leuven)
- The second consisting on a porosity measurement of a polymer block produced by Laser Sintering (at Materialise)
- The third consists in the measurement of injection molding parts (at University of Padova)

The first two studies are excluded from this discussion. Only the third case study is discussed here in detail since it was performed within the framework of this PhD for CT base quality control of micro injection molded parts. Therefore, it is worth investigating the various influencing factors on CT measurement results. In this work, attention will be given to a specific influencing factor, the electron beam alignment, and its influence to the measurement results of CT metrology.

4.2.1 Electron beam alignment

As depicted in Fig. 4.21, the filament generates the electron beam which strikes the target material generating X-rays. The filament gets eroded over time, therefore, it needs to be changed at regular interval. After replacing the filament it is important to perform an alignment of the electron beam, steering the beam to a point where it's wobbling is minimal when a sinusoidal current based signal is applied to the X-Y coils. A poor alignment of the electron beam will lead to a poor focus, an unsharp edge and a loss of contrast between material and background. For instance, CT dataset acquired at particular set of scanning parameters but with a misaligned beam, will lead to erroneous measurements compared to measurements performed on CT data acquired at exactly the same set of scanning parameters but with a properly aligned beam.

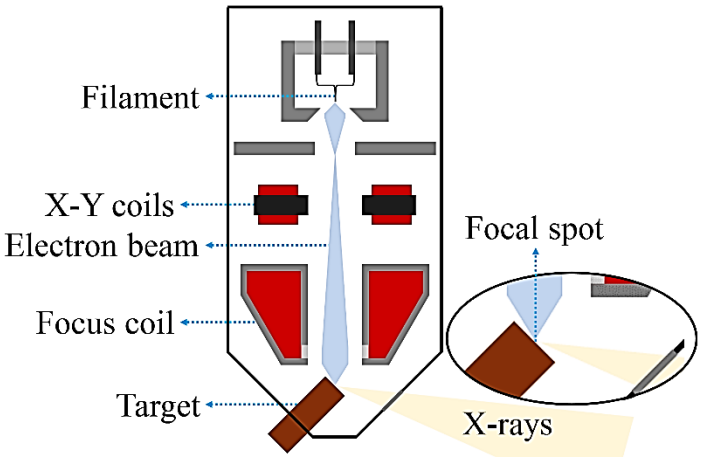

Fig. 4.21: Schematic of an X-ray gun [20]

The usual way of performing the electron beam alignment, prescribed by the manufacturer of the system has been used during the current work. An object with very small features is placed in front of the X-ray window; preferably touching the window in order to achieve the maximum magnification possible. Then, by lowering the exposure time to its minimal value and enabling the modulation on the software, the feature in sight will start to bounce in the radiography image, and to go in and out of focus, this is termed as wobbling. Whereupon, the user has to manipulate the controller in order to find the best combination of parameters which gives, as result, the minimal wobbling. Once these parameters are found, the modulation is switched off and the software takes charge of keeping the electron beam at the chosen position. The alignment shall then be performed until the image pulses in and out of focus rather than moving laterally or vertically.

4.2.2 Methodology

The state-of-the-art micro CT system MCT 225 was used during this work. Two different electron beam alignment conditions were employed during the experiments which are:

1. Interpolation alignment approach
2. Single alignment approach

The interpolation alignment is the procedure prescribed by the manufacturer. First, the beam is physically aligned at mid voltage (e.g. 140 kV). Then, the wobbling behavior is minimized for three voltages (two extremes and one intermediate e.g. 80, 150, 210 kV) by manipulating the x and y-shift on the software; and subsequently, the software makes an interpolation for the entire voltage range with using these three predefined values. On the contrary, the single alignment is the alignment at a particular voltage which is used for measurements (e.g. 100 kV in this case). The interpolation approach is advantageous in way that there is no need to perform the alignment during every scan/measurement; therefore, it is very important to verify the reliability of the interpolation method provided by the manufacturer.

A polymeric micro injection moulded was selected for studying the two beam alignment approaches for CT measurements.

The part has a symmetrical geometry with four identical cylinders. The measurands are the diameter of cylinders (D_1, D_2, D_3 and D_4) and center-to-center distances (C_{13} and C_{24}: between the diagonally placed cylinders 1-3 and 2-4). The nominal values for diameter and center-to-center distance are 0.8 mm and 2.23 mm respectively.

Since the aim was investigation of the effect of beam alignment on the measurement results, other parameters were kept fixed. However, to find out the right settings (voltage and current) for scanning, a number of trials were carried out. The optimized set of scanning parameters are reported in Table 4.6. In order to minimize the noise, averaging of 2 was used which doubles the scan time. Two different magnifications were tested.

Table 4.6: CT scanning parameters employed during the work

Parameter	Value
Voltage, kV	100
Current, µA	87
Exposure time, s	2
Number of Projections	3142
Averaging	2
Magnification	30x and 40x
Repetitions	3

4.2.3 Result and discussion

The measurements were recorded for all three repetitions at both the magnifications (30x and 40x) and the mean values and the standard deviations are reported in Table 4.7. The standard deviation is well below 1 µm which shows a very good repeatability of the CT measurements. The deviations of measured mean values from the nominal values are plotted for all the measurands in Fig. 4.22 and 4.23.

Table 4.7: Measurement results

Measurands	**Interpolation alignment**				**Single alignment**			
	40x		30x		40x		30x	
	Mean	Std. Dev.	Mean	Std. Dev.	Mean	Std. Dev.	Mean	Std. Dev.
D_1 [mm]	0.79877	0.00025	0.79883	0.00015	0.79887	0.00019	0.79925	0.00005
D_2 [mm]	0.80143	0.00048	0.80063	0.00058	0.80003	0.00074	0.80110	0.00090
D_3 [mm]	0.80093	0.00019	0.80080	0.00025	0.80030	0.00054	0.80035	0.00005
D_4 [mm]	0.80180	0.00008	0.80203	0.00017	0.80233	0.00012	0.80190	0.00000
C_{13} [mm]	2.21233	0.00045	2.21203	0.00026	2.21277	0.00100	2.21210	0.00020
C_{24} [mm]	2.21170	0.00099	2.21240	0.00045	2.21253	0.00068	2.21175	0.00005

As mentioned earlier, single alignment is the alignment at a particular voltage which is used for measurements, therefore, it is kept as the base for the comparison of the results. Interpolation is approach employed to save time and not to perform the alignment before each measurement or scan. Fig. 4.23 contains the deviations for the diameter measurements. In general, the interpolation, when compared to the single

alignment, is performing extremely well; furthermore, when the magnification is increased the performance gets improved.

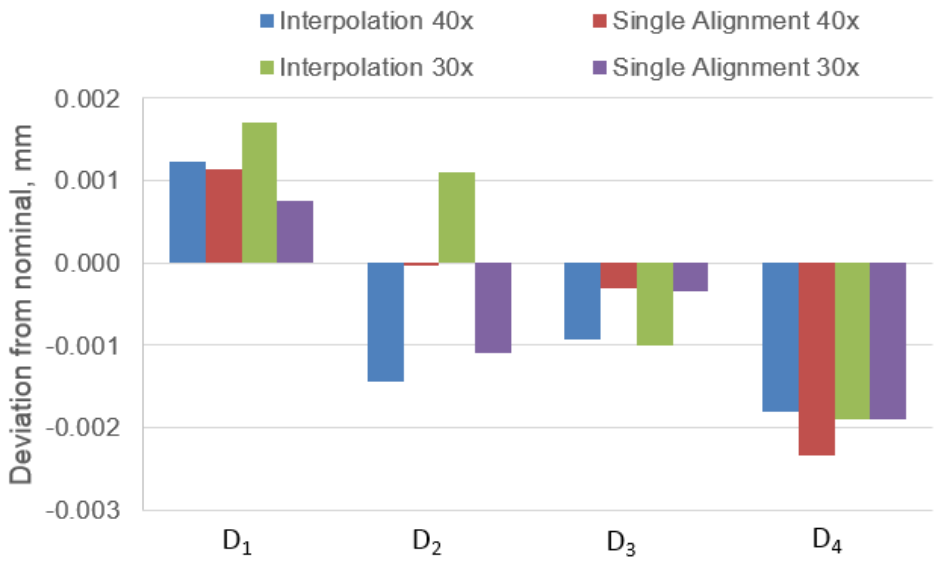

Fig. 4.22: The deviations in the diameter measurements

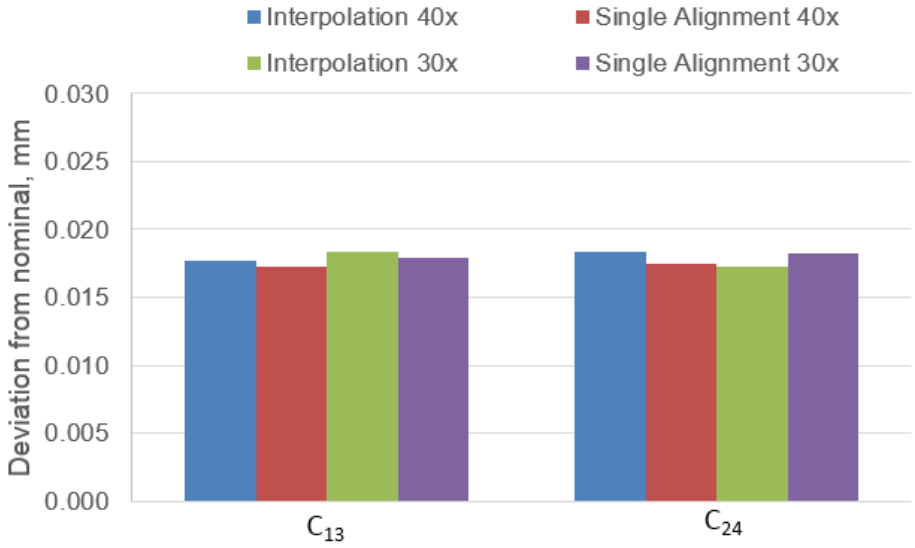

Fig. 4.23: The deviations in the center-to-center measurements

The deviations for center-to-center distance measurements are included in Fig. 4.22. The performance of interpolation approach is quite good in this case as well. It is clear from the two plots that the effect of the measurement conditions is not significant on the measurements. The interpolation seems to be very well optimized. The influence of

magnification is also not visible. However, it will be interesting to see the effect of alignment at lower magnifications.

4.2.4 Conclusions

The study aimed at investigating the influence of electron beam alignment on the measurements of micro injection molded parts. A part produced from micro injection molding was selected and some key features were identified as measurands. Two beam alignment conditions were tested: single alignment approach and interpolation approach to correct for the misalignment introduced when the voltage is changed (as prescribed by the manufactures of the CT system).

The results obtained at interpolation approach were compared against the single alignment approach. The measurement results are in good agreement with the single alignment results and the deviations are extremely minimal (less than 1 µm). There are some exceptions with deviations over 1 µm especially at lower magnification. Overall, the interpolation method perform really well and thus recommended to be used for measurements of such parts. However, it will be interesting to test the method at lower magnifications (below 30x).

Recent studies have also shown that the positioning of the filament in the cup holder also influences the alignment of the electron beam, furthermore, it may increase the focal spot. Further research is needed on how the positioning of the filament influences the electron beam alignment and therefore, CT metrology and quality control.

References

[1] Weber L, Ehrfeld W (1998) Molding of microstructures for high-tech applications. In: Proceedings of the 56th annual technical conference (ANTEC 1998). Part 3 (of 3), Atlanta, GA, USA, 26–30 April 1998.

[2] Angelov, A. K., & Coulter, J. P. (2004). Micromolding product manufacture: a progress report. In ANTEC conference proceedings (Vol. 1, pp. 748-751). Society of Plastics Engineers.

[3] Weber, L., Ehrfeld, W., Freimuth, H., Lacher, M., Lehr, H., & Pech, B. (1996, October). Micro molding—a powerful tool for the large scale production of precise microstructures. In Proc. SPIE (Vol. 2879, pp. 156-167).

[4] Becker H, Locascio L (2002) Polymer microfluidic devices. Talanta 56(2):267–287.

[5] Attia, U. M., Marson, S., & Alcock, J. R. (2009). Micro-injection moulding of polymer microfluidic evices. Microfluidics and nanofluidics, 7(1), 1.

[6] Niggemann, M., Ehrfeld, W., & Weber, L. (1998, September). Fabrication of miniaturized biotechnical devices. In SPIE Conference on Micromach. And Microfab. Process Tech (pp. 204-213).

[7] Piotter V, Guber AE, Heckele M, Gerlach A (2004) Micro moulding of medical device components. Business briefing: medical device manufacturing and technology, 2004.

[8] Yao, D. (2002). Injection molding high aspect ratio microfeatures. Journal of injection molding technology, 6(1), 11.

[9] De Mello, A. (2002). Focus: plastic fantastic?. Lab on a Chip, 2(2), 31N-36N.

[10] Pirskanen, J., Immonen, J., Kalima, V., Pietarinen, J., Siitonen, S., Kuittinen, M., & Pääkkönen, E. J. (2005). Replication of sub-micrometre features using microsystems technology. Plastics, rubber and composites, 34(5-6), 222-226.

[11] Wimberger-Friedl, R. (2000). Injection molding of sub-(mu) m grating optical elements. Journal of Injection Molding Technology, 4(2), 78.

[12] Whiteside, B., Martyn, M. T., & Coates, P. D. (2004). Micromoulding: process evaluation. In ANTEC. Conference proceedings (Vol. 1, pp. 757-761). Society of Plastics Engineers.

[13] Whiteside, B. R., Martyn, M. T., Coates, P. D., Greenway, G., Allen, P., & Hornsby, P. (2004). Micromoulding: process measurements, product morphology and properties. Plastics, rubber and composites, 33(1), 11-17.

[14] Bibber, D. M. (2004). Micro molding challenges. In ANTEC conference proceedings (Vol. 3, pp. 3703-3711). Society of Plastics Engineers.

[15] Rötting, O., Röpke, W., Becker, H., & Gärtner, C. (2002). Polymer microfabrication technologies. Microsystem Technologies, 8(1), 32-36.

[16] Whiteside, B. R., Martyn, M. T., Coates, P. D., Allan, P. S., Hornsby, P. R., & Greenway, G. (2003). Micromoulding: process characteristics and product properties. Plastics, rubber and composites, 32(6), 231-239.

[17] Bariani, P. “Dimensional metrology for micro technology”, Ph.D. thesis, Department of manufacturing Engineering and Management, Technical University of Denmark (2005).

[18] Hansen, H. N., Carneiro, K., Haitjema, H., & De Chiffre, L. (2006). Dimensional micro and nano metrology. CIRP Annals-Manufacturing Technology, 55(2), 721-743.

[19] Weckenmann, A., Jiang, X., Sommer, K. D., Neuschaefer-Rube, U., Seewig, J., Shaw, L., & Estler, T. (2009). Multisensor data fusion in dimensional metrology. CIRP Annals-Manufacturing Technology, 58(2), 701-721.

[20] Kruth, J. P., Bartscher, M., Carmignato, S., Schmitt, R., De Chiffre, L., & Weckenmann, A. (2011). Computed tomography for dimensional metrology. CIRP Annals-Manufacturing Technology, 60(2), 821-842.

[21] Esteban, J., Starr, A., Willetts, R., Hannah, P., & Bryanston-Cross, P. (2005). A review of data fusion models and architectures: towards engineering guidelines. Neural Computing & Applications, 14(4), 273-281.

[22] Galovska, M., Tutsch, R., & Jusko, O. (2012). Data fusion techniques for cylindrical surface measurements. Advanced Mathematical and Computational Tools in Metrology and Testing IX, 84, 179.

[23] Bartscher, M., Hilpert, U., Goebbels, J., Weidemann, G., Puder, H., & Jidav, H. N. (2006). Einsatz von Computertomographie in der Reverse-Engineering-Technologie. Materials Testing, 48(6), 305-311.

[24] Bartscher, M., Hilpert, U., Goebbels, J., & Weidemann, G. (2007). Enhancement and proof of accuracy of industrial computed tomography (CT) measurements. CIRP Annals-Manufacturing Technology, 56(1), 495-498.

[25] Rathore, J. S., Carmignato, S., & Lucchetta, G. (2016). Improving CT quality control of a micro injection molded part by multisensor data fusion. In 6th Conference on Industrial Computed Tomography (iCT 2016).

[26] Ontiveros, S., Yagüe-Fabra, J. A., Jiménez, R., Tosello, G., Gasparin, S., Pierobon, A. & Hansen, H. N. (2012). Dimensional measurement of micro-moulded parts by computed tomography. Measurement Science and Technology, 23(12), 125401.

[27] Carmignato, S., Dreossi, D., Mancini, L., Marinello, F., Tromba, G., & Savio, E. (2009). Testing of x-ray microtomography systems using a traceable geometrical standard. Measurement Science and Technology, 20(8), 084021.

[28] Marinello, F., Savio, E., Carmignato, S., & De Chiffre, L. (2008). Calibration artefact for the microscale with high aspect ratio: The fiber gauge. CIRP Annals-Manufacturing Technology, 57(1), 497-500.

[29] VDI/VDE 2011, Guideline for the application of DIN EN ISO 10360 for coordinate measuring machines with CT-sensors, VDI/VDE 2617 – Part 13 & VDI/VDE 2630 – Part 1.3.

[30] Bartscher, M., Sato, O., Härtig, F., & Neuschaefer-Rube, U. (2014). Current state of standardization in the field of dimensional computed tomography. Measurement Science and Technology, 25(6), 064013.

[31] Probst, G., Pavan, M., Rathore, J., Craeghs, T., Kruth, J. P., Carmignato, S., & Dewulf, W. (2015). Influence of Electron Beam Alignment on Dimensional Metrology by Computed Tomography. In Proceedings of the 2015 International Symposium on Digital Industrial Radiology and Computed Tomography. NDT.net.

CHAPTER 5. FIBER CHARACTERISTICS IN COMPOSITES

Chapter 5.
Fiber characteristics in composites

This chapter is focused on CT based characterization of fiber composite molded parts. The chapter contain two separate parts; the first part includes a comparative study of the CT fiber analysis results on a simulated and a real part. The effect of process parameters on the dimensional accuracy of micro injection molded is investigated in the second part of the chapter.

5.1 Validation of tomographic characterization

Over the recent years, the applications of short fiber reinforced polymers have increased, which is due several advantages including their lightweight, non-corrosiveness, high specific strength and stiffness. These properties are mainly dependent on the amount of fibers, their orientation, length distribution and spatial distribution within the matrix. Therefore, the quantitative assessment of these characteristics is of great significance. X-ray computed tomography (CT) is being successfully used as a three dimensional non-destructive measuring technique in industrial applications. One of recent applications is the analysis of fiber characteristics in fiber reinforced composite materials; however, the accuracy of such analyses depends on various factors (e.g. scanning parameters, resolution), which need to be investigated. The current work focuses on assessment of CT based analysis of fibers characteristics using simulation on a virtual fiber-model, which is followed by the validation of the simulation results with a thin-wall injection molded part.

5.1.1 Introduction

Short fiber reinforced polymer (SFRP) composites constitute relatively short and variously aligned fibers distributed in a continuous polymer matrix [1]. Glass, carbon, graphite and Kevlar are common materials used for short fiber reinforcements. In general, SFRPs are characterized by their versatile properties and low manufacturing cost, which make them extensively useful in automotive, electronics, marine, aerospace and household applications. Superior mechanical properties as compared to the polymer are the main advantage offered by SFRPs. However, these properties are greatly influenced by the fiber characteristics such as fiber-matrix interface strength, fiber volume fraction, fiber orientation distribution and fiber length distribution [1-3].

Injection molding (IM) is one of the most commonly employed manufacturing processes for large scale production of SFRP composites. Precision manufacturing of parts produced by IM recently attracted large attention for electronics applications, including connectors, because of their increasing market trends [3]. Despite the trend of miniaturization observed for IM applications, connectors remain relatively large, because of their complex design, which poses several manufacturing issues [4]. In particular, the thin-wall that characterizes their typical geometry constitutes a major manufacturing constraint [5]. Hence, the commercial breakthrough of new and smaller connectors strongly depends on the necessity to develop low cost mass production technologies, which can provide dimensional accuracy and good part quality [6].

It has been demonstrated in the literature that the quality and dimensional accuracy of injection-molded parts characterized by small thickness mainly depends on the injected polymer [7], the part geometry, the mold design, the selection of process variables [8] and fiber orientation [9]. In order to achieve the desirable fiber characteristics in the final molded product, the manufacturing process has to be optimized well by establishing a correlation of the processing parameters with the fiber characteristics [10]. For example, Oumer et al [11] presented a review of the effect of processing parameters on fiber orientation and effect of mold temperature on motion behavior of short glass fibers was studied by Li et al. [12]. These studies very much rely on the accuracy of the measurement technique for fiber analysis. A comparison between optical and tomographic methods for fiber analysis was performed by Bernasconi et al. [13]. They pointed out that the optical method requires a simpler experimental setup but it is destructive. On the other hand, tomographic technique is non-destructive but requires expensive experimental facilities. However, CT is an efficient tool for analyzing fiber orientation [14] since characterization of fiber orientation and of the skin-core morphology by optical observations of cross sections of the moldings can be very complex for thin-wall parts. In addition, as a non-destructive technique, CT eliminates the distortions introduced by sample cutting and preparation [15]. Nevertheless, CT has evolved over the years as a powerful technique for industrial applications owing to the continuous improvement towards the enhancement of the accuracy and traceability [14].

In the field of composite materials, CT is being used increasingly for various fiber-based analyses [15, 16]. In general, the accuracy of CT based analyses is sensitive to the selection of various scanning parameters (current, voltage and exposure time), spatial resolution (voxel size) and the system limitations (source, detector properties) [14]. In case of SFRP composites, the spatial resolution becomes very crucial due to the small size of fibers e.g. Kastner et al [17] reported the use of high resolution X-ray CT for fiber reinforced polymers. If high resolution is demanded, only a region of interest should be considered for achieving good spatial resolution instead of using the entire part [18]. The aim of this work is to investigate the dependence of the CT based fiber characterization on spatial resolution and scanning parameters by using a model based approach as it

helps in understanding the deviations from the true values. However, the final aim is to validate the findings from simulation using a real injection molded thin-walled part, which could then be used for the quality assessment of the final product.

5.1.2 Materials and methods

The details about the virtual fiber model and the real experimental part are included in this section.

5.1.2.1 Simulated fiber model

The fiber model generation was performed in collaboration with Volume Graphics (Heidelberg, Germany); the details have been published by Konopczyński et al in [19].

A virtual fiber data set of known fiber distribution and orientation was modelled with the aim of depicting the real properties of a specific material, which is eventually manufactured by injection molding for the validation of simulations. The material selected for this study was a commercial grade (BASF, Ultradur B4300 G2); it consists of 10 % (in weight) short glass fibers as reinforcement and polybutylene terephthalate (PBT) as matrix (Fig. 3.2 (c)). PBT is a semi crystalline thermoplastic polymer that is characterized by high shrinkage, making its processing critical in terms of dimensional accuracy. The introduction of fibers further complicates the prediction of the material behavior and thus arises the need to understand the behavior to achieve a desired dimensional accuracy; more details are discussed in Section 5.2.

In order to generate the virtual fiber model, the main a priori information is the fiber volume fraction (*FVF*), which can be deduced from the equation (5.1) using the provided fiber weight fraction (*FWF*) from the material specifications [20].

$$FVF = \left[1 + \frac{\rho_f}{\rho_m}\left(\frac{1}{FWF} - 1\right)\right]^{-1} \quad \textbf{(5.1)}$$

where, ρ_m and ρ_f are the density of matrix and fibers respectively (in g/cm^3). The other fiber properties required for the modeling are provided in Table 5.1.

Table 5.1: Fiber properties used for modeling

Property	Value
Fiber length, µm	500 ± 100
Fiber diameter, µm	13
Density of glass fibers (S-glass), g/cm^3	2.54
Density of matrix (PBT), g/cm^3	1.31

The fiber length is sampled from a normal distribution with a mean and standard deviation of 500 µm and 100 µm. The diameter is taken 13 µm which was roughly estimated from a high resolution (3 µm) CT scan of a PBT pallet as explained in Fig. 5.1.

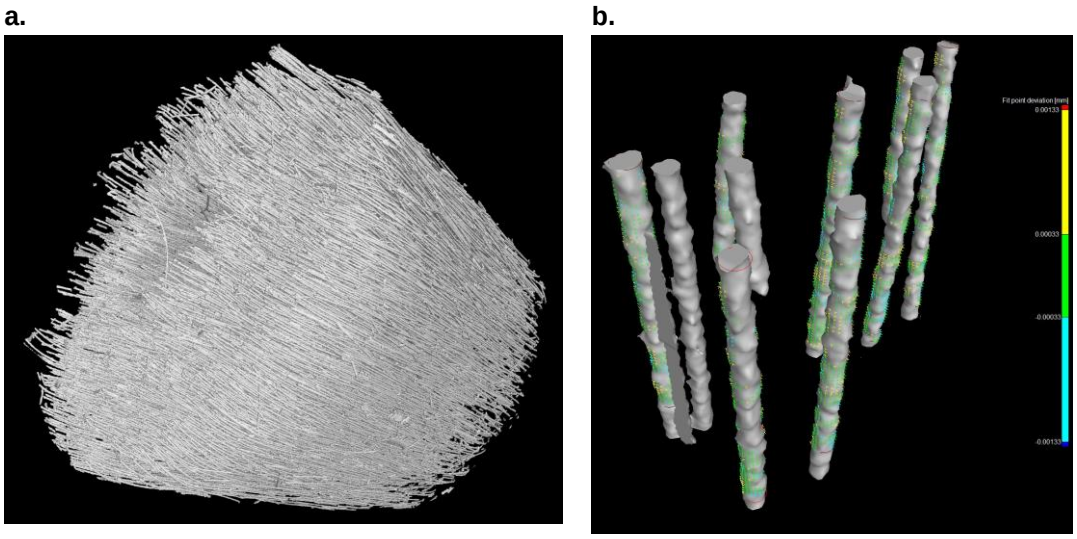

Fig. 5.1: Fiber diameter estimation from CT scan of a pallet

The fibers are assumed as solid cylinders of fixed density (glass) with given diameter and varied length. The surrounding matrix is created using a volume of (2 × 2 × 2) mm^3 to match the fiber calculated fiber volume of 5.39 %.

The model generation algorithm works in an iterative way. Once the desired dimension of the synthetic volume is defined (the dimensions of a cube), the algorithm randomly fits created fibers inside it. At the end of each successful iteration (i.e. an iteration after which a fiber is added to the model), the fiber ratio is calculated based on the provided densities of the fiber and PBT material. The algorithm terminates when the desired fiber ratio or the maximum number of attempts is reached. If the fiber has been generated inside the cube, and fits in such a way that it does not overlap with the previous fibers, it is saved as a set of points defining its surface. Due to the fitting process, the fibers are forced to be almost parallel to the surface of the cube the closer they are to its surface. Computation time depends on the properties of the model. The higher the desired content ratio of fibers the longer it takes to create the model [19].

5.1.2.2 Experimental part

For the validation of the CT analysis, it was desired to use a part produced by injection molding since it is the most commonly used manufacturing process and the fiber characterization is extremely important for such parts. Therefore, a thin-walled plaque geometry of (10 × 10 × 0.35) mm^3 was chosen (Fig. 5.2), which is used to evaluate shrinkage and the orientation tensor using µ-CT according to the conventional injection molding standards and methodologies proposed in the literature for thin-wall parts [21,

22]. More details about manufacturing are covered in Section 5.2.

This plaque geometry is identical to the model geometry except the lower thickness. The reasons for the selection of smaller model geometry are: first, only a small ROI can be considered for achieving high resolution which is limited by the field of view (FOV); second, it reduces the computation time for modeling.

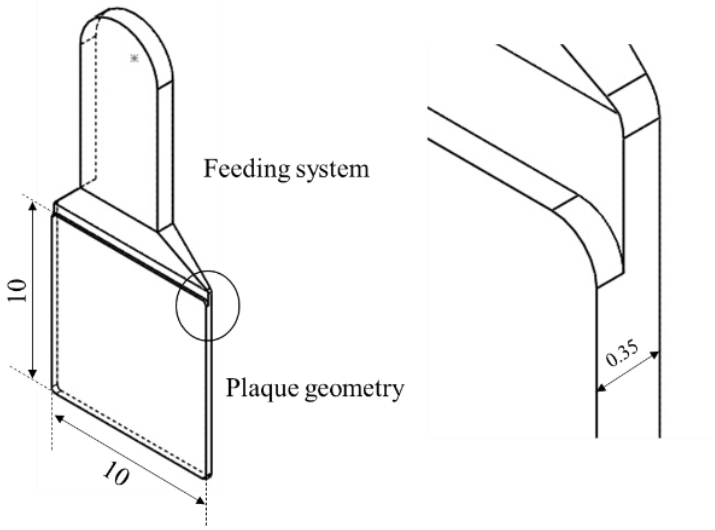

Fig. 5.2: Plaque geometry of 10 × 10 × 0.35 (all dimensions are in mm)

5.1.3 CT data acquisition

The metrological micro CT system (Nikon Metrology, MCT 225) was used for the fiber orientation measurement and analysis. The maximum permissible error (MPE) for this system is given by: (*9 + L/50*) µm (where *L* is the measured length expressed in millimeters) [23]. The metrological performances of the CT system were evaluated using specific procedures and a fiber-based calibrated object [24, 25].

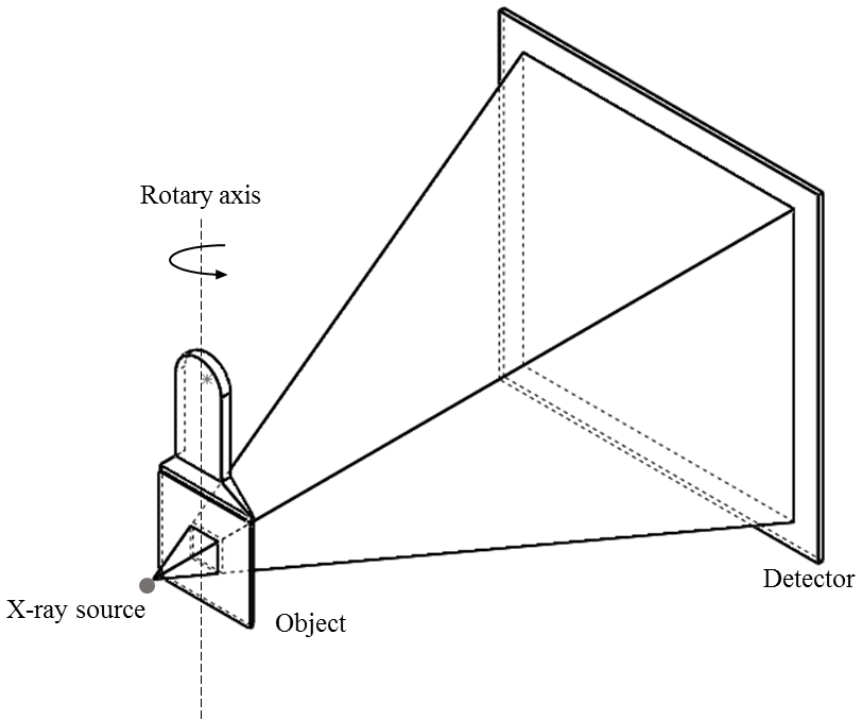

Fig. 5.3: Schematic representation of the CT scanning layout

Table 5.2: Different magnification settings

SOD, mm	15.69	23.54	33.62	47.08
Voxel size, µm	2.7	4	5.7	8
Notation	BR	HR	MR	LR

The part placement for the scanning is schematically shown in Fig. 5.3. The source-to-detector distance (SDD) is 1177 mm and four different source-to-object distances (SOD) were chosen, resulting in different magnifications (see Table 5.2) with corresponding resolution defined by a cubic voxel (volumetric pixel). The best, high, medium and low resolutions are termed as BR, HR, MR and LR respectively. Higher resolution is achieved by placing the object closer to the source but at the cost of smaller field of FOV. The X-ray projections are acquired for a complete rotation cycle and subsequently reconstructed into a 3D volumetric dataset. The CT scanning parameters were chosen with consideration of material density and by analyzing the grey value histogram on the projections. Two sets of CT parameters (see Table 5.3) were finalized to understand their effect on the results.

Table 5.3: CT data acquisition parameters

Factor	Set-1	Set-2
Voltage, kV	120	95
Current, µA	71	74
Exposure time, s	1.4	2.8
Number of Projections, Nr.	2000	1800
Averaging, Nr.	4	2
Scanning time, min.	~ 190	~ 150

- Simulation

ARTIST (Analytical RT Inspection Simulation Tool) software package from BAM, Germany, was used for CT simulation within the scope of this work [26]. The generated STL model of fibers was uploaded and embedded inside a cube geometry, which serves as the matrix. The material density and composition are required for the X-ray attenuation, which are used as reported in Table 5.1. The detector and source parameters were set based on the characteristics of the Nikon MCT225 X-ray CT system. The detector size has been set to 2048 x 2048 pixels, with a pixel resolution of 0.2 mm. For the noise factor, the signal to noise ratio (SNR) of the air of a real experimental projection was checked and adapted to the simulation.

5.1.4. Results and discussion

The various results obtained are presented and discussed in this section and interpretations are made. Mainly this section is divided into two parts based on the results of the fiber model and real part.

5.1.4.1 Fiber model

- Model statistics

The proposed computational model of SFRP composite has been set to match the fiber content of 5.40 %, which was calculated using the densities of glass fiber and matrix. The fiber model generation took around 6 hours of computational time on single CPU. The generated model is characterized by the properties listed in Table 5.4. The obtained fiber model and the corresponding length distribution are presented in Fig. 5.4. This virtual composite part was used for the CT simulation in ARTIST.

Table 5.4: Fiber model statistics obtained from the modeling

Number of fibers (n)	Total fiber volume ($n\pi r^2 l_{avg}$)	Average length (l_{avg})	Fiber volume fraction
	mm^3	µm	%
6628	0.432	491.231	5.399

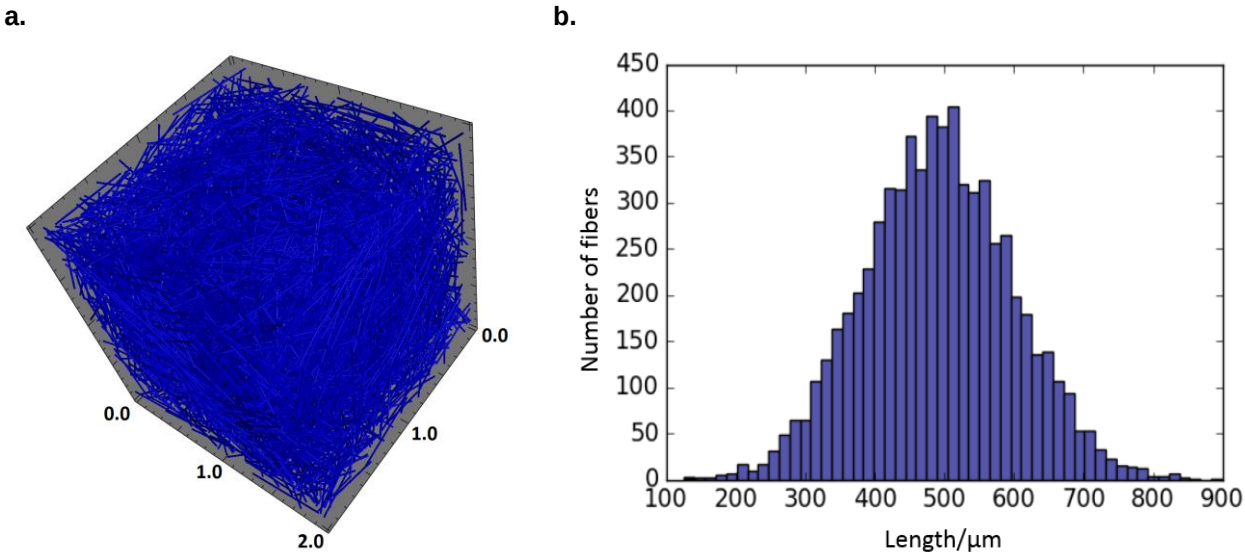

Fig. 5.4: Generated fiber model with a cubic matrix of 2 mm size (a) and the corresponding length distribution [19] (b)

- CT fiber analysis

The reconstruction of the CT projections was performed by use of the standard filtered back projection (FBP) reconstruction algorithm implemented in the reconstruction module of the commercial software VGStudio Max 3.0 (Volume Graphics GmbH, Germany). A common thresholding (ISO-50%) [27] method was used for determining the surface. In-built fiber analysis tool was utilized for obtaining fiber orientation and fiber volume results for all the simulated scans. A work flow for the analysis is shown in Fig. 5.5.

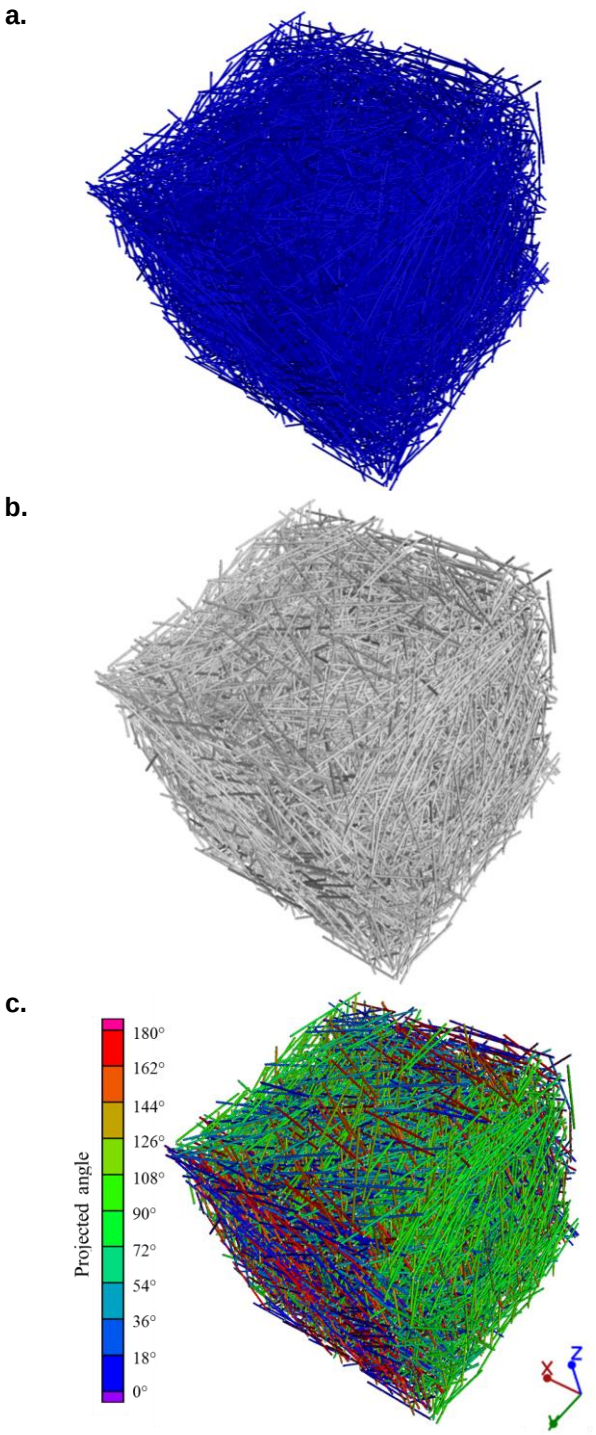

Fig. 5.5: Work flow: Fiber model for CT simulation (a) Reconstruction and surface determination (b) and Fiber analysis (c)

For fiber orientation, the mode “plane projection” was selected since it is preferred when injection molding parts with a preferred plane or surface of orientation are analyzed. It calculates the 3D orientations of the fibers, projects them into a user-defined plane and then calculates the projected angle from the reference axis within that plane (see Fig. 5.5 (c)). The fiber orientation tensor is extracted for better interpretation is plotted against the

thickness of the part and the results are shown in Fig. 5.6. The tensor has three principal components (A_{11}, A_{22}, A_{33}); only the first principal component (A_{11}) is considered reported here for the comparison. The results show almost identical behavior; neither the CT settings nor the resolution are significantly affecting the fiber orientation results for the chosen resolutions. This information is useful because sometimes it is not practically possible to achieve very high resolutions.

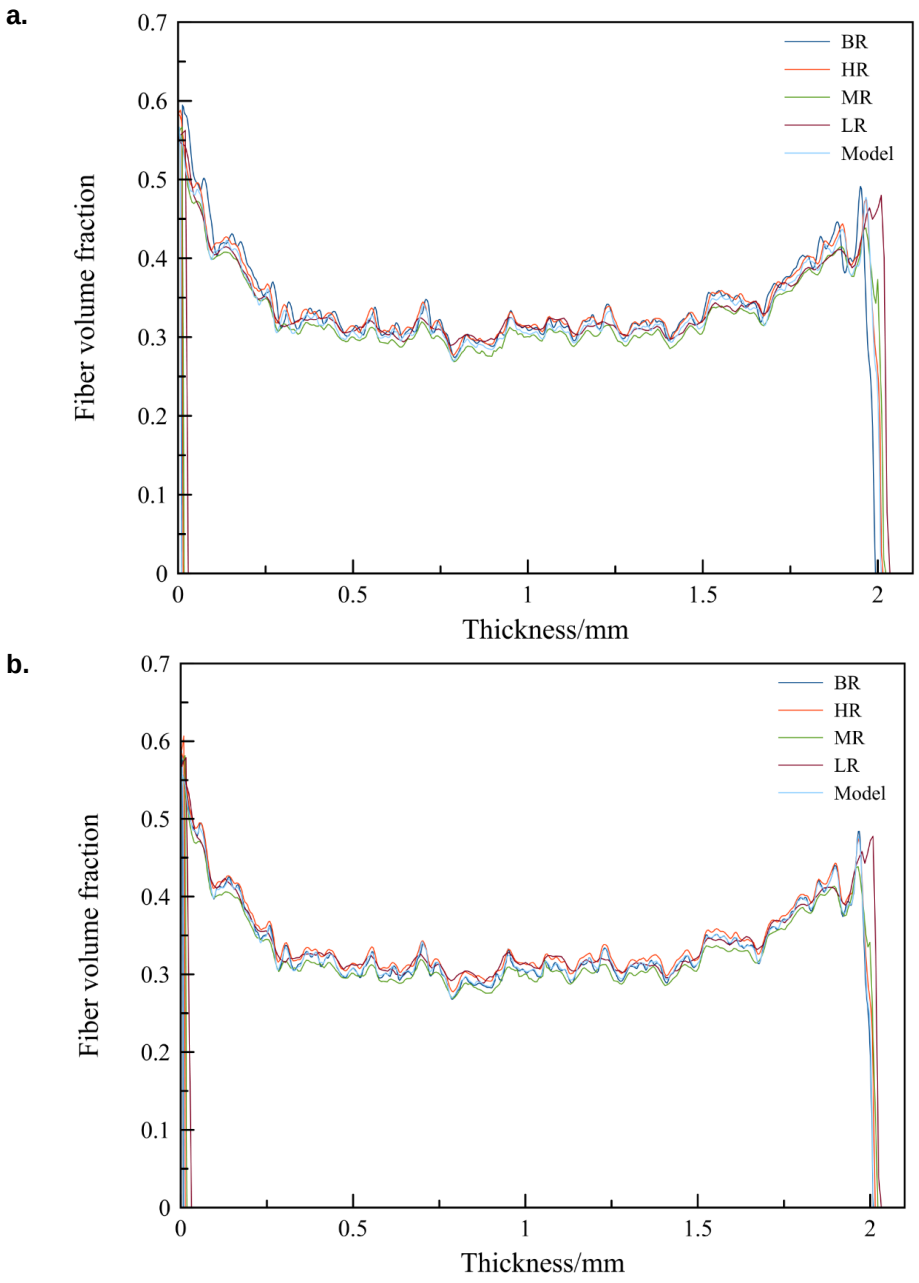

Fig. 5.6: Fiber orientation tensor component for (a) Set-1 and (b) Set-2

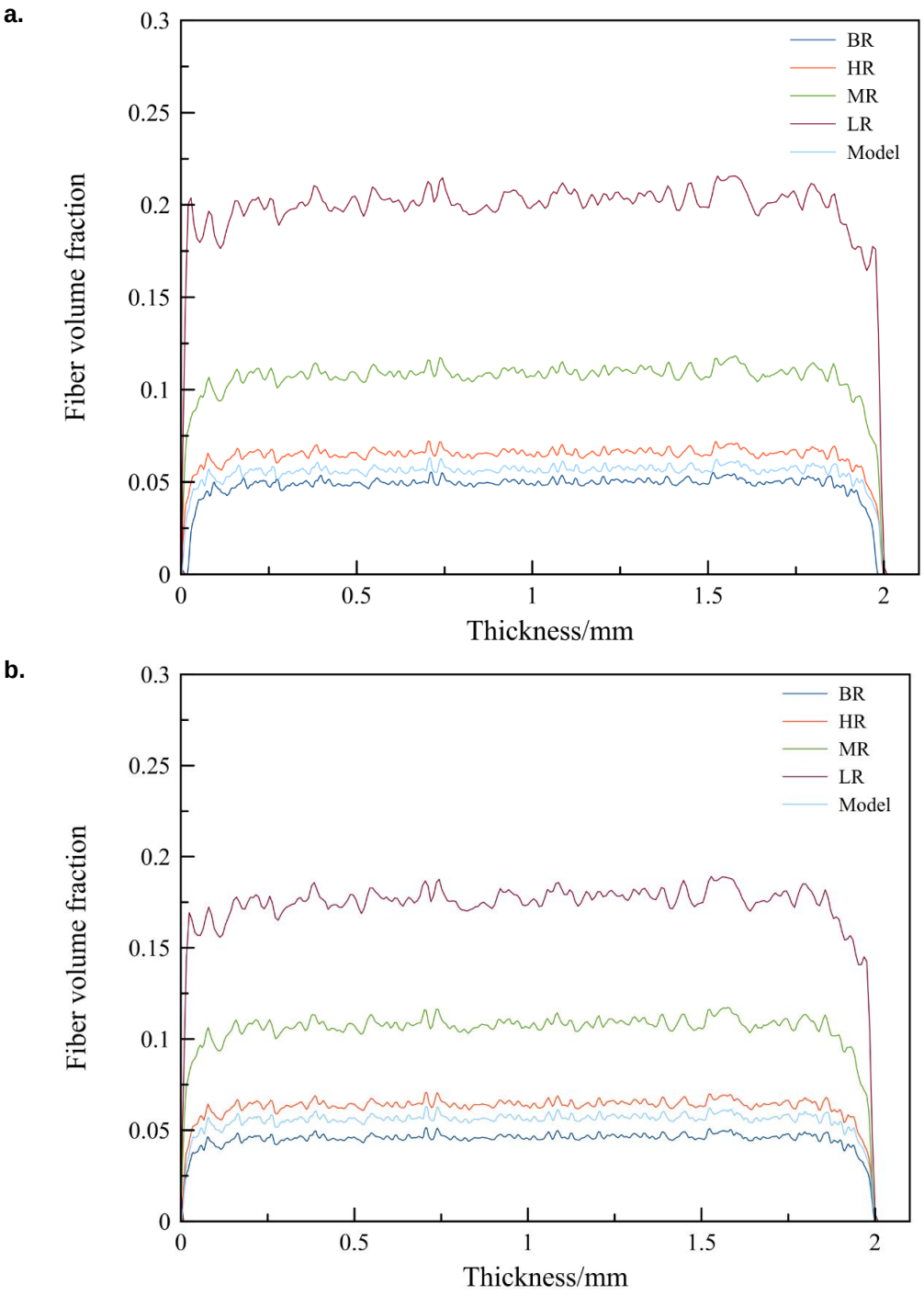

Fig. 5.7: Fiber volume content as a function of thickness for (a) Set-1 and (b) Set-2

On the other hand, the fiber volume content is greatly affected by the resolution, see Fig. 5.7. It becomes more evident in the (Otsu) segmented 2D slices taken at the center of the part (Fig. 5.8 a-d) that the fiber content is overestimated with lower magnifications, which is due to the increased voxel size. Increasing the voxel size (i.e. decreasing the spatial resolution) from 2.7 µm to 8 µm, results in 300 % higher estimation in fiber content. In order to get comparable results it is recommended to use voxel size ≤ 4 µm. It

is also visible from the cross section that the error in volume is mainly due to the overestimation of diameter.

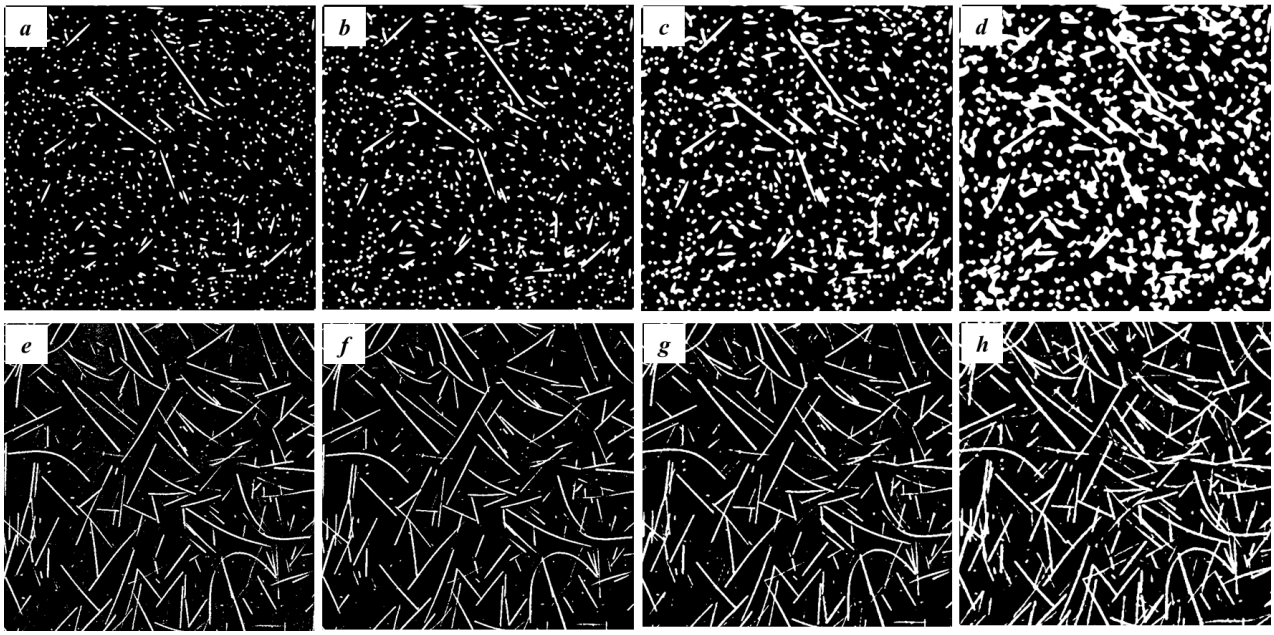

Fig. 5.8: 2D cross-section obtained at the center of the simulated part (*a,b,c,d*) and real part (*e,f,g,h*) for BR (*a,e*), HR (*b,f*), MR (*c,g*) and LR (*d,h*)

5.1.4.2 Real part

The manufactured part was scanned in order to validate the simulation results; since both the sets of CT parameters produced almost identical results for the virtual part, only the set-2 parameters were employed for scanning the real part due to its lower scanning time. The part was scanned at all the four magnifications; however, the scanned area for the BR and HR scans was partial due to the limited FOV, as explained in Fig. 5.3. Therefore, a common area of (2 × 2) mm^2 through the thickness was chosen for the analysis of all the magnifications. The area was precisely selected at the center of the part as shown in Fig. 5.9.

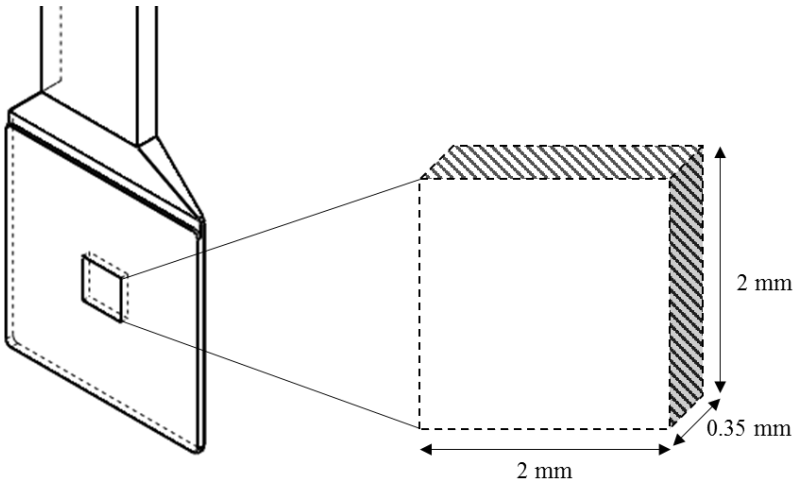

Fig. 5.9: ROI selection on the real part

- Fiber orientation

It is important to understand the fiber orientation in the flow and transverse direction for injection molded parts, which are considered for the analysis and the obtained results are reported in Fig. 5.10. The results are in good agreement with the simulated results, as the resolution is not affecting the fiber orientation. However, the lowest resolution (LR) produced slight deviation in the transverse direction as compared to the identical results of other three resolutions (MR, HR, BR); which could be explained by the fact that further lowering the resolution might produce longer deviations. Therefore, it is concluded that the resolution does not affect the fiber orientation results but up to a certain voxel size.

a.

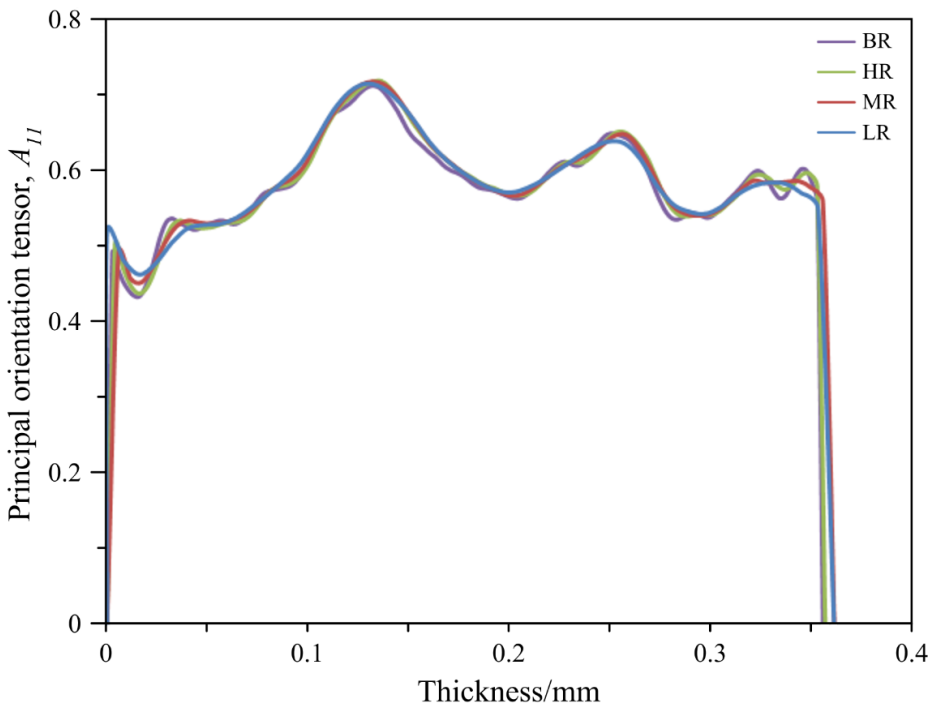

b.

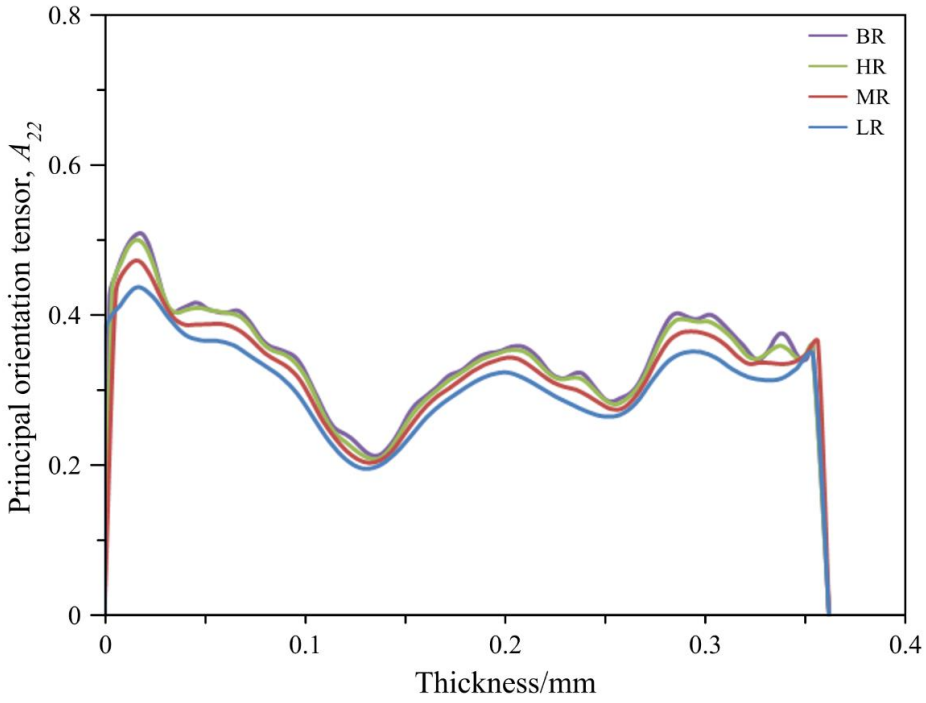

Fig. 5.10: Fiber orientation results obtained from the real part for all four magnifications (a) tensor component A_{11} (along the flow direction) and (b) tensor component A_{22} (along the transverse direction)

- Fiber volume content

The fiber volume content results obtained on the real part for different resolutions are shown in Fig. 5.11 (a). The results follow similar trends, which were observed in the simulations. The fiber volume content along the thickness direction is overestimated when using a lower resolution. As already stated, the increased voxel size results in significant error in the evaluation of diameter of the fibers, which is responsible for the large overestimation of the volume as visible in the cross sections in Fig. 5.8 (e-h). However, an important thing to be noticed in both the simulation and real scans is a slight underestimation in the volume at the best resolution (Fig. 5.11 (b)). This unusual behavior is rather difficult to quantify but can be explained with the increased X-ray image blurring at higher magnification and the resulting shift of the surface determination is shifted towards the material side [27].

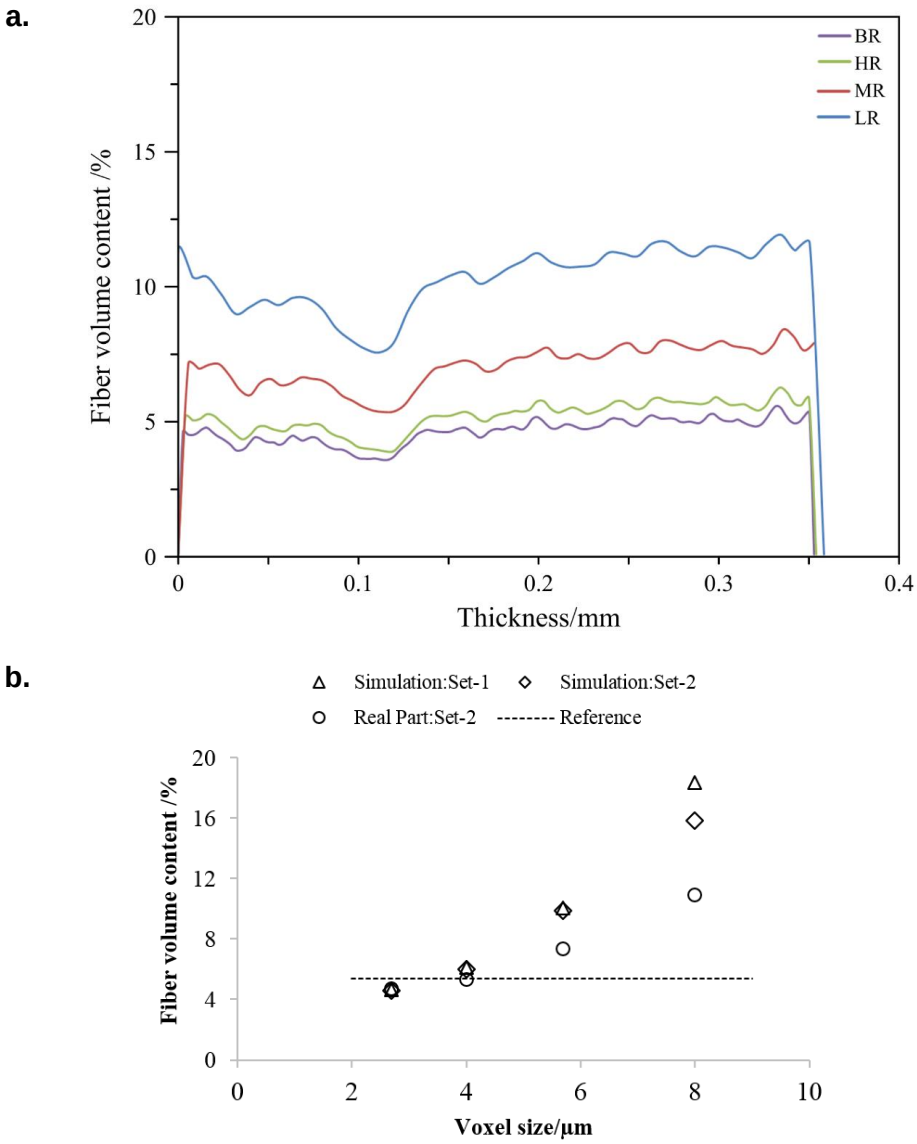

Fig. 5.11: Fiber volume content results obtained from the real part for all four magnifications (a) and the obtained fiber volume content as a function of voxel size (b)

From Fig. 5.11 (b), it can be observed that the results from both the simulation and real part are in good agreement for BR and HR i.e. up to the voxel size 4 µm; moreover, further increasing the voxel size yields deviations in the results. It can be concluded that the voxel size does not affect the volume evaluation to a very limited voxel size, which is considerably higher (~ 4 µm). In industrial practices, it is difficult to achieve such high resolutions, therefore, there is need to find a correction of the overestimation. From Fig. 5.8, it is visible that the main cause of volume overestimation seems to be error in diameter. However, with the help of fiber diameter (d) and average fiber length (l_{avg}) and the number of fibers (n), the mean error in diameter can be calculated with the equation (5.2) since $l_{avg} >> d$, the error in length can be neglected.

$$V = n\pi \left(\frac{d+e}{2}\right)^2 l_{avg} \quad \textbf{(5.2)}$$

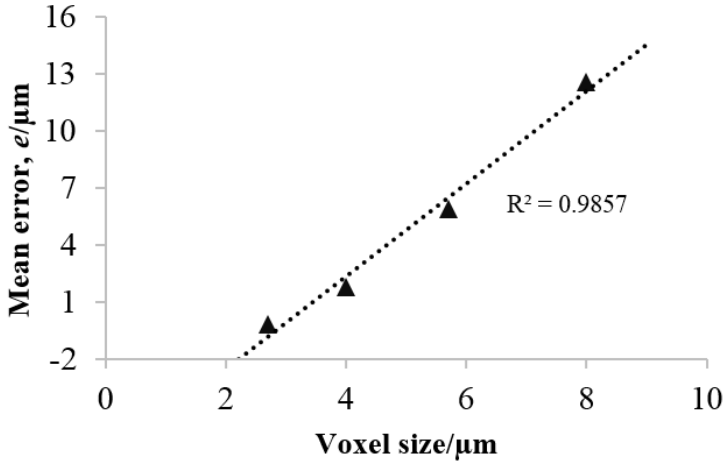

Fig. 5.12: The estimated error in diameter as a function of voxel size

As shown in Fig. 5.12, the mean error in the diameter was calculated for the simulation results thanks to the known information about *n*, *d* and l_{avg}. It can be seen that the mean error is linearly increasing with the voxel size; therefore, it can be compensated with known information of number of fibers, average length and diameter. However, for real parts this could be difficult as the true values of these parameters are unknown due to the fact that the processing parameters affect *n* and l_{avg}.

5.1.5 Conclusions

First, CT based characterization of short glass fiber composites is analyzed using simulations of a virtual composite part of a commercially used material and second, the findings from simulations are validated based on experiments on a real composite part of the same material.

The major advantage of CT technique is its non-destructive nature, though which is partially true when high resolution is required and the part is longer than the field of view. Thanks to the simulation study, it is evident that the fiber orientation results are not significantly affected by the resolution and the employed CT settings. This observation was confirmed by the experimental results from the real part. On the other hand, the fiber volume is greatly affected by the voxel size of the CT data, e.g. 300 % overestimation for voxel size 8 µm. Similar results have also been observed from the experiments on the real part with a good agreement up to a voxel size of 4 µm and then large deviations in both the simulated and real part results are witnessed. It was also demonstrated that the

error in volume measurement can be compensated with the known fiber length, diameter and number of fibers.

It can be concluded that the effect of the spatial resolution on the fiber orientation results is negligible for the voxel sizes tested in this work. Therefore, a large area of the part/full part can be considered for the fiber orientation analysis of the experimental part. On the other hand, it is recommended to use higher resolution for analyzing the fiber volume content from CT.

5.2 Effect of process parameters on dimensional accuracy

The effect of injection molding conditions on the dimensional accuracy of thin-walled fiber composite material parts is investigated in this work. The correlation between the distribution of short glass fibers within the part and its dimensional accuracy was achieved by using X-ray computed tomography. A design of experiment was performed for the statistical analysis. The experimental results demonstrated that melt temperature and packing pressure were the most significant processing parameters affecting the shrinkage of thin-wall parts. Particularly, a selection of high values for these parameters allowed for the minimization of the dimensional difference between the mold and the final parts. The analysis of the cross sections of the molded parts allowed the observation of an almost flat trend of the orientation tensor for parts molded at lower injection speed, indicating the absence of the core layer. It caused a higher shrinkage along the transverse direction that eventually led to a differential shrinkage and to the warpage of the final part. This work was a joint effort between the injection molding and the X-ray CT research groups of University of Padova. The main findings of the work have been published by Davide et al. in [10].

5.2.1 Introduction

Injection molding has established as one of the most flexible, reliable and cost effective manufacturing technologies to produce complex plastic components [28]. Precision manufacturing of parts produced by injection molding recently attracted large attention for electronics applications, including connectors owing to their increasing market trends [3]. Despite the trend of miniaturization observed for molding applications, connectors remain relatively large, because of their complex design, which poses several manufacturing issues [5]. In particular, the thin wall that characterizes their typical geometry constitutes a major manufacturing constraint [6]. Hence, the commercial breakthrough of new and smaller connectors strongly depends on the necessity to develop low cost mass production technologies, which can provide dimensional accuracy and good part quality [7].

It has been demonstrated in the literature that quality and dimensional accuracy of injection-molded parts characterized by small thickness mainly depends on the injected polymer [8], the part geometry, the mold design and the selection of process variables [9]. Shrinkage and warpage are common defects resulting from the IM process that can impair quality and functionality of final parts [29]. In this sense, reducing and controlling shrinkage is very important to control dimensional accuracy of products, especially when manufacturing parts characterized by tight tolerances [30].

The intrinsic cause for polymer shrinkage is the thermodynamic behavior of polymers, which is responsible for dimensional variations in injection-molded parts. In order to guarantee process quality, it is then important to minimize the difference between the mold and the part dimensions, especially for applications requiring tight fit tolerances.

When dealing with injection molding, it is necessary to control many process parameters that can influence the dimensional accuracy of the parts by altering their shrinkage behavior [31]. For this reason, it is important to understand the effect of the controllable process parameters in order to improve the quality of the final parts. In general, shrinkage minimization of injection-molded parts is better performed with the adoption of statistical approaches [32]. Researchers reported in the literature that the main injection molding parameters affecting the overall shrinkage are cooling time, packing pressure [33, 34], melt temperature [35] and injection speed [36]. However, the identification of the most critical processing parameters influencing the dimensional accuracy cannot be separated from material properties and part design [37]. The combination of these factors in the case of thin-wall parts makes the shrinkage behavior and the process parameters selection particularly critical.

The achievement of structural and thermal stability are fundamental requirements for the manufacturing of micro connectors, thus leading to the selection of high performance materials, characterized by good mechanical and thermal properties, such as fiber-filled polymers [38]. However, the use of reinforced polymers poses some processing issues, related to the anisotropic distribution of fibers within the parts, which eventually affects the shrinkage of the parts [39]. Azaman et al numerically investigated the injection molding of thin-wall parts (thickness 0.70 mm) indicating that the presence of 10% weight glass fibers affect the shrinkage of the parts [40]. Glass fibers affect the shrinkage of thin-wall injection molded parts by modifying their morphology. Cadena-Perez et al. showed that the addition of fiber fillers completely change the shrinkage behavior of the polymer parts [41]. In particular, they showed their significant effect in the melt flow direction and the null effect in the transverse one.

The fiber orientation in injection-molded parts is determined and affected by the geometry of the mold and by the molding parameters [42]. Several researchers have studied how the fiber orientation tensor is influenced by the injection molding parameters [43, 44]. Nevertheless, the correlation between fiber distribution and parts shrinkage has not been investigated for thin-wall parts yet.

Experimental studies about the IM process demonstrated that shrinkage is affected by scale effects [45], especially due to the different morphology of the parts, which is caused by the high shear rates that characterize the thin-wall IM process [46, 47]. In general, fiber orientation within injection-molded parts is explained considering the 'fountain-flow' model [48]: the shear effect is more marked in the skin layer and consequently is the orientation in the melt flow direction; conversely, in the core region, the melt flow is subjected to the minimum shear and the orientation is considerably

lower. However, this behavior can be modified by the diverse thickness ratio between the skin and core layers in the case of very small thickness [49].

Characterization of the skin-core morphology and of fiber orientation by means of optical observations of cross sections of the moldings can be very complex for thin-wall parts. In this sense, micro computed tomography is a powerful technique to analyze fiber orientation [50]. As a non-destructive testing method, micro CT analysis can also eliminate the distortions introduced by sample cutting and preparation [51].

5.2.1.1 Motivation

Production of micro connectors is one of the applications where high precision is demanded due to the complexity of features and strict tolerances as shown in Fig. 5.13.

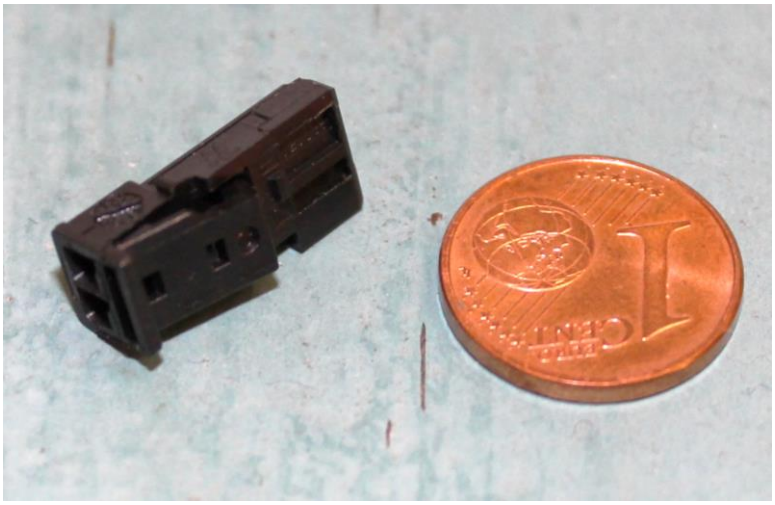

Fig. 5.13: A type of a micro connector with complex features

This is manufactured with fiber reinforced material due to the offered advantage such better mechanical properties, durability etc. Nevertheless, the use of fiber-reinforced polymers also affects the desired accuracy, as visible from CT scan results in Fig. 5.14. A large amount of porosity and for deviations are present which could attributed to the fiber characteristics. Due to the complex geometry it is difficult to study the influences whether its process induced or part related defects. Therefore, it is much easier to understand the effects of processing conditions on the part quality using a simplified geometry. The findings can also be extended to broad application domain.

In this work, the effects of fiber orientation and process parameters on the dimensional accuracy of injection-molded thin-wall parts were experimentally investigated. The design of experiments (DoE) approach was used to understand the effects of process parameters on the shrinkage. The results of this first dimensional analysis were then complimented using micro CT to characterize short glass fiber orientation and its correlation with the injection molding process parameters. The resulting skin-shear-core morphology among the thin-wall parts was then characterized using micro CT data, allowing the understanding of its relationship with the part shrinkage.

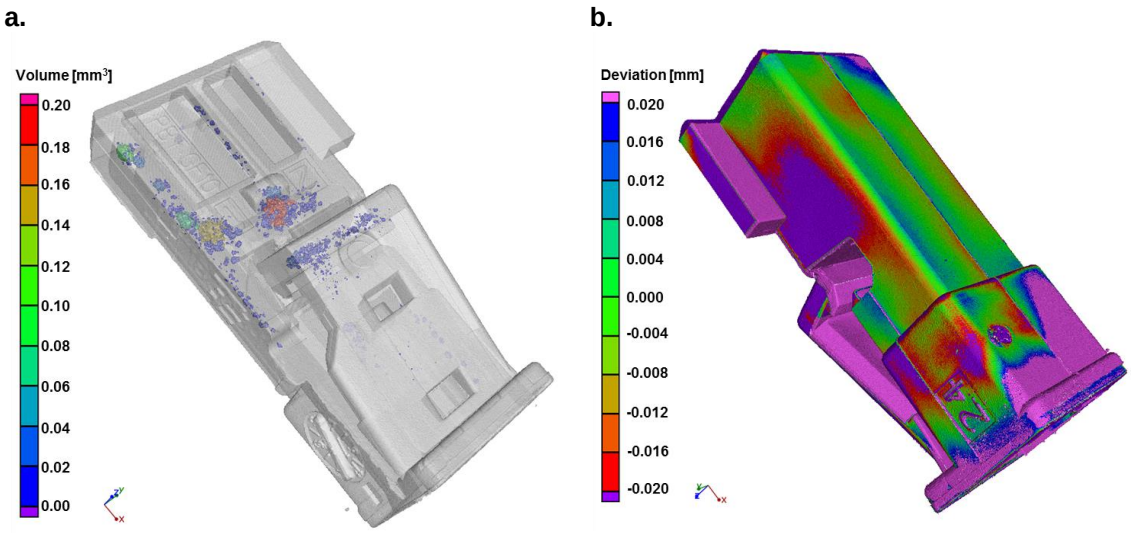

Fig. 5.14: CT analysis performed on the micro connector shown in Fig. 5.13

5.2.2 Micro injection molding

5.2.2.1 Part and mold design

The part considered in this study is similar to the previous studies with detailed experimental investigation. The square plaque with a side length of 10 mm, as shown in Fig. 5.2. The part was specifically designed to allow an accurate evaluation of the shrinkage and of the orientation tensor using micro CT, according to conventional injection molding standards [21] and methodologies proposed in the literature for thin-wall parts [22]. In order to maximize the effect of the thin-wall mold cavity on the shrinkage, a thickness of 350 µm was chosen for the plaque.

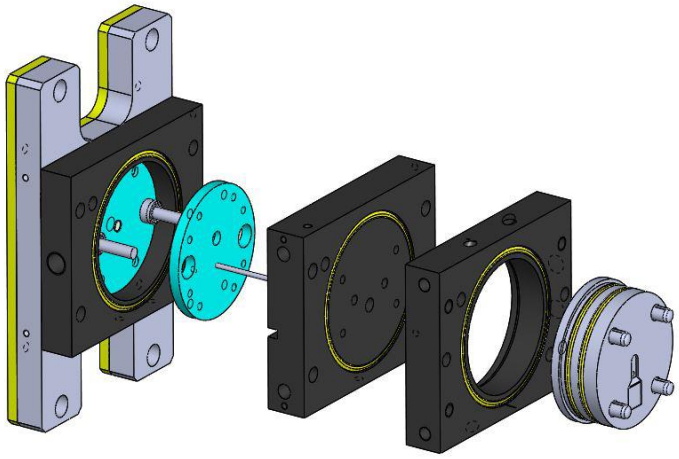

Fig. 5.15: Schematic representation of Model of the moving half of the mould [52]

As shown in Fig. 5.15, the square cavity was positioned on the moving half at the end of a fan gate (thickness: 0.2 mm), which ensured a linear flow front and a balanced filling.

The polymer was fed through a fan gate and a runner with a rectangular cross-section (dimensions: 5x1 mm), directly connected to the nozzle of the injection molding machine.

The square cavity was machined with a 5-axis micro-milling machine (Kugler, Micromaster 5X) and its dimensions were measured using a multi-sensor coordinate measuring machine (Werth, Video-Check-IP 400). The average dimensions of the cavity were of 9.899 mm in the flow direction and of 9.906 mm in the perpendicular direction. In order to prevent a possible deformation of the part during the demolding phase, due to its reduced thickness, a single ejector with a diameter of 2 mm was positioned adjacent to the runner.

5.2.2.2 Material and manufacturing

A commercial polybutylene terephthalate PBT (BASF, Ultradur B4300 G2) reinforced with short glass fibers (10% in weight) was used for the injection molding experiments (Fig. 3.2 (c)). The material was selected because of its strength, stiffness and impact resistance, which make it suitable for electronics applications, such as housings, plugs and connectors. However, PBT is a semi-crystalline thermoplastic polymer thus being characterized by marked shrinkage properties, making its processing critical in terms of dimensional accuracy. This is especially critical for application requiring coupling with other components and it is accentuated for thin-wall parts, such as connectors. The main properties of the injected polymer are summarized in Table 5.5.

Table 5.5: Main properties of the Ultradur B4300 G2 PBT

Property	Test Method	Value
Grade name	ISO 1183	Ultradur B4300 G2
Density, g/cm^3	ISO 1133	1.37
MVR (250°C - 2.16 kg), cm^3/10min		16
Melt temp., °C		250 - 275
Mold temp., °C		60 - 100
Drying temperature, °C		80-120
Drying time, h		4

The micro injection molding machine (Wittmann Battenfeld, MicroPower 15) with a maximum injection speed of 750 mm/s and a maximum clamping force of 150 kN was used for the experiments (more details in Section 3.1). A mold heating system was realized using four electrical cartridges, two for each mold half. Two thermocouples allowed the control of two temperature zones, one for each mold half.

5.2.2.3 Experimental Approach

A four-factor full factorial plan was designed to characterize the effect of the injection molding process on both shrinkage and fiber orientation of the thin-wall parts. Melt temperature (T_b), injection speed (V_{inj}), packing pressure (P_h) and cooling time (t_c) are the most important factors that can affect the final part quality; however, cooling time was excluded from the DoE based on initial investigation. The range values for the DoE plan and the fixed parameters values were defined considering the literature, recommendations of the material supplier (e.g. max. nozzle melt temperature, mold temperature) and technological limitations of the available experimental setup.

Table 5.6: Full factorial design of experiments

T_b [°C]	V_{inj} [mm/s]	P_h [bar]	t_c [s]
270	200	200	3
270	200	200	15
270	200	600	3
270	200	600	15
270	600	200	3
270	600	200	15
270	600	600	3
270	600	600	15
290	200	200	3
290	200	200	15
290	200	600	3
290	200	600	15
290	600	200	3
290	600	200	15
290	600	600	3
290	600	600	15

During the injection molding experiments, the following parameters were kept constant:

- mold temperature: 80°C;
- metering size: 7.5 mm^3;
- velocity/pressure switch-over point: 90% of maximum injection pressure;
- packing time: 2 s;
- clamping force: 150 kN

The response variables selected for the DoE campaign were the shrinkage (in the flow direction (S_f) and in the transverse direction (S_t) respectively) and the average and the maximum values of the orientation tensor (evaluated along the flow direction).

For each run of the DoE plan, ten molding cycles were carried out before the collection of the first part to stabilize the injection molding process. Then, three specimen were collected for the shrinkage and fiber orientation characterization, one every five molding cycles, for each combination of molding conditions. The entire experimental campaign was run for over a hundred parts including the discarded parts. Finally, 48 specimen (three repetitions of each parameter settings) were collected for the characterization and the computation of all the selected response variables.

5.2.3 Characterization of the molded parts

The manufactured specimen were characterized to obtain quantitative and qualitative information about the parts according to the requirements of the response variables.

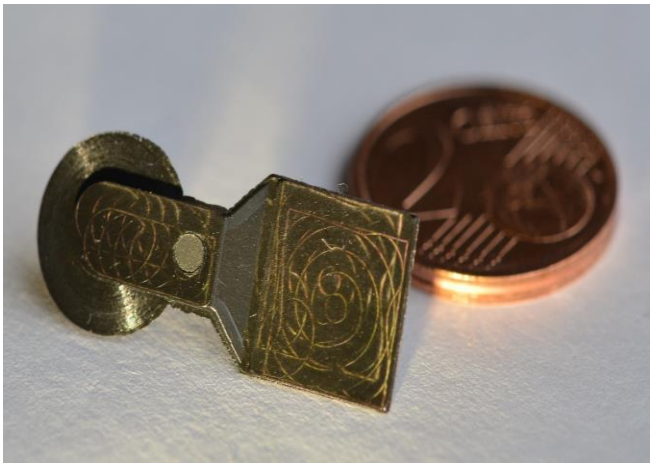

Fig. 5.16: The real manufactured real parts [52]

5.2.3.1 Shrinkage measurements

The linear shrinkage of the molded thin-wall parts was determined according to Fischer's definition as the "difference between the linear dimension of the mold at room temperature and that of the molded part at room temperature within 48 hours following the ejection" [53].

The dimensional measurements of the parts were evaluated by means of a multi-sensor coordinate measuring machine (Werth, Video-Check-IP 400), using a video imaging sensor and a direct episcopic illumination, which allowed identifying the edges of the samples [23]. The following measuring procedure was applied (Fig. 5.17):

i. Fig. 5.17 (a): acquisition of the coordinates of five equally spaced points for each edge of the square molded parts

ii. Fig. 5.17 (b): association of a straight line for each one of the plaque edges by fitting to the acquired points

iii. Fig. 5.17 (c): creation of two symmetry lines in the flow and transverse directions, followed by intersection of the symmetry lines with the lines representing the edges of the specimen, to determine a midpoint for each edge

iv. Fig. 5.17 (d): evaluation of the dimensions as the distance between the midpoints on the opposite edges of the parts

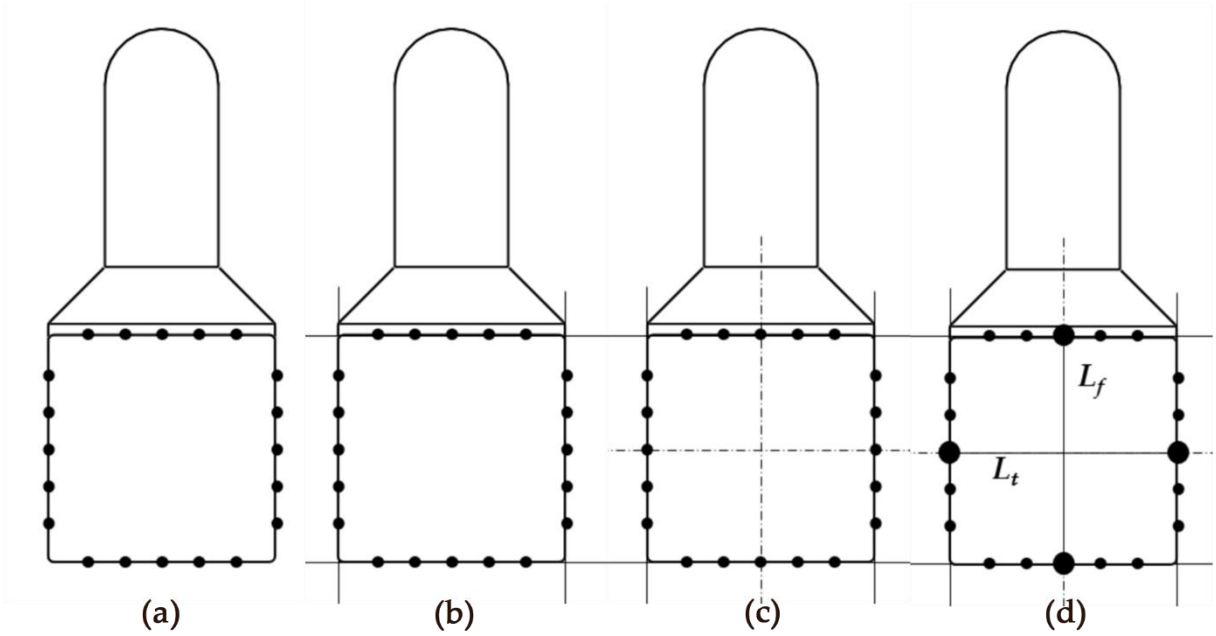

Fig. 5.17: Procedure adopted to evaluate the dimensions of molded thin-wall parts [10]

The shrinkage of the molded parts was calculated as a percentage reduction from mold dimensions. The following equations were applied for each run of the DoE plan to obtain the response variables for the analysis:

$$S_f[\%] = \frac{L_{fpart} - L_{fmold}}{L_{fmold}} \cdot 100 \quad \textbf{(5.3)}$$

$$S_t[\%] = \frac{L_{tpart} - L_{tmold}}{L_{tmold}} \cdot 100 \quad \textbf{(5.4)}$$

where L_{fpart} and L_{tpart} are the dimensions of the molded part, measured with the coordinate measuring machine in the flow and transverse direction respectively; L_{fmold} and L_{tmold} are the dimensions of the mold in the two directions.

5.2.3.2 Fiber orientation measurements

As mentioned in the first part of the chapter, Nikon Metrology, X-Tek MCT 225 was used for measuring the molded parts and analyzing their fiber orientation. The X-ray projections were acquired for a complete rotation cycle (see Fig. 5.18) and subsequently reconstructed into a 3D volumetric dataset. The CT metrological software VGStudio MAX 3.0 was used to process and evaluate the acquired data. Table 5.7 reports the parameters employed for the micro CT scans.

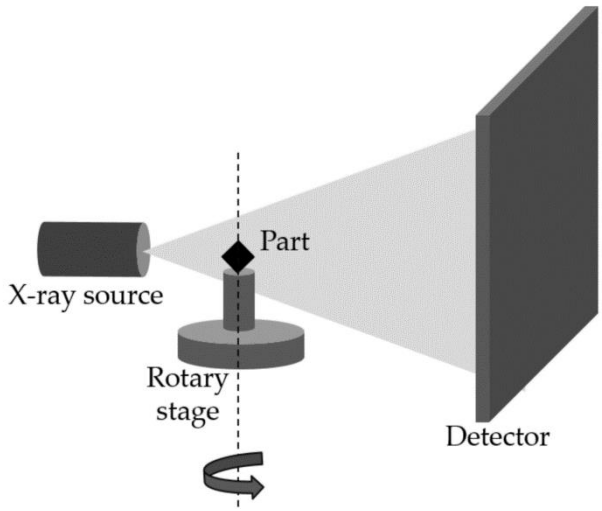

Fig. 5.18: Schematic representation of the CT scanning procedure [10]

Table 5.7: Parameters used for the μ-CT scans

Parameter	Value
Voltage, kV	95
Current, μA	74
Exposure times	2.8
Number of projections	2500
Averaging	2
Physical filtering	No
Voxel size, μm	8.3

It is possible to select a region of interest (ROI) on the CT data for performing a particular analysis. Therefore, it was crucial to select an optimum ROI, which represents the overall fiber orientation behavior. The exterior portion of the part may lead to some irregularities attributed to the manufacturing steps, e.g. the warpage of the part results in bending at the edges. On the other hand, a very small ROI may not be good enough to be a

representative. In this study, several squared (*a x a x t*) ROIs, symmetrical with the centre of the part were examined; where a (in mm) is the desired size of the ROI and t is the thickness of the part (see Fig. 5.19). It can be seen that for smaller ROIs (for a values: 1, 0.5 and 0.3 mm) the orientation tensor is quite irregular (without any trend) and for bigger ROIs (for a value: 9 mm) it flattens. The chosen ROI for the fiber analysis study was with *a* equals 5 mm.

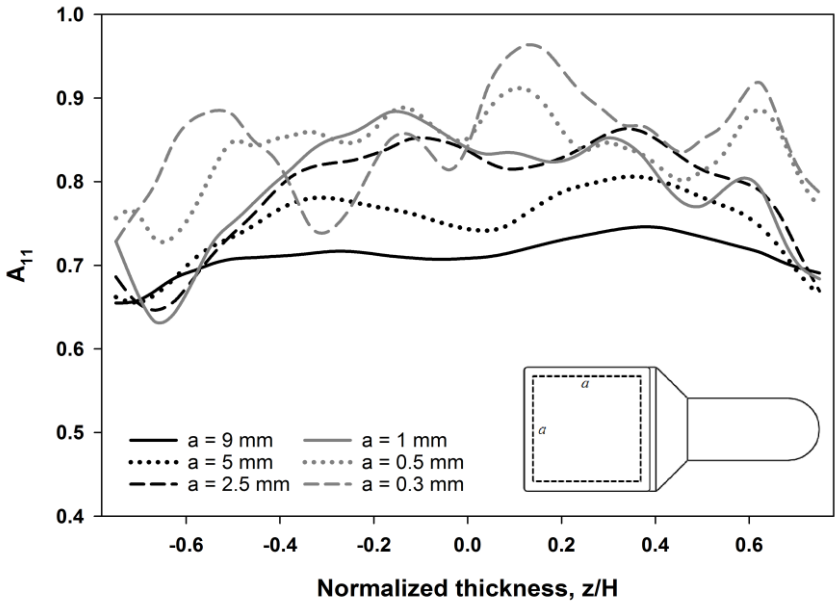

Fig. 5.19: Fiber orientation component obtained on the same part with different ROIs

The acquired datasets were analyzed by calculating the orientation tensor within the selected region of interest (dimensions: 5 x 5 mm) along the whole thickness of the molded thin-wall parts. The three-dimensional orientation was described using a second order tensor as suggested by Advani and Tucker [54]. The major components of the tensor are A_{11}, A_{22}, A_{33}, which represents the orientation in the flow direction, the transverse direction and the out of the plane direction. Fig. 5.20 reports the results of the fiber orientation analysis performed on the thin-wall molded samples in the three directions.

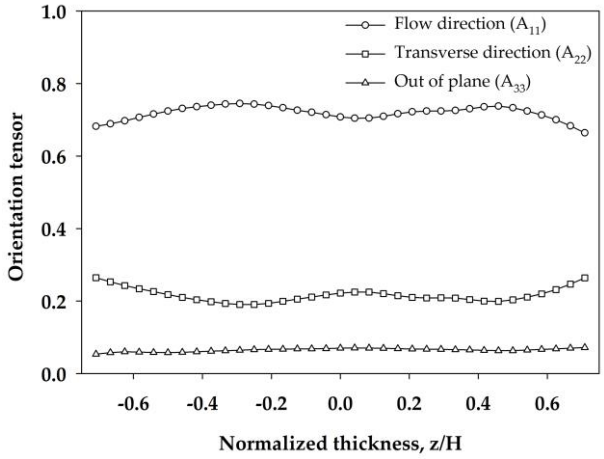

Fig. 5.20: Major components of the orientation tensor evaluated for the molded thin-wall parts using μ-CT [10]

In injection molding, because of their kinematics, the fibers are mainly oriented in the flow direction and A_{11} is the highest component. For this reason, the molded parts in the following experiments were characterized considering the orientation in the melt flow direction (A_{11}), which contains the quantitative information about the microstructure and is the most sensitive to flow, processing and material changes.

5.2.4 Results and discussion

The results of the experimental campaign were analyzed collecting each one of the selected response variable. Table 5.8 and 5.9 report the measurement results for shrinkage and fiber orientation respectively.

Table 5.8: Results of the experimental campaign for shrinkage

T_b [°C]	V_{inj} [mm/s]	P_h [bar]	t_c [s]	Shrinkage [%]			
				Parallel (S_f)		Perpendicular (S_t)	
				Mean	Std. Dev.	Mean	Std. Dev.
270	200	200	3	0.85	0.05	1.66	0.12
270	200	200	15	0.91	0.05	1.63	0.03
270	200	600	3	0.72	0.16	1.16	0.05
270	200	600	15	0.62	0.10	1.13	0.09
270	600	200	3	0.92	0.06	1.41	0.08
270	600	200	15	0.97	0.03	1.33	0.11
270	600	600	3	0.67	0.03	0.87	0.07
270	600	600	15	0.57	0.03	0.94	0.12
290	200	200	3	0.87	0.05	1.38	0.07
290	200	200	15	0.84	0.01	1.41	0.08
290	200	600	3	0.57	0.04	1.09	0.02

290	200	600	15	0.54	0.07	1.05	0.07
290	600	200	3	0.95	0.15	1.32	0.02
290	600	200	15	1.01	0.04	1.35	0.03
290	600	600	3	0.54	0.05	0.89	0.03
290	600	600	15	0.55	0.05	0.78	0.07

Table 5.9: Results of the experimental campaign for fiber orientation

T_b [°C]	V_{inj} [mm/s]	P_h [bar]	Avg. Orientation		Max. Orientation	
			Mean	Std. Dev.	Mean	Std. Dev.
270	200	200	0.73	0.01	0.80	0.01
290	200	200	0.67	0.01	0.75	0.02
270	600	200	0.62	0.01	0.74	0.01
290	600	200	0.61	0.01	0.68	0.01
270	200	600	0.70	0.01	0.79	0.01
290	200	600	0.68	0.01	0.78	0.02
270	600	600	0.64	0.01	0.73	0.01
290	600	600	0.58	0.01	0.65	0.01

For each treatment, the factorial design was analyzed in order to evaluate the factors and the first-order interactions that significantly affect the selected response variables. A General Linear Model was used to perform a univariate analysis of variance (ANOVA) for the designed factorial plan. The terms included in the model are all the main factors implemented in the design of the experimental plan. The statistical identification of significant parameters was carried out considering the p-values, for which the threshold value was fixed at 0.05. Then, factors having a p-value inferior to 0.05 are statistically significant to the selected response.

5.2.4.1 Effect of process parameters on shrinkage

From Table 5.10, the analysis of variance (ANOVA) results indicate that the melt temperature and the packing pressure are the main parameters which affect the dimensional accuracy, both in terms of parallel shrinkage (S_f) and perpendicular shrinkage (S_t). Moreover, the injection speed was observed to affect the shrinkage, but only in the transverse direction. In contract, the cooling time resulted statistically not significant for the shrinkage, thus excluded from the fiber orientation analysis. The reduced thickness of the part led to very high cooling rates, which did not allowed a higher cooling time to affect the shrinkage of the micro parts.

Table 5.10: Results of the ANOVA considering shrinkage as the response variable

Factor	*p*-value	
	S_f	S_t
T_b	0.156	0.003
V_{inj}	0.056	0.000
P_h	0.000	0.000
t_c	0.627	0.167
$T_b \cdot V_{inj}$	0.048	0.274
$T_b \cdot P_h$	0.486	0.745
$T_b * t_c$	0.528	0.872
$V_{inj} \cdot P_h$	0.006	0.495
$V_{inj} * t_c$	0.519	0.695
$P_h * t_c$	0.054	0.341

The main effect plots for presented in Fig. 5.21 and 5.22 for shrinkage in flow and transverse directions respectively. The shrinkage of the micro parts was also reduced by an increase of the melt temperature, as shown in Fig. 21 (a) and Fig. 5.22 (a). In particular, the main effect of varying the melt temperature from 270 to 290 °C was to reduce the shrinkage by 6% and 9%, respectively in the flow and transverse directions. This is explained considering the reduction of viscosity that followed an increase in the melt temperature, which led to a smaller pressure drop during the injection phase and consequently to more material being injected inside the cavity. Increasing the injection speed from 200 to 600 mm/s resulted in a decrease by 15% of the shrinkage in the direction transverse to the flow, as shown in Fig. 5.22 (b). This is further investigated and discussed, considering the effect of this parameter on fibers orientation, in the next sections by analyzing the different fibers distributions along micro parts thickness. By varying the packing pressure from 200 to 600 bar, the shrinkage reduces by 35% in the flow direction (Fig. 5.21(c)) and by 31% in the transverse direction (Fig. 5.22 (c)). Indeed, in agreement with polymers PVT behavior, the higher is the pressure applied to the polymer the lower is the specific volume, and so is the shrinkage. It is also clear from the plots in Fig. 5.21 (d) and Fig. 5.22 (d) that the cooling time is insignificant

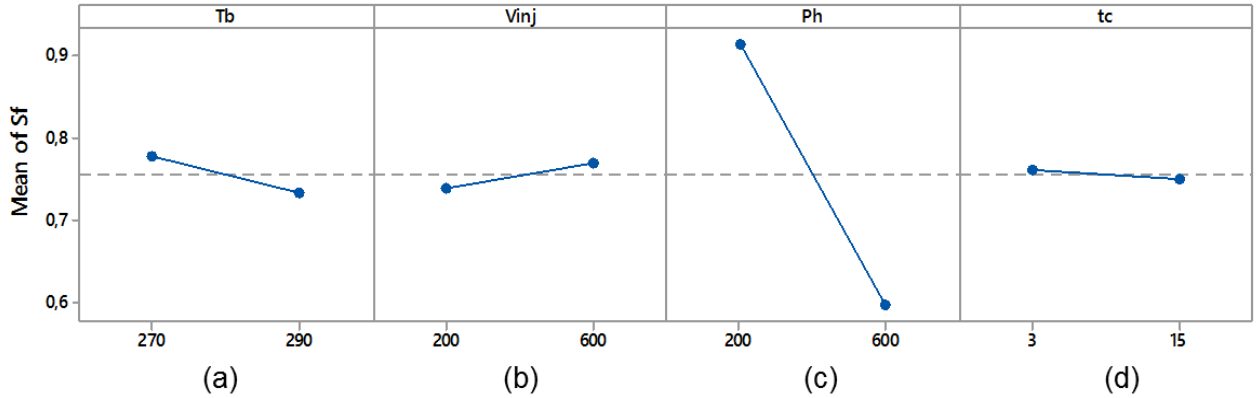

Fig. 5.21: Main effect plots for the shrinkage in the flow direction

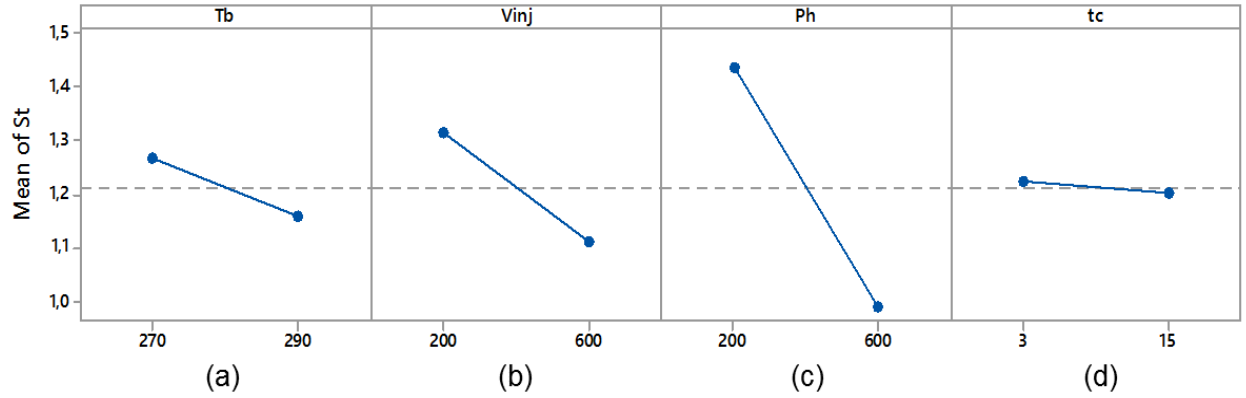

Fig. 5.22: Main effect plots for the shrinkage in the transverse direction

As far the interactions of parameters are concerned; no significant first order interaction was observed for the shrinkage measured in the transverse direction. From Fig. 5.23 (a), the interaction between the melt temperature and the packing pressure indicated that a higher value of the packing pressure can be exploited to reduce the shrinkage in the flow direction only when applying high values of the melt temperature. In fact, the lower is the melt polymer viscosity (i.e. the higher the melt temperature) the more is the material that is force into the cavity during the packing phase and so the higher is the shrinkage compensation, consequent to the higher density. From Fig. 5.23 (b), the interaction between the injection speed and the packing pressure indicated that when molding with a low value of the packing pressure the micro parts produced with a high injection speed shrink more. On the contrary, the effect of the injection speed on the shrinkage in the flow direction is negligible when the packing pressure was set to its higher value.

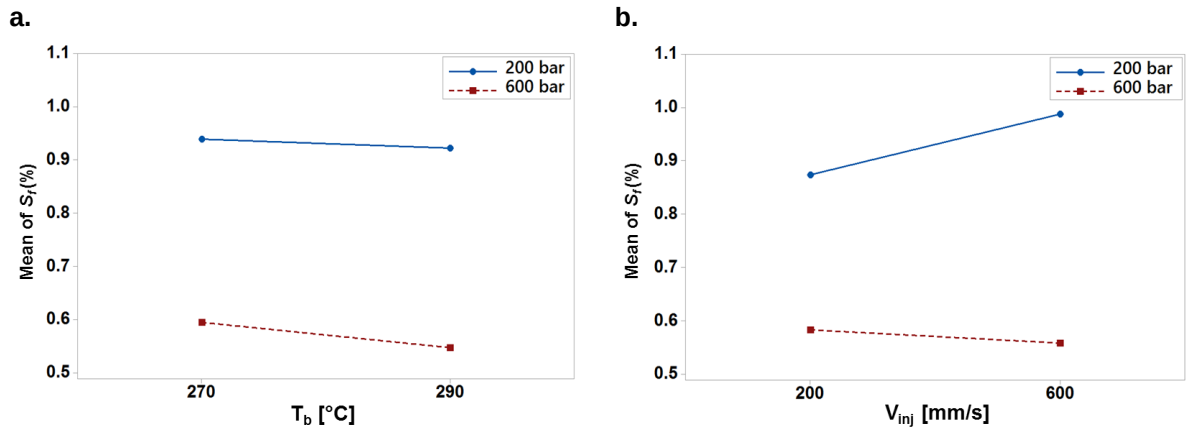

Fig. 5.23: Interaction plots for shrinkage: melt temperature and packing pressure (a) and injection speed and packing pressure (b)

5.2.4.2 Effect of process parameters on fiber orientation

The fiber orientation tensor, obtained from the CT data, was analyzed using the VGStudio MAX 3.0 software. The main components of the orientation tensor (i.e. in the flow direction) were determined along the thin-wall parts thickness and the average and maximum values were used to perform the ANOVA for the DoE plan (Table 5.11). The main effects of both melt temperature and injection speed resulted statistically significant. Conversely, the packing pressure did not affect fiber orientation, as it was determined during the filling phase. The main effects of the statistically significant parameters were plot in Fig. 5.24 and Fig. 5.25.

Table 5.11: Results of the ANOVA considering fiber orientation as the response variable

Factor	*p*-value	
	Avg. Orientation	**Max. Orientation**
T_b	0.000	0.000
V_{inj}	0.000	0.000
P_h	0.467	0.613
$T_b \cdot V_{inj}$	0.550	0.007
$T_b \cdot P_h$	0.559	0.366
$V_{inj} \cdot P_h$	0.873	0.051

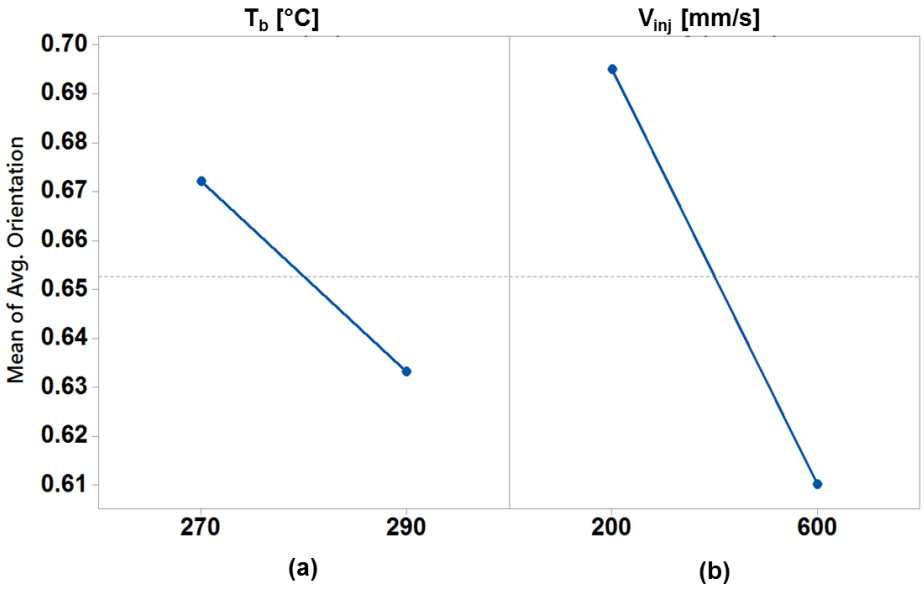

Fig. 5.24: Effect of melt temperature (a) and injection speed (b) on the average orientation of fibers

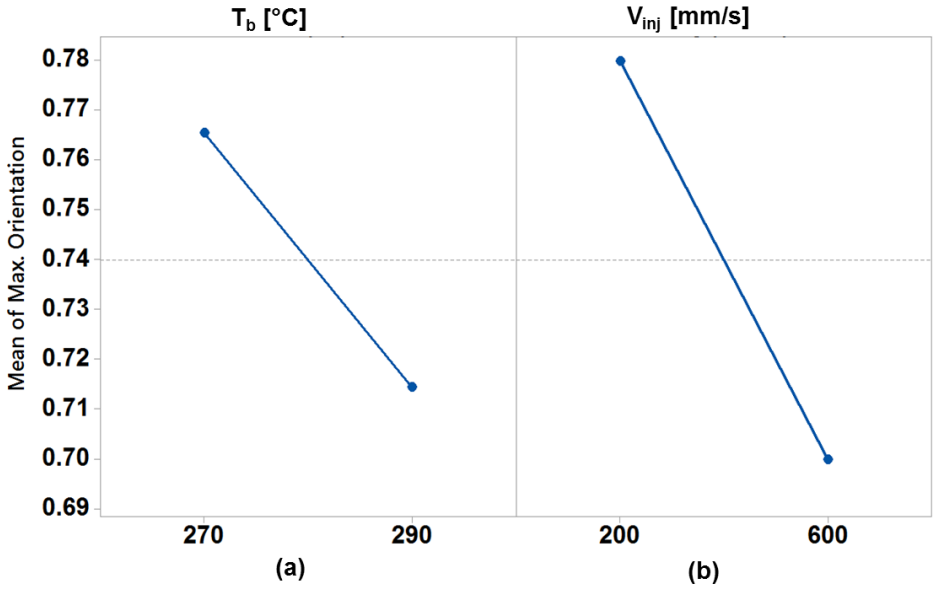

Fig. 5.25: Effect of melt temperature (a) and injection speed (b) on the maximum orientation of fibers

The melt temperature variation from 270 to 290 °C reduced the average orientation by 6.2% (Fig. 5.24 (a)) and the maximum orientation by 6% (Fig. 5.25 (a)). Indeed, increasing this parameter causes a slower solidification near the cavity walls and thus resulting in thinner shear layers within the thin-wall parts. Consequently, at higher melt temperature the number of oriented fibers, which are prevalent in the shear layers, decreases with the layers thickness.

The main effect of increasing the injection speed from 200 to 600 mm/s was a reduction of the average orientation by 12.3% (Fig. 5.24 (b)) and a reduction of the maximum orientation by 11.6% (Fig. 5.25 (b)). Certainly, changing the flow rate led to different kinematics for the fibers injected into the thin-walled cavity, modifying the skin-core morphology along the thickness.

Furthermore, the first order interaction between the two factors ($T_b \cdot V_{inj}$) also resulted significant for fiber orientation (Fig. 5.26). In particular, when molding with a low injection speed the effect of a higher melt temperature was the reduction of the average and maximum fiber orientation by 3.1% and 1.9%, respectively. The trend becomes more evident at higher injection speed. An increase of 20 °C in the melt temperature caused a reduction of both the response variables by 10%. This is explained considering that at high injection speed the increased heat, convected by the polymer melt, counteracts more significantly the skin solidification and, therefore, the thickening of those shear layers that host the oriented fibers.

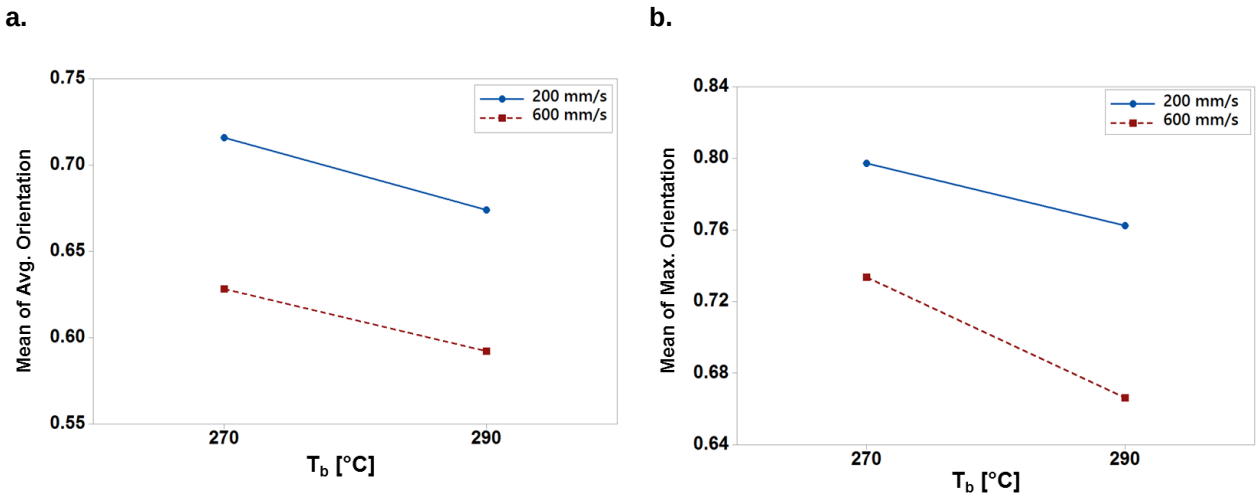

Fig. 5.26: Interaction plot between melt temperature and injection speed for (a) the average value and (b) the maximum value of the fiber orientation tensor

5.2.4.3 Skin-shear-core morphology

The fountain-flow filling pattern that characterizes the IM process generates a 5-layer structure composed of two surface (skin), two sub-surface (shear) and one core layer in the edge section. The resulting higher shear stress near the cavity walls inducted a marked fiber orientation along the flow direction in the shear layers, and a more random distribution in the core (Fig. 5.27). However, the ratio between the shear and core layers, and the consequent overall fibers distribution, is affected by the IM process parameters, and in particular by the injection speed.

The higher fiber orientation observed at lower injection speed (Fig. 5.27 (a)) was explained considering the formation of thicker shear layers. In fact, the lower the flow rate, the higher the cooling rate between the polymer melt and the mold, hence allowing

for a thinner core and consequently a higher overall orientation. Conversely, at higher injection speed the orientation in the shear layers is lower, as shown in Fig. 5.27 (b).

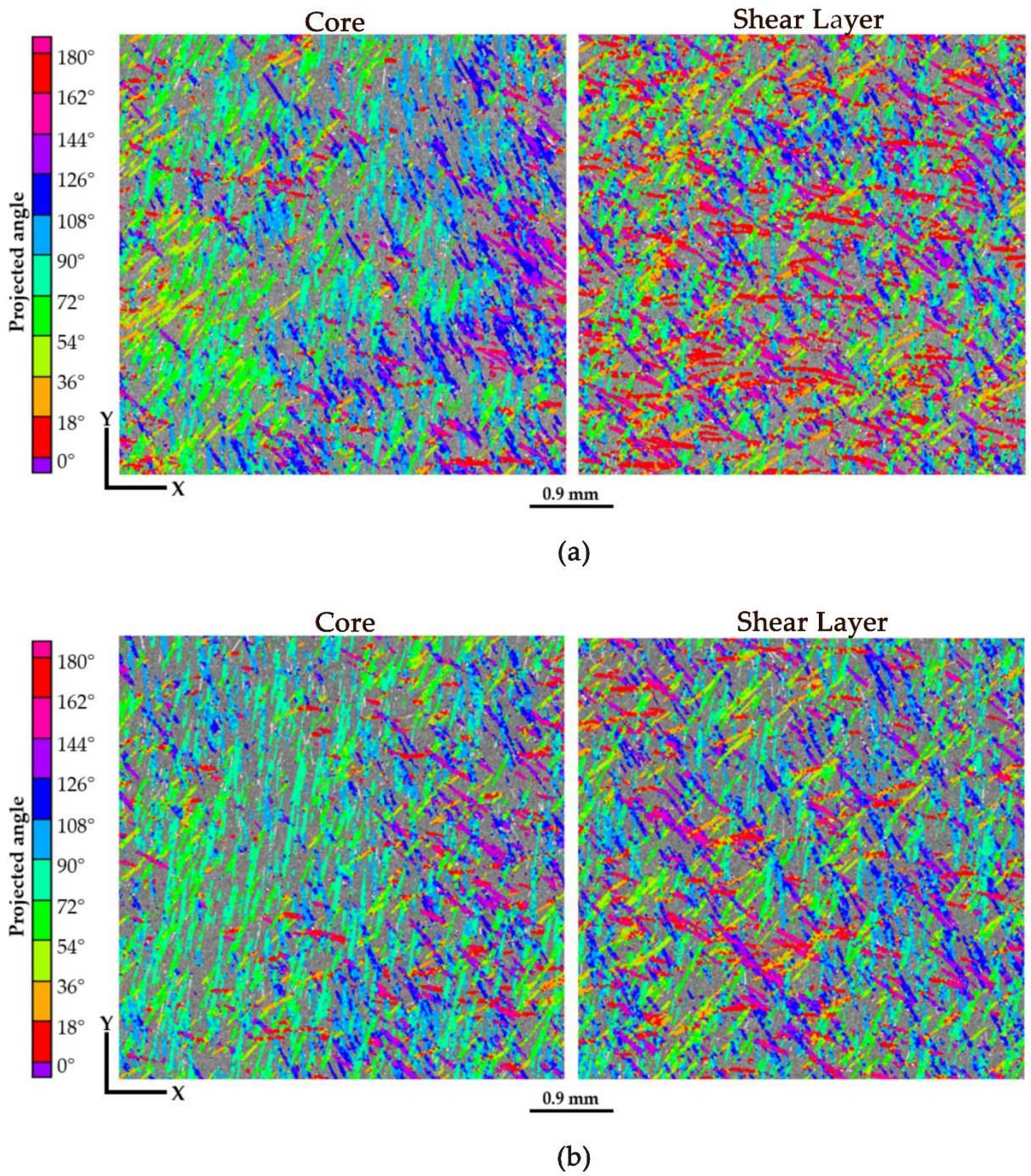

Fig. 5.27: Cross sections extracted form µ-CT 3D measurements of thin-wall parts molded at (a) low injection speed and (b) high injection speed [10]

The analysis of the orientation tensor also indicated that the thickness ratio between the shear and core layers is very high compared to conventional injection molding due to the

very small depth of the mold cavity. In conventional injection molding, the orientation of the fibers is markedly higher in the shear layers (i.e. in the proximity of the cavity walls) and orientation tensors indicate higher value of the orientation tensor components. Conversely, in thin-wall injection molding, the extremely reduced cavity thickness resulted in an almost flat pattern of the orientation tensor. However, the skin-shear-core morphology of the molded parts was modified by different selection of the injection molding process parameters. For parts molded at lower injection speed, especially for a high melt temperature (Fig. 5.28 (a)). The trend was less evident at lower melt temperature as the orientation tensor indicated higher orientation in the shear layers than in the core (Fig. 5.28 (b)), confirming the effect of the interaction between the investigated IM parameters (Fig. 5.26). This indicates that, apart from differences induced by the variations of process parameters, the core layer was very thin and in some cases not even present.

The consequence of a higher orientation along the melt flow direction, observed for lower injection speed, is that the shrinkage of the thin-wall parts is markedly higher along the cross-flow direction. In fact, owing to their higher stiffness and lower thermal expansion coefficient, the fibers hinder the polymer matrix from shrinking in the flow direction. Hence, the result is the differential shrinkage of the molded thin-wall parts.

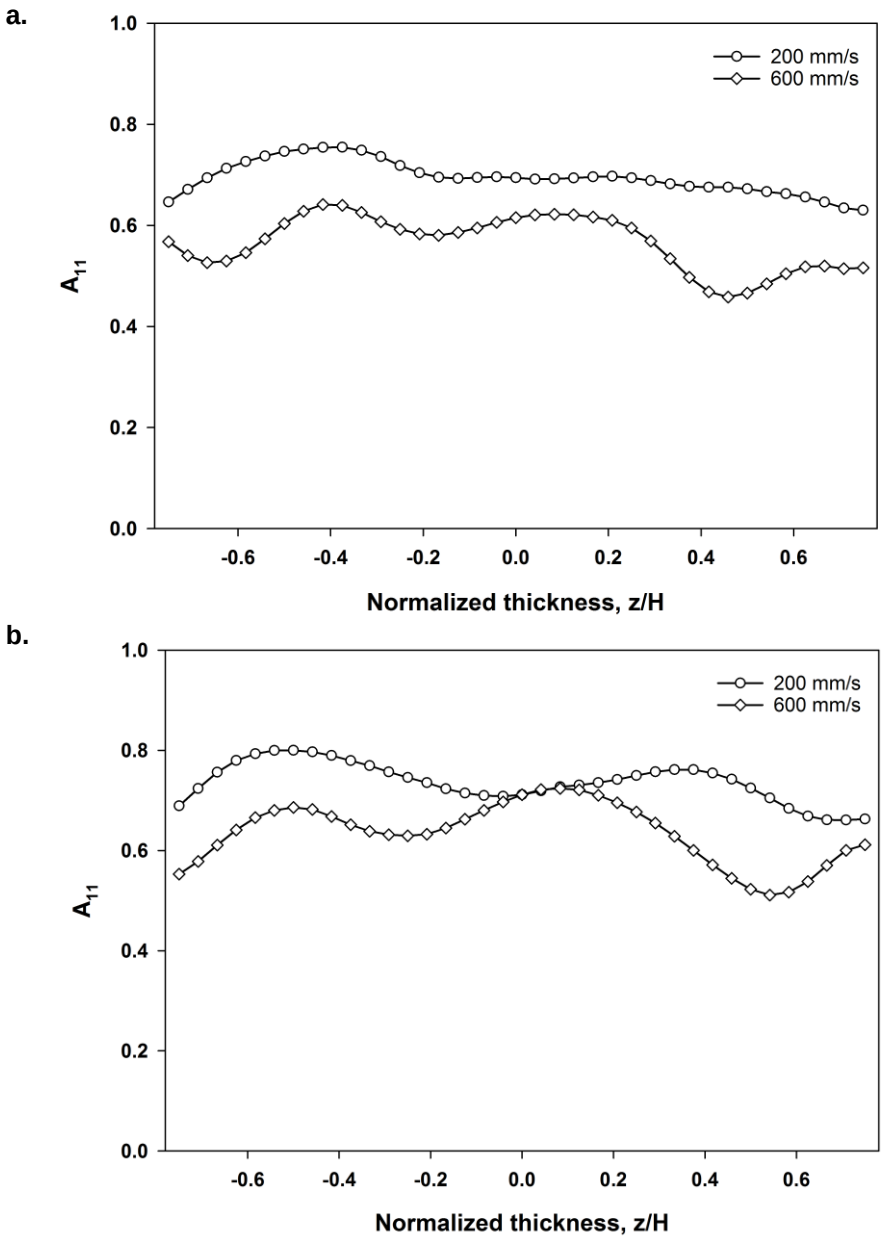

Fig. 5.28: Average fiber orientation tensors evaluated for parts molded at a melt temperature of (a) 290 °C and of (b) 270 °C [10]

The volumetric comparison between the micro CT scan and the CAD model, displayed in Fig.5.29, showed that because of the differential shrinkage in the in-flow and cross-flow directions the final warpage of the micro part was unbalanced.

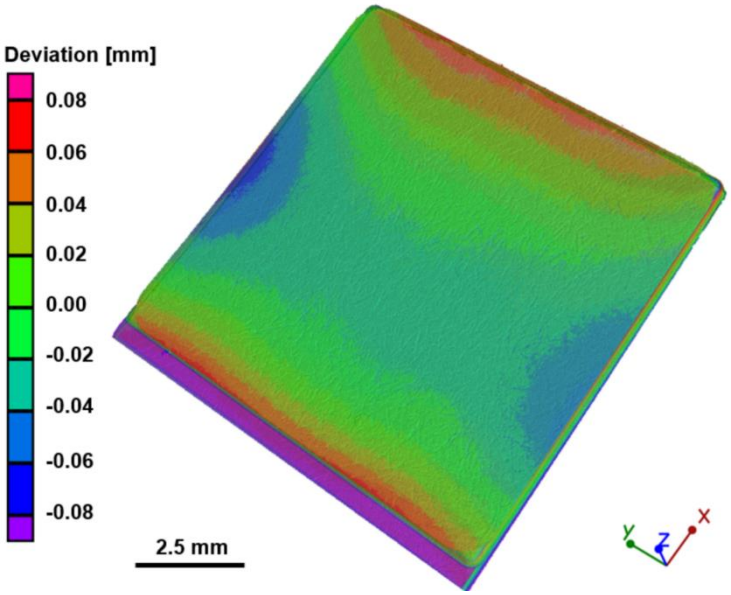

Fig. 5.29: Comparison of real part (CT scan) with CAD model [10]

5.2.5 Conclusions

This study was focused on analyzing the impact of the injection molding processing conditions on the dimensional accuracy of thin-wall fiber-reinforced parts with respect to shrinkage and fiber orientation. The shrinkage reduction, which is related to the pressure and temperature applied to the polymer during the process, was taken into consideration analyzing the final dimensions and the distribution of short glass fibers of a specifically designed thin-wall part.

The analysis of variance was performed on the experimental data, which depicted that only the packing pressure (-8%) is affecting shrinkage in both the melt flow and the transverse directions among the selected process parameters. Shrinkage in the transverse direction was further reduced by increasing the melt temperature (-9%) and the injection speed (-15%), due to their effect on fiber orientation along the thickness of the molded parts.

The analysis of fiber orientation within the thin-wall parts, performed using micro CT, indicated that the injection molding process affected both average and maximum values of the orientation tensor. However, they were affected by different selection of process parameters. In particular, a selection of higher values for both injection speed (-11%) and melt temperature (-7%) yielded a reduction of fiber orientation. Furthermore, the CT based analysis of the cross sections of the thin-wall parts, revealed the 'skin-shear-core' morphology. The thickness ratio of the shear and core layers was affected by the process especially by the injection speed. The extremely thin cavity results in a nearly flat trend of the orientation tensor for parts obtained at lower injection speed which could

be attributed to the absence of the core layer. Thus, a higher shrinkage along the transverse direction led to a differential shrinkage in the part and to the warpage of the final part.

In general, the results indicate how the dimensional accuracy of the molded thin-wall parts can be optimized by considering the effects of injection molding process parameters. In particular, the linear shrinkage of the molded parts was significantly reduced by adopting high values of the melt temperature, the packing pressure and the injection speed.

References

[1] Fu, S.Y., Lauke, B. and Mai, Y.W., 2009. Science and engineering of short fibre reinforced polymer composites. Elsevier.

[2] Fu, S.Y. and Mai, Y.W., 2003. Thermal conductivity of misaligned short-fiber-reinforced polymer composites. Journal of applied polymer science, 88(6), pp.1497-1505.

[3] Wallrabe, U., Dittrich, H., Friedsam, G., Hanemann, T., Mohr, J., Müller, K. & Zißler, W., 2002. Micromolded easy-assembly multi fiber connector: RibCon®. Microsystem technologies, 8(2-3), 83-87.

[4] Meneghetti, G., Ricotta, M., Lucchetta, G., & Carmignato, S. (2014). An hysteresis energy-based synthesis of fully reversed axial fatigue behaviour of different polypropylene composites. Composites Part B: Engineering, 65, 17-25.

[5] Lucchetta, G., Sorgato, M., Carmignato, S., & Savio, E., 2014. Investigating the technological limits of micro-injection molding in replicating high aspect ratio micro-structured surfaces. CIRP Annals-Manufacturing Technology, 63(1), 521-524.

[6] Selden, R., 2000. Thin wall molding of engineering plastics--a literature survey. Journal of Injection Molding Technology, 4(4), 159.

[7] Oh, H. J., Lee, D. J., Lee, C. G., Jo, K. Y., Lee, D. H., Song, Y. S., & Youn, J. R., 2013. Warpage analysis of a micro-molded parts prepared with liquid crystalline polymer based composites. Composites Part A: Applied Science and Manufacturing, 53, 34-45.

[8] Sorgato, M., Masato, D., & Lucchetta, G., 2016. Effect of vacuum venting and mold wettability on the replication of micro-structured surfaces. Microsystem Technologies, 1-10.

[9] Masato, D., Sorgato, M., & Lucchetta, G., 2016. Analysis of the influence of part thickness on the replication of micro-structured surfaces by injection molding. Materials & Design, 95, 219-224.

[10] Masato, D., Rathore, J., Sorgato, M., Carmignato, S., Lucchetta, G., 2017. Analysis of the shrinkage of injection-molded fiber-reinforced thin-wall parts. Materials & Design.

[11] Oumer, A.N. and Mamat, O., 2013. A review of effects of molding methods, mold thickness and other processing parameters on fiber orientation in polymer composites. Asian Journal of Scientific Research, 6(3), pp.401-410.

[12] Li, X.P., Zhao, G.Q. and Yang, C., 2014. Effect of mold temperature on motion behavior of short glass fibers in injection molding process. The International Journal of Advanced Manufacturing Technology, 73(5-8), pp.639-645.

[13] Bernasconi, A., Cosmi, F. and Hine, P.J., 2012. Analysis of fibre orientation distribution in short fibre reinforced polymers: A comparison between optical and tomographic methods. Composites Science and Technology, 72(16), pp.2002-2008.

[14] Carmignato, S. (2012). Accuracy of industrial computed tomography measurements: experimental results from an international comparison. CIRP Annals-Manufacturing Technology, 61(1), 491-494.

[15] Thi, T.B.N., Morioka, M., Yokoyama, A., Hamanaka, S., Yamashita, K. and Nonomura, C., 2015. Measurement of fiber orientation distribution in injection-molded short-glass-fiber composites using X-ray computed tomography. Journal of Materials Processing Technology, 219, pp.1-9.

[16] Shen, H., Nutt, S. and Hull, D., 2004. Direct observation and measurement of fiber architecture in short fiber-polymer composite foam through micro-CT imaging. Composites science and technology, 64(13), pp.2113-2120.

[17] Kastner, J., Plank, B., Salaberger, D., 2013. High resolution X-ray computed tomography for quantitative characterization of fiber reinforced polymers and heterogeneous light metals, Proceeding ASNT 22nd Annual Research Symposium, Memphis, USA.

[18] Ontiveros, S., Yagüe-Fabra, J.A., Jiménez, R., Tosello, G., Gasparin, S., Pierobon, A., Carmignato, S. and Hansen, H.N., 2012. Dimensional measurement of micro-moulded parts by computed tomography. Measurement Science and Technology, 23(12), p.125401.

[19] Konopczyński, T., Rathore, J., Kröger, T., Zheng, L., Garbe, C. S., Carmignato, S., & Hesser, J. (2017). Reference Setup for Quantitative Comparison of Segmentation Techniques for Short Glass Fiber CT Data. In 7th Conference on Industrial Computed Tomography (iCT 2017).

[20] O'Gara, J.F., Novak, G.E. and Wyzgoski, M.G, 2010. Predicting the tensile strength of short glass fiber reinforced injection molded plastics. In Proceedings of the 10th Annual SPE® Automotive Composites Conference & Exhibition (ACCE), Troy, MI, USA.

[21] BS EN ISO 294-3: 2003, Plastics – Injection Moulding of Test Specimens of Thermoplastic Materials - Part 3: Small Plates.

[22] Annicchiarico, D., Attia, U.M. and Alcock, J.R., 2013. A methodology for shrinkage measurement in micro-injection moulding. Polymer testing, 32(4), pp.769-777.

[23] Carmignato, S., Voltan, A., & Savio, E. (2010). Metrological performance of optical coordinate measuring machines under industrial conditions. CIRP Annals-Manufacturing Technology, 59(1), 497-500.

[24] Carmignato, S., Dreossi, D., Mancini, L., Marinello, F., Tromba, G. and Savio, E., 2009. Testing of x-ray microtomography systems using a traceable geometrical standard. Measurement Science and Technology, 20(8), p.084021.

[25] Marinello, F., Savio, E., Carmignato, S., & De Chiffre, L. (2008). Calibration artefact for the microscale with high aspect ratio: The fiber gauge. CIRP Annals-Manufacturing Technology, 57(1), 497-500.

[26] Gerd-Rüdiger, J., Bellon, C., and Ewert, U., 2008. "aRTist–Analytical RT Inspection Simulation Tool for Industrial Application." *Proceedings of the 17th World Conference on Non-Destructive Testing, Shanghai, China, International Committee on NDT, CDrom paper*. Vol. 64.

[27] Kruth, J. P., Bartscher, M., Carmignato, S., Schmitt, R., De Chiffre, L., & Weckenmann, A. (2011). Computed tomography for dimensional metrology. CIRP Annals-Manufacturing Technology, 60(2), 821-842.

[28] Yang, C., Yin, X. H., & Cheng, G. M. (2013). Microinjection molding of microsystem components: new aspects in improving performance. Journal of Micromechanics and Microengineering, 23(9), 093001.

[29] Liao, S. J., Chang, D. Y., Chen, H. J., Tsou, L. S., Ho, J. R., Yau, H. T., ... & Su, Y. C. (2004). Optimal process conditions of shrinkage and warpage of thin-wall parts. Polymer Engineering & Science, 44(5), 917-928.

[30] Annicchiarico, D., & Alcock, J. R. (2014). Review of factors that affect shrinkage of molded part in injection molding. Materials and Manufacturing Processes, 29(6), 662-682.

[31] Ozcelik, B., & Sonat, I. (2009). Warpage and structural analysis of thin shell plastic in the plastic injection molding. Materials & Design, 30(2), 367-375.

[32] Chiang, Y. C., Cheng, H. C., Huang, C. F., Lee, J. L., Lin, Y., & Shen, Y. K. (2011). Warpage phenomenon of thin-wall injection molding. The International Journal of Advanced Manufacturing Technology, 55(5-8), 517-526.

[33] De Santis, F., Pantani, R., Speranza, V., & Titomanlio, G. (2010). Analysis of shrinkage development of a semicrystalline polymer during injection molding. Industrial & Engineering Chemistry Research, 49(5), 2469-2476.

[34] Pontes, A. J., & Pouzada, A. S. (2006). Predicting shrinkage in semi-crystalline injection mouldings–the influence of pressure. In Materials science forum (Vol. 514, pp. 1501-1505). Trans Tech Publications.

[35] Altan, M. (2010). Reducing shrinkage in injection moldings via the Taguchi, ANOVA and neural network methods. Materials & Design, 31(1), 599-604.

[36] Pomerleau, J., & Sanschagrin, B. (2006). Injection molding shrinkage of PP: Experimental progress. Polymer Engineering & Science, 46(9), 1275-1283.

[37] Cellere, A., & Lucchetta, G. (2010). Identification of CRIMS model parameters for warpage prediction in injection moulding simulation. International Journal of Material Forming, 3(1), 37-40.

[38] De, S. K., & White, J. R. (Eds.). (1996). Short fibre-polymer composites. Elsevier.

[39] Sadabadi, H., & Ghasemi, M. (2007). Effects of some injection molding process parameters on fiber orientation tensor of short glass fiber polystyrene composites (SGF/PS). Journal of Reinforced Plastics and Composites, 26(17), 1729-1741.

[40] Azaman, M. D., Sapuan, S. M., Sulaiman, S., Zainudin, E. S., & Khalina, A. (2015). Numerical simulation analysis of unfilled and filled reinforced polypropylene on thin-walled parts formed using the injection-moulding process. International Journal of Polymer Science, 2015, Article ID 659321.

[41] Cadena-Perez, A. M., Yañez-Flores, I., Sanchez-Valdes, S., Rodriguez-Fernandez, O. S., Fernandez-Tavizon, S., de Valle, L. F. R., & Sanchez-Cuevas, J. L. (2017). Shrinkage reduction and morphological characterization of PP reinforced with glass fiber and nanoclay using functionalized PP as compatibilizer. International Journal of Material Forming, 10, 233-240.

[42] Laun, H. M. (1984). Orientation effects and rheology of short glass fiber-reinforced thermoplastics. Colloid and Polymer Science, 262(4), 257-269.

[43] Bright, P. F., Crowson, R. J., & Folkes, M. J. (1978). A study of the effect of injection speed on fibre orientation in simple mouldings of short glass fibre-filled polypropylene. Journal of Materials Science, 13(11), 2497-2506.

[44] Shokri, P., & Bhatnagar, N. (2007). Effect of packing pressure on fiber orientation in injection molding of fiber-reinforced thermoplastics. Polymer Composites, 28(2), 214-223.

[45] Huang, M. C., & Tai, C. C. (2001). The effective factors in the warpage problem of an injection-molded part with a thin shell feature. Journal of Materials Processing Technology, 110(1), 1-9.

[46] Giboz, J., Copponnex, T., & Mélé, P. (2009). Microinjection molding of thermoplastic polymers: morphological comparison with conventional injection molding. Journal of Micromechanics and Microengineering, 19(2), 025023.

[47] Lucchetta, G., Masato, D., Sorgato, M., Crema, L., & Savio, E. (2016). Effects of different mould coatings on polymer filling flow in thin-wall injection moulding. CIRP Annals-Manufacturing Technology, 1(65), 537-540.

[48] Rose, W. (1961). Fluid-fluid interfaces in steady motion. Nature, 191, 242-243.

[49] Vincent, M., Giroud, T., Clarke, A., & Eberhardt, C. (2005). Description and modeling of fiber orientation in injection molding of fiber reinforced thermoplastics. Polymer, 46(17), 6719-6725.

[50] Wirjadi, O., Godehardt, M., Schladitz, K., Wagner, B., Rack, A., Gurka, M. & Noll, A. (2014). Characterization of multilayer structures in fiber reinforced polymer employing synchrotron and laboratory X-ray CT. International Journal of Materials Research, 105(7), 645-654.

[51] Shen, H., Nutt, S., & Hull, D. (2004). Direct observation and measurement of fiber architecture in short fiber-polymer composite foam through micro-CT imaging. Composites Science and Technology, 64(13), 2113-2120.

[52] Nicola, G. (2016). Prediction of shrinkage in micro injection moulded parts via determination of the CRIMS model coefficients. Master thesis, University of Padova.

[53] Fischer, J. (2012). Handbook of molded part shrinkage and warpage. William Andrew.

[54] Advani, S. G., & Tucker III, C. L. (1987). The use of tensors to describe and predict fiber orientation in short fiber composites. Journal of Rheology, 31(8), 751-784.

CHAPTER 6. QUALITY CONTROL BY DEFECT MINIMIZATION

Chapter 6.
Quality control by defect minimization

Other than dimensional accuracy and preferred fiber characteristics, there are several other quality criteria for process optimization depending on the applications. These quality criteria correspond to different kinds of defects which may appear in injection molded part. Over the years, a strong know-how has been developed to get rid of the defects by fine tuning the processing conditions, design of part/mould etc. However, the complexity of functional features leaves very limited scope of design changes on the product side and the only way to minimize the defects is by better understanding the effect of process parameters. In this chapter, an application based study has been carried out with a goal of minimizing internal void defects by varying the process parameters and finding the best set of process parameters with respect to different quality criteria.

6.1 Introduction

In the injection molding process, hot melt of plastic is forced into a cavity of desired shape (mold) and the hot melt is allowed to solidify. Then, the solidified net shape product is ejected out of the mold upon opening. Each of the processing steps may cause a one or more type of defects, if not optimized well. The most common are: splay marks, sink marks, voids, weld/meld lines, air traps, burn marks etc. There defects can be categorized as attribute related defects in order to differentiate them from the dimensional related defects [1]. Table 6.1 contains some of the common defects, the possible cause and remedial measures to prevent them.

Table 6.1: A summary of the various defects in injection molded parts taken from [2]

Defect	Appearance	Cause	Remedy
Short Shot		Plastic melt is not reaching the mold cavity section	- Increase melt temperature - Increase mold temperature - Increase injection speed - Increase injection pressure if process is pressure limited - Check if the mold is vented in the - area of short shots - Increase gate and runner sizes

Flash		Plastic melt is flowing into unwanted sections of the mold cavity	- Check for Mold shut-off and mold damage - Decrease melt temperature - Decrease mold temperature - Decrease injection speed
Sink		Plastic is shrinking as it cools but additional plastic cannot be for further compensation of the shrinkage	- Increase pack and hold Pressures - Increase pack and hold times - Decrease mold temperatures - Decrease melt temperatures
Splay		A layer/ streak of a unwanted gaseous by product from the melt or moisture in the material comes in between the melt flow and the cavity walls preventing the texture from being picked up and in addition eventually leaving a residue	- Dry plastic to suggested moisture levels - Decrease injection speeds - Decrease melt temperature - Decrease screw rotation speeds - Decrease back pressure - Increase mold temperatures - Increase venting - Increase gate sizes
Burn Marks		When air and gasses get trapped inside the mold cavity during plastic injection, the high pressure results in the dieseling of the plastic resulting in the burning of the plastic.	- Increase venting in the mold - Decrease injection speed - Decrease melt temperature - Decrease Screw Rotation Speeds
Contamination/ Black Specs		This can be degraded plastic and/or foreign material that can get mixed with the plastic that needs to be molded.	- Reduce melt temps - Reduce injection speeds - Reduce screw speeds - Find source of foreign material
Voids	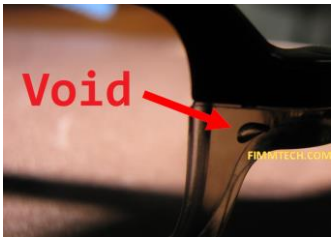	Usually occur with the parts are thick. The walls solidify and the plastic melt shrinks towards the wall and therefore sucks a vacuum void on the inside of the part	- Decrease mold temperature - Lower injection speed - Increase pack and hold pressures - Increase pack and hold times
Bubbles	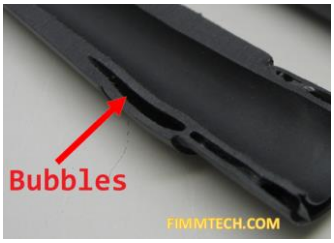	When moisture and/or a gaseous by product gets mixed with the melt and is injected in the mold cavity this moisture or gas if embedded inside the melt can show up as	- Dry material to suggested moisture levels - Increase back pressure - Reduce melt temperature

		bubbles	
Gate Blush		Shows up at the gate when the material is sheared differently compared to the rest of the part	- Slow down the injection speeds in the gate area - Profile the injection speeds if necessary - Experiment with increasing and decreasing melt temperatures or hot tip temperatures in case of hot runner molds
Jetting		Usually seen with the part is thick causing the injected plastic to 'snake fall' on to the cold mold surface and start freezing immediately. When the fresh plastic come in it does not blend well with the first material causing the jetting marks	- Reduce injection speed - Increase melt temperature - Change gate location
Weld Lines		The melt flow front is usually cold due to the exposure to the cold cavity. When two flow fronts meet as in a flow around a mold pin they do not fuse uniformly causing a weld line. Sometimes air can also get trapped in to form the defect	- Increase melt temperature - Increase mold temperatures - Increase injection speeds - Increase venting

6.1.1 Voids/Bubbles

Bubbles can be defined as a voided area trapped within a molded plastic part. It differs from a blister in that there is no surface protrusion with a bubble. Bubbles are usually caused by trapped gases or air pockets, but can also be caused by differential shrinkage.

According to the Moldflow design guide by Shoemaker [3]: "Sink marks and voids are caused by localized shrinkage of the material at thick sections without sufficient compensation when the part is cooling (Fig. 6.1). Once the outer material has cooled and solidified, the core material starts to cool. When shrinkage pulls the surface of the main wall inward, it causes a sink mark; and if the skin is rigid enough, as in engineering resins, deformation of the skin may be replaced by formation of a void in the core.

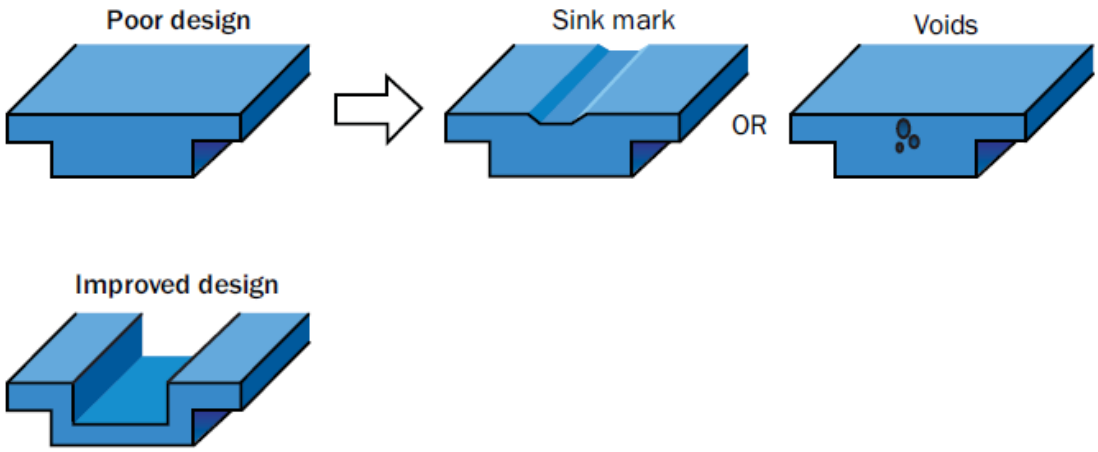

Fig. 6.1: The design aspect of void/sink mark formation [3]

The causes of such defects are discussed here in detail, which are categorized in machine, mold, material and operator related as explained by Bryce [4]:

6.1.1.1 Machine

Low injection pressure or hold time

When injection pressure or hold time are too low, the molten material is not forced into the mold cavity and trapped gases and air will form voids as the gases will not be forced out of the mold through vent paths. Increasing the injection pressure and/or the hold time to force the gases out as the plastic is pushed into the cavity.

Insufficient material

Insufficient material feed will have the same effect as low injection pressure. The material will not be forced into the cavity and gases will remain trapped, forming voids due to a lack of molecular packing. It is important to establish a feed setting that allows a cushion of material at the end of the injection stroke. Without the cushion, there is no material against which holding pressure can be applied to force the material into the cavity.

Improper injection temperature profile

The injection temperature profile addresses four heating zones of the injection barrel. These are commonly known as rear, center, front, and nozzle. The rear is also known as the feed zone, the center is known as the transition zone, and the front is known as the metering zone. The purpose of the feed zone is to start the material through the heating process. The heat is kept lower at this point but high enough to begin softening the plastic. The transition zone heats the plastic higher and begins to compress it, squeezing

out the trapped gases. In the metering zone the material is brought up to the final, ideal temperature and is further compressed and sheared, which also introduces more heat. In the nozzle zone the material is simply kept at the upper temperature as it is injected into the mold. Any imbalance in the temperature values of these zones may result in plastic particles that are not properly melted at the right time. This will not allow gases to escape and voids will appear. Maintaining a proper temperature profile is best way to avoid the bubbles.

Excessive injection speed

The injection speed determines how fast the material is injected into the mold. If it is too slow, the material tends to cool off and solidify before the mold is filled, which results in a short shot. If it is too fast, the material tends to tumble and become turbulent, which traps air and gases in the resin. These gases then show up as bubbles as they were not able to reach the vented areas of the mold. Therefore, a good practice would be starting with material specifications and adjusting up or down according to the results.

Insufficient back pressure

Back pressure is used to help mix the material and homogenize it. It also helps remove trapped air and densifies the melt. If back pressure is insufficient the gases and trapped air are not allowed to escape and remain in the plastic melt as bubbles that can be molded into the finished part.

6.1.1.2 Mold

Improper venting

Most molds do not have adequate venting. Usually the mold maker elects to “wait and see” where the venting needs to be located and then assigns an arbitrary size. While size is not necessarily as important as location, there is a tendency to use a minimum number of oversized vents rather than an adequate number of properly sized vents. If improper venting is used (or no venting), any trapped air or generated gases cannot escape. This will result in voids, bubbles, shorts, and burns.

Vent the mold even before the first shot is taken by grinding thin pathways on the shutoff area of the cavity blocks. Vents should take up approximately 30% of the perimeter of the molded part. Vent the runner, too. Any air that is trapped in the runner will be pushed into the part.

Section thickness too great

Most plastic parts are not of uniform wall thickness. There is usually a need to change the wall thickness for such reasons as additional strength. Unfortunately, when that happens, there is a pressure loss in the thicker section as the molten material shrinks more there as it solidifies. The material pulls away from the cavity wall leaving a voided area (Fig. 6.1). If the void is captured below the part surface, the void will appear as a bubble. A good rule-of-thumb is that any wall thickness should not exceed any other wall thickness by more than 25%. There will be little tendency for bubbles at that ratio.

Improper runners or gates

Runners or gates that are too small will restrict the molten material in the flow pattern and may cause non-packed parts. If gates are placed to flow material from a thin section into a thicker section, the restricted flow in the thin section will keep the thicker section from packing. Both of these conditions can result in a loss of filling pressure and cause sinks to evolve in the molded part. These sinks can take the shape of bubbles and voids if they are trapped within the part rather than on the surface.

Gates should be of a depth that is equal to at least 50% of the wall they are placed at and should always be located to flow material from the thickest section to the thinnest. Runner diameters should be adequate to avoid a pressure drop as the material fills. Thus, the farther the travel, the larger the initial runner diameter should be. It is a good practice to place gates and runners in individual inserts so they can be easily replaced and/or reworked.

Low mold temperature

A mold that is too cold for a specific resin or product design will not allow the molten material to fill and pack all of the mold properly before the resin starts to solidify. Any air or gases present in the plastic at the time will be trapped under the surface as bubbles. Raise the mold temperature in small increments until the bubbles disappear. Allow 10 cycles for each change in adjustment (up or down) for the mold temperature to stabilize.

6.1.1.3 Material

Selection of material

Selection of material can also play important role in void formation. During injection molding, shrinkage always occurs due to the change in density of the polymer when solidified. Higher the shrinkage in the part, higher the probability of void formation, especially in thick section (Fig. 6.1). In general, amorphous materials are considerably less prone to shrinkage than semi-crystalline materials as depicted in the Fig. 6.2.

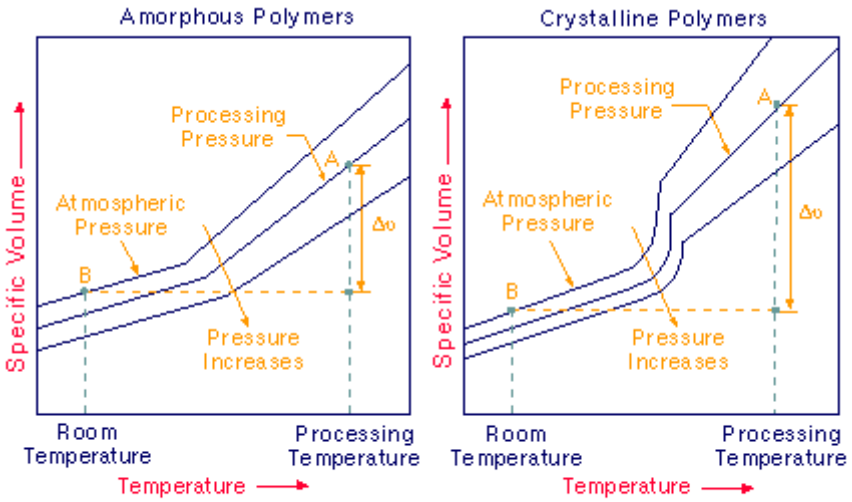

Fig. 6.2: Shrinkage in amorphous and crystalline polymers [5]

Excessive moisture

Excessive moisture is one of the most frequent causes of bubbles. Moisture causes bubbles as the water droplets actually turn to pockets of steam when heated in the injection unit, causing voided areas between molecules. If the voided areas are trapped beneath the surface of the part they appear as bubbles.

Although it is commonly understood that non-hygroscopic materials do not require drying. Nevertheless, it is good practice to dry all materials. It may be that fillers used in the material are hygroscopic and they will absorb moisture. Every plastic material requires specific drying conditions. And each material should be dried according to the material supplier's recommendations. The desired moisture content is between $1/10^{th}$ of 1 percent and $1/20^{th}$ of 1 percent by weight. It means the dry air being used to take moisture from the material should have a dew point of - 20 to - 40 °F.

6.1.1.4 Operator

Inconsistent process cycle

It is possible that the machine operator is the cause of delayed or inconsistent cycles. This will result in excessive residence time of the material in the injection barrel. If such a condition exists, materials may flow more easily and be injected too quickly, resulting in trapped air and gases being held in the resin and not being vented as required. The gases will form bubbles if held under the molded part surface.

The above mentioned causes and remedies are very generic and may not be applicable to a specific part. In that case, it requires additional control strategies to avoid such defects. Every application has several design restrictions due to the functionality and

leaves very limited room for design changes (e.g. changing the wall thickness etc.); therefore, the process has to be optimized by developing a clear understanding with respect to the desirable quality criteria.

6.1.2 Case study

This study was performed in collaboration with an industrial partner and the specific part details about the geometry, dimensions and material are not included here due to confidentiality agreement. The part was produced by micro injection molding and referred as V-shaped polymeric part in this discussion. The quality of the part is very much affected by the void defects appearing during the injection molding stage.

6.2 Methodology

This section consists of the design of experiments approach for the micro injection molding experiments and the CT characterization of molded parts.

6.2.2 Design of experiments

The main objective for using the design of experiment is to identify the critical parameters affecting the quality aspects as well as their interactions. Four critical process parameters were included in the design of experiment in order to determine their influence on the micro injection moulding process:

- Melt temperature (T_m)
- Mold/tool temperature (T_t)
- Injection speed (V_{inj})
- Packing pressure (P_h)

A full factorial design was created with 2 levels of melt temperature, injection speed and holding pressure each and 3 levels of tool temperature; a total 24 molding experiments were performed (see Table 6.2). The velocity/pressure switch-over point was set at 90% of the maximum injection pressure. Constant process parameters were back pressure, cooling time and metering speed. Ten test specimens were moulded for every set of process conditions. When changing from one experiment to another, the first five test specimens were discarded to allow the process to reach a steady state.

Table 6.2: Full factorial design of experiments for the injection moulding of the test specimens. T_t: tool temperature, T_m: melt temperature, V_{inj}: injection speed and P_h: packing pressure

ID	T_t [°C]	T_m [°C]	V_{inj} [mm/s]	P_h [bar]
1	80	190	100	625
2	80	190	100	1000
3	80	190	400	625
4	80	190	400	1000
5	80	210	100	625
6	80	210	100	1000
7	80	210	400	625
8	80	210	400	1000
9	100	190	100	625
10	100	190	100	1000
11	100	190	400	625
12	100	190	400	1000
13	100	210	100	625
14	100	210	100	1000
15	100	210	400	625
16	100	210	400	1000
17	120	190	100	625
18	120	190	100	1000
19	120	190	400	625
20	120	190	400	1000
21	120	210	100	625
22	120	210	100	1000
23	120	210	400	625
24	120	210	400	1000

6.2.3 CT Characterization

Metrological micro-computed tomography (µCT) system MCT225 was used for acquiring CT data. Four parts are placed on a sample holder to be scanned at one time. Two out of the four parts are repetitions at one process setting from the Table 6.2. Physical markings are used for identification as all parts look identical in appearance. The scanning parameters are provided in Table 6.3.

Table 6.3: CT scanning parameters

Factor	Value
Voltage, kV	120
Current, µA	45
Exposure time, s	2
Projections	1800
Scan time, min.	60
Voxel size, µm	10.47

6.3 Results and discussion

The three responses variable have been identified for the part quality assessment which are void volume (V_v), part volume (V_p) and wall thickness (t_w). In order to test the repeatability, two parts were measured for every set of process conditions. In this way, it was possible to perform an analysis of variance (ANOVA) to understand how the process conditions affect the part quality based of the response variables. Results of part measurements and analysis are reported in the following Table 6.4; a detailed discussion is followed. For settings ID:10, ID:17 and ID:22, incomplete moldings were resulted, which are excluded from the this discussion. The desirability with respect to the responses are: the void volume should be minimized, the part volume should be maximized and the wall thickness should remain consistent. The minimum and maximum values reported for the DoE are:

Table 6.4: Measurements of the moulded parts for the DoE

ID	V_v [mm^3]		V_p, [mm^3]		t_w [mm]	
	Mean	**Std. dev.**	**Mean**	**Std. dev.**	**Mean**	**Std. dev.**
1	0.464	0.024	43.65	0.180	0.186	0.007
2	0.443	0.014	44.67	0.079	0.194	0.002
3	0.415	0.043	43.96	0.088	0.191	0.002
4	0.398	0.010	44.65	0.101	0.194	0.002
5	0.403	0.006	44.57	0.049	0.193	0.003
6	0.388	0.013	44.41	0.090	0.193	0.001
7	0.385	0.006	44.47	0.061	0.194	0.002
8	0.381	0.005	44.20	0.182	0.192	0.001
9	0.420	0.007	44.44	0.087	0.193	0.002
10	-	-	-	-	-	-
11	0.428	0.004	44.36	0.058	0.183	0.024
12	0.397	0.002	44.86	0.051	0.183	0.024
13	0.385	0.002	44.33	0.082	0.192	0.003
14	0.379	0.004	44.38	0.132	0.195	0.002
15	0.377	0.012	44.39	0.028	0.193	0.002
16	0.374	0.002	44.37	0.044	0.193	0.002
17	-	-	-	-	-	-
18	0.368	0.000	44.64	0.000	0.193	0.002
19	0.440	0.004	44.55	0.039	0.194	0.002
20	0.366	0.004	44.48	0.083	0.193	0.001
21	0.438	0.011	43.87	0.137	0.192	0.000
22	-	-	-	-	-	-
23	0.430	0.005	43.98	0.027	0.192	0.000
24	0.345	0.009	44.64	0.052	0.192	0.001

6.3.1 Void volume

The void or bubbles are the main contributor to the low quality of the manufactured parts and thus it was considered as the most important quality criterion. The surface determination based porosity module was used for the void volume analysis in the VGStudioMax 3.0. The quantitative results of the void volume are reported in the Table 6.4 for the full DoE plan. The process settings with ID:24 yield the minimum void volume, the settings contain all the four factors at high level (T_m = 210°C; T_t = 120°C V_{inj} = 400 mm/s and P_h = 1000 bar). On the other hand, the process settings with ID:1 yield the

maximum void volume, the settings contain all the four factors at low level (T_m = 190°C; T_t = 80°C V_{inj} = 100 mm/s and P_h = 625 bar). However, the effect of process parameters on void volume is straightforward but it needs to be understood further in order to find out the optimized conditions considering the other quality criteria.

The voids are mainly located in the central symmetrical plane (core) of the part with size ranging from 0.010 mm^3 to 0.10 mm^3; which is due to the fact that the material around the central plane is the last to solidify and therefore, is more prone to air/gas entrapment and/or differential shrinkage. The study of cross section along this plane is of importance to understand the morphology of the void e.g. the size and the pattern. However, the graphical data is not included here for the confidentiality.

At tool temperature 80 °C, presence of large voids of volume of 0.09 mm^3 and above is very evident especially at lower melt temperature and lower packing pressure, which could be attributed to the material insufficiency. At tool temperature 100 °C, the voids are comparatively smaller and remains smaller than 0.06 mm^3. A similar trend can also be observed at the tool temperature of 120 °C; however the number of bigger voids is reduced with the increment of tool temperature.

6.3.2 Part volume

The part volume is the estimation of the shrinkage of the part. Lower volume corresponds to higher shrinkage. When compared with the nominal geometry, the V-shaped part exhibits larger deviation at both the ends and the central portion shows minimum deviations. This could be due to the flexibility at the open ends. However, the deviations are not very crucial from the quality point of view; the important aspect could be the total part volume. Based on the determined surface, the total value can be measured; which is included in Table 6.4 for the entire DoE.

6.3.3 Wall thickness

One of the important quality parameter identified according to the functional requirement was the wall thickness at the V-point or the junction point. The algorithm for calculating the wall thickness of a part in VGStudio MAX 3.0 is based on the result of the surface determination routine. It is possible to apply the wall thickness calculation to specifically selected regions of interest (ROIs) within the CT dataset thus limiting the total amount of computational time needed to analyze a dataset. Therefore, it was applied only in the V-point region.

For the quantitative analysis, the minimum wall thickness was chosen and six measurements were taken along the x-axis at a fixed y and z positions. The mean values is reported in Table 6.4. The wall thickness seems to be consistent (± 5 µm) except for process settings ID: 1, 11 and 12, where the difference is over 10 µm. Moreover, a non-uniformity was observed at process settings ID: 2 and 5; which is more prominent at lower packing pressure due to incomplete filling. At higher tool temperature (120 °C),

there was a presence of some flash material which could be attributed to the more material entering in the cavity.

6.3.4 Statistical analysis

Analysis of variance (ANOVA) is a statistical method for identifying the significant factors that affect a certain response. In this case, the effect of tool temperature, melt temperature, injection speed and packing pressure on void volume, part volume and wall thickness are investigated as well as their interactions. Tables 6.5 and 6.6 and 6.7 report the analysis of variance for the void volume, part volume and wall thickness respectively.

Table 6.5: Anova table for void volume

Source	DF	Adj SS	Adj MS	F-Value	P-Value
T_t	2	0.000938	0.000469	58.64	0.092
T_m	1	0.003033	0.003033	379.15	0.033
V_{inj}	1	0.000448	0.000448	56.02	0.085
P_h	1	0.003961	0.003961	495.15	0.029
T_t*T_m	2	0.000388	0.000194	24.25	0.142
T_t*V_{inj}	2	0.000885	0.000443	55.32	0.095
T_t*P_h	2	0.002864	0.001432	179.02	0.053
T_m*V_{inj}	1	0.000031	0.000031	3.92	0.298
T_m*P_h	1	0.000047	0.000047	5.9	0.249
V_{inj}*P_h	1	0.000018	0.000018	2.3	0.371
Error	1	0.000008	0.000008		
Total	20	0.019183			

Table 6.6: Anova table for part volume

Source	DF	Adj SS	Adj MS	F-Value	P-Value
T_t	2	0.14444	0.07222	305.33	0.04
T_m	1	0.07346	0.073458	310.56	0.036
V_{inj}	1	0.00312	0.003119	13.18	0.171
P_h	1	0.33674	0.336738	1423.65	0.017
T_t*T_m	2	0.25678	0.128392	542.81	0.03
T_t*V_{inj}	2	0.00893	0.004467	18.89	0.161
T_t*P_h	2	0.00371	0.001853	7.83	0.245
T_m*V_{inj}	1	0.00011	0.000107	0.45	0.623
T_m*P_h	1	0.09059	0.09059	382.99	0.033
$V_{inj}*P_h$	1	0.03021	0.030211	127.72	0.056
Error	1	0.00024	0.000237		
Total	20	1.78108			

Table 6.7: Anova table for wall thickness

Source	DF	Adj SS	Adj MS	F-Value	P-Value
T_t	2	0.000014	0.000007	2.72	0.394
T_m	1	0.000014	0.000014	34.31	0.108
V_{inj}	1	0.000005	0.000005	21.83	0.134
P_h	1	0.000003	0.000003	29.31	0.116
T_t*T_m	2	0.000037	0.000018	6.43	0.269
T_t*V_{inj}	2	0.000036	0.000018	53.57	0.096
T_t*P_h	2	0.000006	0.000003	0.18	0.856
T_m*V_{inj}	1	0.000006	0.000006	10.61	0.19
T_m*P_h	1	0.000002	0.000002	12.82	0.173
$V_{inj}*P_h$	1	0.000001	0.000001	19.64	0.141
Error	6	0.000057	0.000009		
Total	20	0.000222			

The Analysis of variance showed important information as far as the influence of process parameters is concerned. From the ANOVA tables the significant factors and interactions can be pointed out with p-values less than 0.05. As far as the void volume is concerned, the significant factors are: melt temperature, packing pressure, the interaction between melt temperature and packing pressure and the interaction between tool temperature and packing pressure. For part volume, tool temperature, melt temperature and packing pressure are significant and interactions of tool and melt temperature and melt temperature and packing pressure. No significant effect has been observed for the wall thickness. These results are analyzed in detail with the help of main effect plots, interaction plots.

6.3.4.1 Main effects plots

The main effect plots for void volume, part volume and wall thickness are presented in Fig. 6.3.

In Fig. 6.3 (a), the effect of tool temperature on void volume shows a minimum at the middle level, which indicates that increasing the tool temperature further can have adverse effects. Increasing the melt temperature and injection speed reduces the void content to some extent; however the most significant is the packing pressure. Increasing packing pressure from 625 to 1000 bar, reduced the void content by around 10 %. Higher pressure helps in removing the trapped air and densifies the melt.

As shown in Fig. 6.3 (b), the part volume is significantly affected by the packing pressure, which is explained by the fact that increasing packing pressure increases the amount of material entering the cavity; as a result, shrinkage decreases. The other factors are not really significant as the change in the part volume is very minimal.

Although the effect of parameters on wall thickness is not so significant (Fig. 6.3 (c)); the small increase in the wall thickness by increasing the melt temperature and packing pressure can be explained by more material entering the cavity. An increase in melt temperature reduces the viscosity of material, hence allows more material.

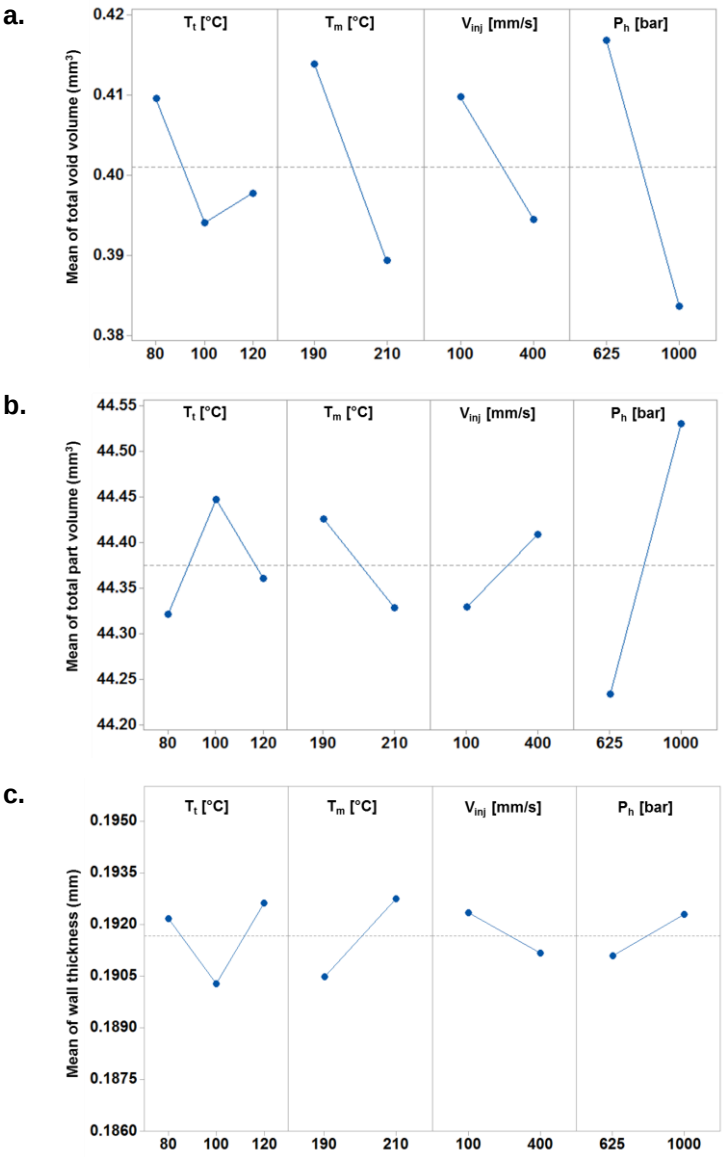

Fig. 6.3: Main effect plots: void volume (a), part volume (b) and wall thickness (c)

6.3.4.2 Interaction effect plots

Interaction plots are used to visualize interactions DoE; parallel lines in an interaction plot indicate no interaction and the greater the difference in slope between the lines, the higher the degree of interaction.

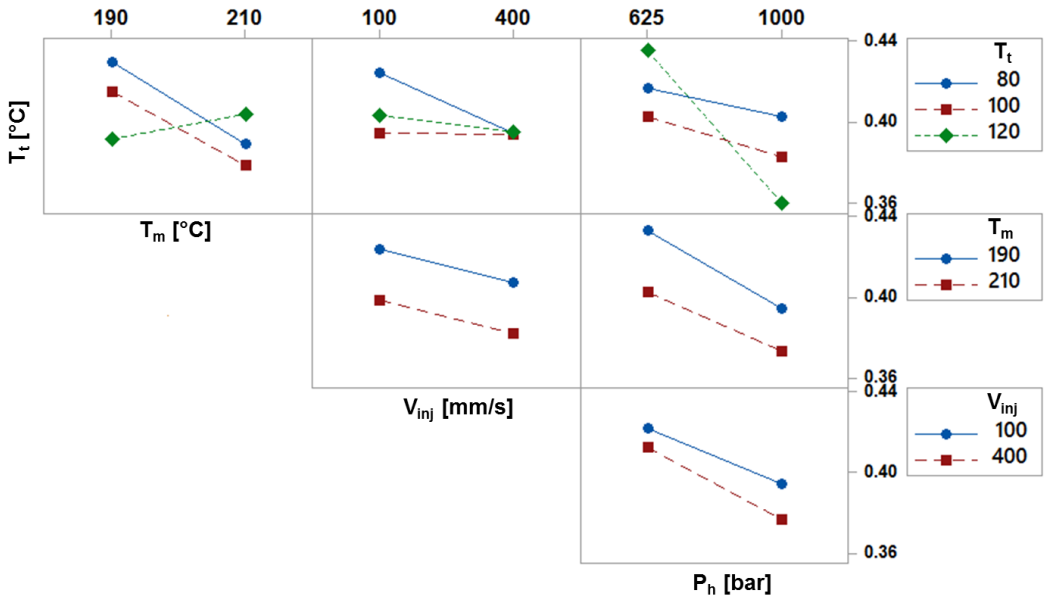

Fig. 6.4: Interaction plots for void volume

Fig 6.4 represents the interaction plots for response variable void volume. The most significant interactions are tool temperature - melt temperature and tool temperature - pressure. The interactions are mainly at the high tool temperature (120 °C); higher value of melt temperature reduces the void content for tool temperature 80 and 100 °C but slightly increase the void content at 120 °C; which could be due the combined effect of both the melt and tool temperatures.

As far as the part volume is concerned the most significant interaction is between tool temperature and melt temperature which was also true for void volume (see Fig. 6.5). The part volume is reduce (higher shrinkage) at higher mold temperature (100 and 120 °C) when the melt temperature is increased. This is surprising since high mold temperature reduces the post molding shrinkage due to the stress relaxation and additional crystallization within the molded part. The complexity of the relationship between melt and mold temperature is due to the curvature in the response surface graphs as presented in Fig. 6.6.

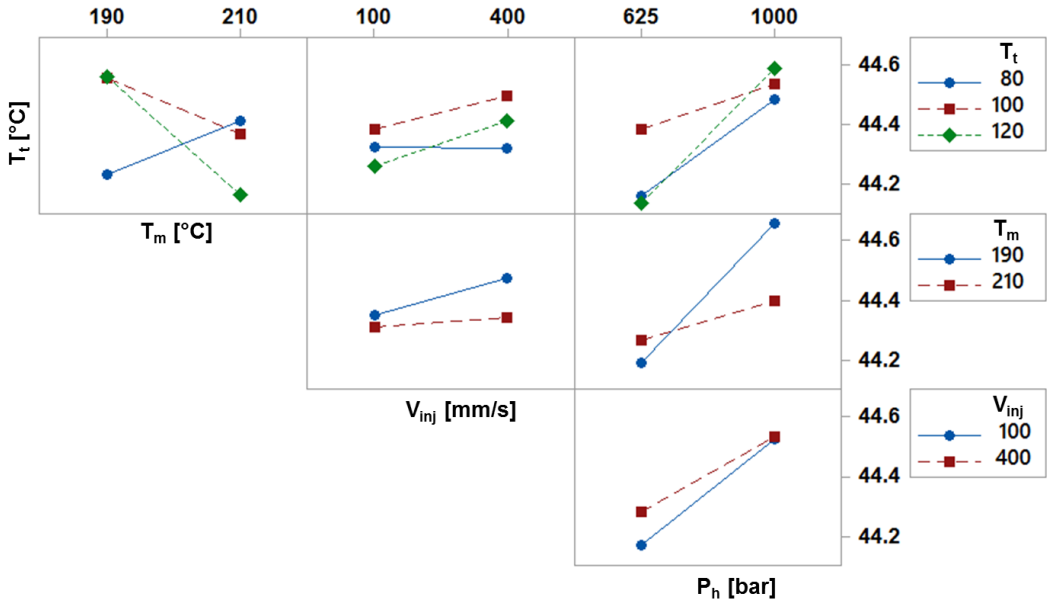

Fig. 6.5: Interaction plots for part volume

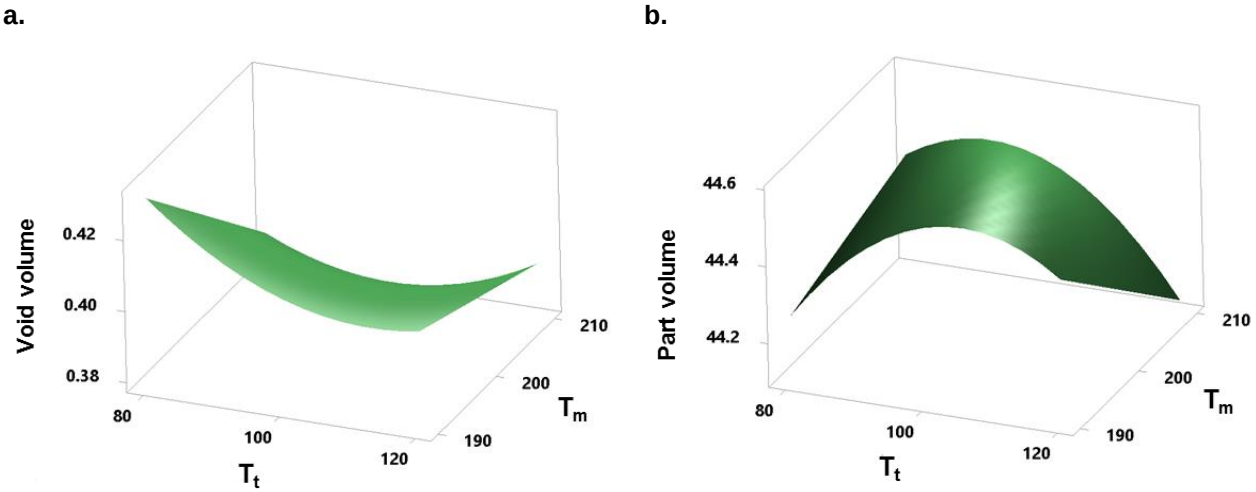

Fig. 6.6: Response surface for void volume (a) and part volume (b)

6.3.5 Optimal solution

Since wall thickness is not much affected by the process settings, an optimal solution identifying the combination of input variable settings that optimize the void content and part volume according to the desirability is presented here. The desirability is to minimize void volume and maximize part volume. Minitab response optimizer calculates an optimal solution and draws an optimization plot, which is shown in Fig. 6.7. The top row of the graph corresponds to the composite desirability and the remaining row corresponds to a response variable (part volume and void volume). The horizontal blue line shows the

best set of responses with a composite desirability (D) of 0.892. The optimized variable setting is indicated by the red lines (the exact details are not revealed due to confidentiality)

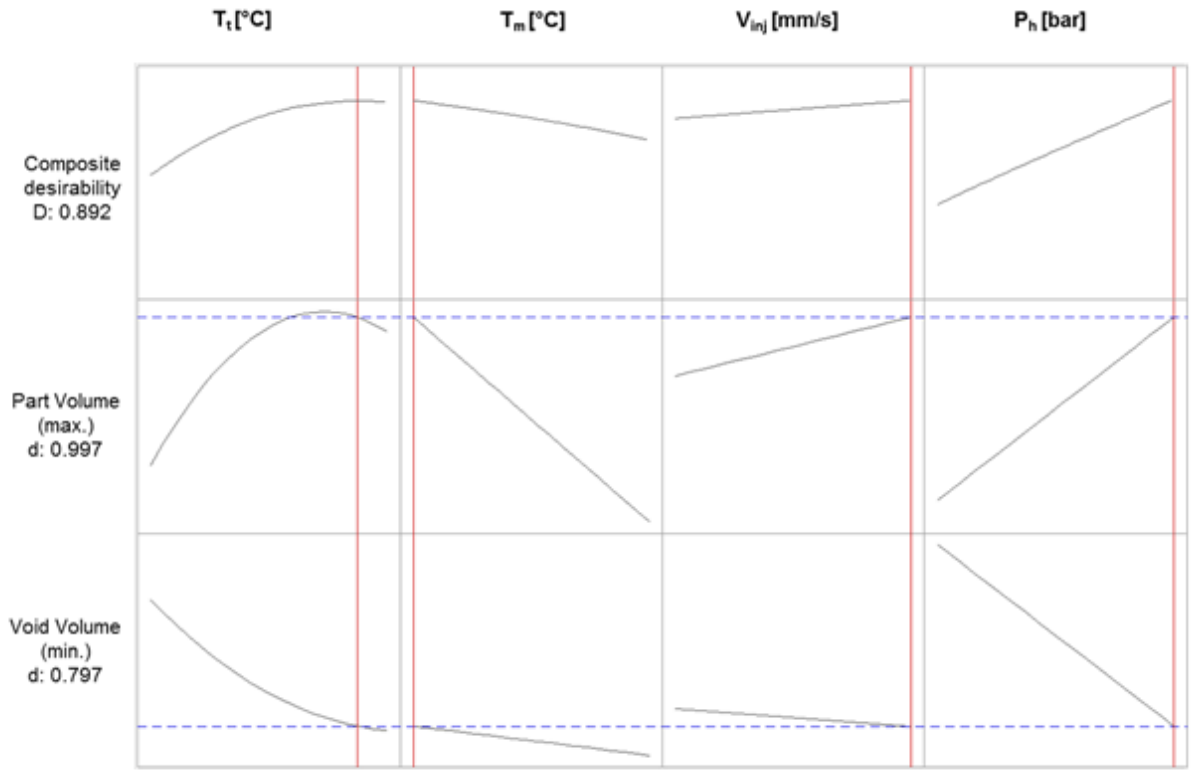

Fig. 6.7: Optimization plot

6.4 Conclusions

An application based study was carried out with the goal of minimizing the internal defects and finding out the best set of processing parameters.

Thanks to DoE analysis the critical molding parameters were identified based on the three quality aspects: void volume, part volume and wall thickness. Void volume corresponds to the total amount of internal void or bubble defects. The part volume is related to the shrinkage of the part.

Based on the qualitative analysis, it was shown that the voids are mainly located in the central symmetrical plane of the part. The lower tool temperature 80 °C resulted into large voids of volume of 0.09 mm^3 and above which gets adverse at the combination low melt temperature and low packing pressure. The higher level of all the process variables resulted in the minimum void content. The wall thickness seems to be consistent (± 5 µm); a non-uniformity was observed at lower packing pressure due to incomplete filling.

The quantitative analysis highlighted the most significant factors and their interactions thanks to the ANOVA study. As far as the void volume is concerned, the significant factors are: melt temperature, packing pressure, the interaction between melt temperature and packing pressure and the interaction between tool temperature and packing pressure. For part volume, tool temperature, melt temperature and packing pressure are significant and interactions of tool and melt temperature and melt temperature and packing pressure. No significant effect has been observed for the wall thickness. An optimal solution was proposed by minimizing the void volume and maximizing part volume.

The future work will include the part manufacturing with the calculated optimum settings followed by CT characterization. A new DoE with narrow range of variable is also proposed to be conducted.

References

[1] Mathivanan, D., Nouby, M., & Vidhya, R. (2010). Minimization of sink mark defects in injection molding process–Taguchi approach. International Journal of Engineering, Science and Technology, 2(2), 13-22.

[2] http://www.fimmtech.com (Retrieved on October 5, 2017)

[3] Shoemaker, J. (Ed.). (2006). Moldflow design guide: a resource for plastics engineers (Vol. 10). Hanser Verlag.

[4] Troubleshooting Guide For Injection Molders by Douglas M. Bryce http://www.plastictroubleshooter.com/ThePlasticTroubleshooter/bubbles.htm (Retrieved on October 27, 2017)

[5] Santa Clara University Engineering Design Center (2006). Shrinkage and warpage. http://www.dc.engr.scu.edu/cmdoc/dg_doc/develop/process/physics/b3500001.htm (Retrieved on October 5, 2017)

CHAPTER 7. CONCLUSIONS AND FUTURE OUTLOOK

Chapter 7.
Conclusions and Future Outlook

The increasing demands of miniaturized products with stringent quality requirements in terms of dimensional accuracy was the motivation behind this PhD work. The low production cost and ease of fabrication make injection molding as the most preferred manufacturing method for mass micro replication. However, before mass replication a product has to go through a development phase where, the quality has to be reached to the desired standards by process optimization. The recent inclusion of X-ray CT in the industrial environments for quality control is seen as a very promising solution for the micro injection molding industry as well. Within the current framework, these two technologies are combined where the main objectives are:

- Designing new optimization control strategies for innovative injection molding applications using the CT technology.
- Using new methods and approaches to further improve CT based quality control of micro injection molded part

The general findings of this PhD work are summarized below:

From the first study, it was demonstrated that the X-ray CT can be utilized for measuring shrinkage and warpage of microfluidics system, however, the limited resolution is not sufficient for measuring the micro channels. Nevertheless, when combined with other sensor/techniques using data fusion methods, the holistic quality control is achieved. Moreover, further investigation is proposed in applying different data fusion algorithms to examine the accuracy of fused datasets.

Effect of electron beam alignment conditions (interpolation and single alignment) was investigated on the CT measurements of a micro molded part. The interpolation method is an efficient way to perform electron beam alignment which works of CT measurements for the entire voltage range (0-225 kV). On the other hand, single alignment is basically performing alignment at each measurement voltage which takes long time. The results showed that interpolation method is very well optimized and performs really well.

The second part of PhD work was concerning fiber reinforced composite molded parts. The influence of CT scanning parameters and resolution on the fiber characterization results (fiber orientation and fiber volume content) was investigated using a model based approach. The chosen two sets of scanning parameters were not significantly affecting the results. The resolution (voxel size) was affecting the fiber volume content estimation significantly; the lower the resolution, the higher the overestimation of the fiber volume which is due to the bigger voxel size. Interestingly, the resolution is not affecting the fiber orientation results, which supports using larger area/entire part for fiber orientation

analysis rather than sectioning the part to achieve higher resolution. These findings were utilized in the subsequent study of effect of molding conditions on the dimensional accuracy of final parts. The thickness ratio of the shear and core layers was affected by the process especially by the injection speed. The extremely thin cavity results in a nearly flat trend of the orientation tensor for parts obtained at lower injection speed which could be attributed to the absence of the core layer. Thus, a higher shrinkage along the transverse direction led to a differential shrinkage in the part and to the warpage of the final part.

The last part of PhD was dedicated to an application based study where the part quality was drastically affected by the presence of internal voids. A series of experimentation was performed using design of experiment approach. The quantitative analysis highlighted the most significant factors and their interactions thanks to the ANOVA study. As far as the void volume is concerned, the significant factors are: melt temperature, packing pressure, the interaction between melt temperature and packing pressure and the interaction between tool temperature and packing pressure. For part volume, tool temperature, melt temperature and packing pressure are significant and interactions of tool and melt temperature and melt temperature and packing pressure. No significant effect has been observed for the wall thickness. An optimal solution was proposed by minimizing the void volume and maximizing part volume. The future work will include the part manufacturing with the calculated optimum settings followed by CT characterization. A new DoE with narrow range of variable is also proposed to be conducted.